uOttawa

L'Université canadienne
Canada's university

FACULTÉ DES ÉTUDES SUPÉRIEURES ET POSTOCTORALES

uOttawa

L'Université canadienne
Canada's university

FACULTY OF GRADUATE AND POSDOCTORAL STUDIES

Ngoc Vuong

AUTEUR DE LA THÈSE / AUTHOR OF THESIS

M.Sc. (Biochemistry)

GRADE / DEGREE

Department of Biochemistry, Microbiology and Immunology

FACULTÉ, ÉCOLE, DÉPARTEMENT / FACULTY, SCHOOL, DEPARTMENT

Imaging the Nicotinic Acetylcholine Receptor in Reconstituted Membranes by Atomic Force Microscopy

TITRE DE LA THÈSE / TITLE OF THESIS

Linda Johnston

DIRECTEUR (DIRECTRICE) DE LA THÈSE / THESIS SUPERVISOR

John Baenziger

CO-DIRECTEUR (CO-DIRECTRICE) DE LA THÈSE / THESIS CO-SUPERVISOR

Danielle Carrier

Mary Alice Hefford

Gary W. Slater

Le Doyen de la Faculté des études supérieures et postdoctorales / Dean of the Faculty of Graduate and Postdoctoral Studies

Imaging the Nicotinic Acetylcholine Receptor in Reconstituted Membranes by Atomic Force Microscopy

Ngoc Quang Vuong

Thesis submitted to the Department of Biochemistry in partial fulfillment of the requirements for the degree of Master of Science

University of Ottawa
Ottawa, Ontario, Canada
February, 2010

Your file Votre référence
ISBN: 978-0-494-66239-7
Our file Notre référence
ISBN: 978-0-494-66239-7

To my parents, Hong Phan and Loc Vuong, who have been supporting and encouraging me in achieving my goals in life.

Abstract

Several recent studies have suggested that the nicotinic acetylcholine receptor (nAChR) segregates lipids into domains in reconstituted bilayers. These studies, however, lack direct evidence (e.g., microscopic images) to show domain formation. Atomic force microscopy (AFM) has been used extensively to image both lipid domains and proteins in membranes, but has not been applied extensively to reconstituted membrane proteins due to the lack of available protocols for preparing suitable planar bilayers on AFM supports. The aim of the work presented in this thesis was to image the nAChR in planar reconstituted membranes by AFM. I developed a novel method for reconstituting the nAChR in POPC (POPC-nAChR) to generate vesicles with high lipid-to-protein (L:P) ratios (i.e., greater than 100:1 w/w). Freeze-thaw cycles are required to improve vesicle homogeneity. The high L:P vesicles must also be isolated from protein-free vesicles using sucrose density gradients. Finally, the preparation of planar bilayers from the high L:P ratio proteoliposomes requires an appropriate sample load and incubation time on a defined area of mica surface (the solid AFM support) and an appropriate level of calcium. AFM images of a POPC-nAChR bilayers show a number of features that protrude out of the bilayer with an average height of 3 nm and diameter of 4 – 9 nm, which is appropriate for the dimensions of the cytoplasmic side of the nAChR. My results thus represent the first AFM images of the nAChR in a reconstituted membrane environment. Now that the key parameters governing nAChR reconstitution and planar bilayer preparation for AFM imaging are understood, they will undoubtedly be useful for reconstituting and imaging the nAChR in more complex bilayers.

Acknowledgements

My accomplishments here would not have been possible if it were not for the support and encouragement of my dear family, friends and mentors.

- First and foremost I'd like to thank Dr. Linda Johnston (supervisor #1) who has been with me through thick and thin in my career. Your mentorship was highly consistent and accessible throughout my study. Thanks seem not enough…
- Special thanks to Dr. John Baenziger (supervisor #2) for being a great mentor. I have learnt and developed many invaluable scientific skills from you. You have made the ion channels that much more interesting.
- Member of my thesis advisory committee: Dr. Natalie Goto. Your suggestions were very helpful.
- Thank the members in Drs. Baenziger and Johnston lab for your friendship and supports. Members in Dr. Baenziger lab: Casey Carswell, Lopa Dey, Mike Goodreid, Danny Hill, Yi Huo, Prateek Khatri, Nadine Lavine, Marc Rigden, Ali Sayed, Wajid Sayed, Michel Sturgeon, and Shuzi Wang. Members from Dr. Johnston's lab: Daniel Ramirez, Mukundan Chakrapani, Oana Coban, Anatolli Ianoul, Zhengfang Lu, Kirk Mulligan, Ira Probodh, Mauro Tomietto, Dusan Vobornik, Anna Carnini, Zygmunt Jakubek.
- My family members who have always been with me through every thing: Hong Phan, Loc Vuong, Nhung Vuong, Minh Vuong, and Tuan Phan.
- My friends and colleagues that have made my student life so much more enjoyable. Especially BaeBae, Leslie, Natalia, and Sujeeve.

Table of Contents

Table of Figures

List of Abbreviations

Å	Angstrom
αBTx	α-Bungarotoxin
αBTx-A488	Alexa-488 conjugated α-Bungarotoxin
A_{400}	Absorbance at 400 nm
AChBP	Acetylcholine binding protein
AFM	Atomic force microscopy
ATR	Attenuate total internal reflection
BCA	Bicinchonicic acid
Carb	Carbamylcholine
cDNA	Complementary deoxyribonucleic acid
Chol	Cholesterol
Da	Dalton
DEC221	DOPC/eSM/Chol (2:2:1 mole/mole)
DOPC	1,2-dioleoyl-sn-glycero-3-phosphocholine
DPPC	1,2-dipalmitoyl-sn-glycero-3-phosphocholine
DRM	Detergent resistant membrane
EDTA	Ethylenediaminetetraacetic acid
EPR	Electron paramagnetic resonance
eSM	Egg sphingomyelin
FTIR	Fourier transform infrared
GM1	Monosialotetrahexosylganglioside
GPI	Glycosylphosphatidyl inositol
HEPES	4-(2-hydroxyethyl)-1-piperazineethanesulfonic acid
kDa	Kilodalton
L:P	Lipid to protein
μg	Microgram
μl	Microliter
μm	Micrometer
ml	Milliliter
nAChR	Nicotinic acetylcholine receptor
nm	Nanometer
NMR	Nuclear magnetic resonance
OD	Optical density
PA	1,2-diacyl-sn-glycero-3-phosphate
PC	1,2-diacyl-sn-glycero-3-phosphocholine
PE	1,2-diacyl-sn-glycero-3-phosphoethanolamine
PG	1,2-diacyl-sn-glycero-3-phosphoglycerol
PI	1,2-diacyl-sn-glycero-3-phosphoinositide
POPA	1-palmitoyl-2-oleoyl-sn-glycero-3-phosphate
POPC	1-palmitoyl-2-oleoyl-sn-glycero-3-phosphocholine
PS	1,2-diacyl-sn-glycero-3-phosphoserine
TIRF	Total internal reflection fluorescence

Tm	Melting temperature
SDS-PAGE	Sodium dodecyl sulfate polyacrylamide gel electrophoresis
SM	Sphingomyelin
STM	Scanning tunneling microscopy
TDB	Tris dialysis buffer
TRB	*Torpedo* ringer buffer
TR-DHPE	Texas red dihexadecanoyl-PE

Chapter 1: Introduction

1.1 The Cell Membrane

The cell membrane is a complex multifunctional biological structure. It provides a boundary to all cells and organelles. It functions as a selectively permeable barrier to polar or charged molecules allowing cells and organelles to establish and maintain the proper solute concentrations within their compartments. At the same time, the cell membrane orchestrates numerous important biological processes such as signal transmission and transduction, homeostasis regulation, and cell adhesion and differentiation. How is the cell membrane organized to carry out such a vast array of tasks so effectively? This question can only be answered by careful examination of the machineries and building blocks of which the cell membrane is constituted.

1.1.1 The main components of the cell membrane

The cell membrane can be viewed as a thin fluid film made of mainly lipids and proteins (Figure 1.1). The lipids form a thin bilayer, where the hydrophilic head groups of lipids interact with water and the hydrophobic tails are sandwiched in the middle. Due to the hydrophobic core of the bilayer, the membrane effectively serves as a physical barrier to polar or charged molecules, but non-polar molecules diffuse relatively easily through the lipid bilayer.

Another component of the cell membrane is protein. There are two main types of membrane proteins, namely peripheral and integral proteins. Peripheral membrane proteins typically associate loosely with the bilayer surface and do not span the hydrophobic core of the membrane. These proteins can be removed from the membrane with mild treatments that do not disrupt the membrane structure. For example, high ionic strength buffers are typically sufficient to remove peripheral membrane proteins from the cell membrane. On

Figure 1.1. A model of the cell membrane adopted from the National Institute of Standards and Technology (http://www.ncnr.nist.gov/programs/reflect/cnbt/). The cell membrane can be viewed as a thin fluid film made of mainly lipids and proteins. The lipids form a thin bilayer, where the hydrophilic lipid head groups interact with water and hydrophobic tails are sandwiched in the middle. There are two main types of membrane protein, namely peripheral and integral membrane proteins. Peripheral membrane proteins are typically anchored in the bilayer through their acylated moieties and/or small hydrophobic peptide(s) that do not span the length of the membrane. Integral membrane proteins on the other hand are embedded in the bilayer through their transmembrane domain(s) which span the length of the bilayer.

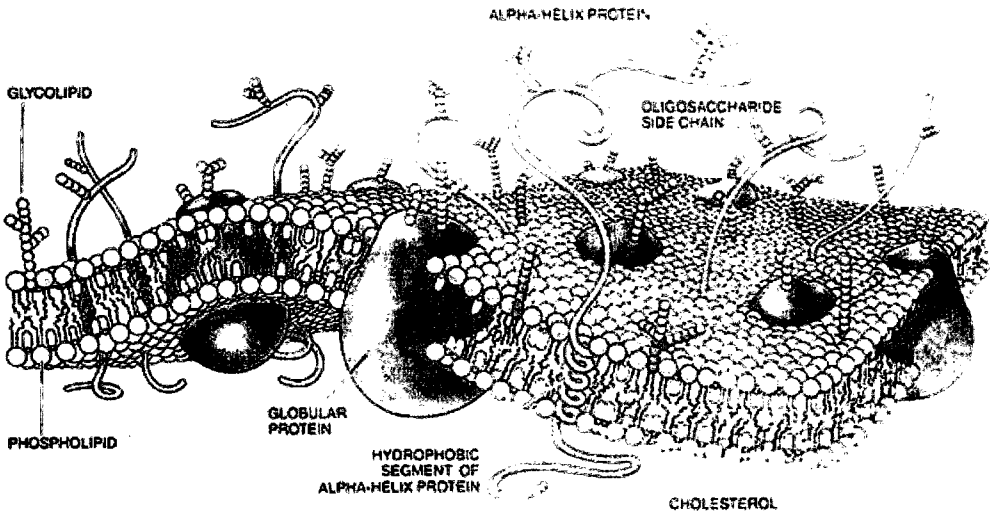
ALPHA-HELIX PROTEIN
GLYCOLIPID
OLIGOSACCHARIDE SIDE CHAIN
GLOBULAR PROTEIN
PHOSPHOLIPID
HYDROPHOBIC SEGMENT OF ALPHA-HELIX PROTEIN
CHOLESTEROL

the other hand, integral membrane proteins require detergent to remove them from the cell membrane, conditions under which the membrane structure is highly compromised. The reason detergent is required to extract integral membrane proteins is because they are embedded in the membrane through their hydrophobic domain(s) which span the length of the hydrophobic core of the membrane.

The presence of membrane proteins in the bilayer allows the cell membrane to carry out numerous vital biological processes. For example, the Na^+ and K^+ ion channel and Na^+/K^+ pump regulate the concentrations of Na^+ and K^+ across the cell membrane (Voet et al., 1999). The G protein and G-protein-coupled receptors (e.g., rhodopsin and serotonin) translate external signals to the interior of the cell (Voet et al., 1999). The insulin receptor stimulates the uptake of glucose into the cell. The nicotinic acetylcholine receptor, which is the subject of this thesis, converts extracellular chemical signals into electrical signals and facilitates neuronal cell to cell communication (Voet et al., 1999). Undoubtedly, membrane proteins must be highly organized and regulated in the cell membrane for proper functioning of the cell. Therefore, understanding the organization of the cell membrane is important.

1.1.2 The organization of the cell membrane

Singer and Nicolson proposed a fluid mosaic model for the cell membrane in 1972 and suggested that lipids and proteins form a bilayer in which both components can diffuse freely in the lateral dimension of the membrane (Singer and Nicolson, 1972). This model remains essentially correct, although accumulating evidence suggests that lipids and proteins do not diffuse as freely in a membrane as suggested in the fluid mosaic model (Laude and Prior, 2004; Vereb et al., 2003). Rather, both the lipids and proteins can segregate into domains to serve specific structural and/or functional purposes (Laude and Prior, 2004;

Zeyda and Stulnig, 2006). One possibility is the "pickets and fences" theory which proposes that transmembrane proteins (pickets) and actin-based membrane cytoskeletons (fences) form a mesh-like structure that confines the diffusion of lipids and membrane proteins within certain areas of the plasma membrane (Kusumi et al., 2005; Nakada et al., 2003; Sako and Kusumi, 1995). By contrast, the "lipid rafts" theory suggests that some lipids in the cell membrane are organized into domains to provide platforms for proteins to dock for trafficking or signaling (Simons and Ikonen, 1997). The cell membrane is undoubtedly a sea of lipids and proteins in which complex and dynamic organization among these components have important structural and functional implications. Understanding the organization of the cell membrane is clearly an important goal of membrane biology. The ultimate goal of my thesis is to examine whether the nicotinic acetylcholine receptor influences the formation of rafts in biological membranes. To understand how the nAChR may influence the formation of rafts, I will examine the lipid rafts concept in further detail.

1.1.3 Rafts in the cell membrane

The concept of lipid rafts in cell membranes was first introduced by Simons and Ikonen in 1997. This model suggests rafts are microdomains in the cell membrane that are composed mainly of cholesterol and saturated lipids such as sphingomyelin (Figure 1.2). Rafts are believed to exist in a liquid ordered phase (see *section 1.2.2* for more information), and are surrounded by unsaturated lipids in the liquid crystalline phase (see *section 1.2.2*). It was suggested that lipid rafts may function as platforms in the fluid membrane for specific proteins to dock for trafficking or signaling purposes (Simons and Ikonen, 1997).

Figure 1.2. A lipid raft model in the cell membrane (Simons and Ikonen, 2000). Ordered lipids such as saturated lipids (pink) and cholesterol segregate to form rafts surrounded by a fluid phase containing unsaturated lipids (blue) in the cell membrane.

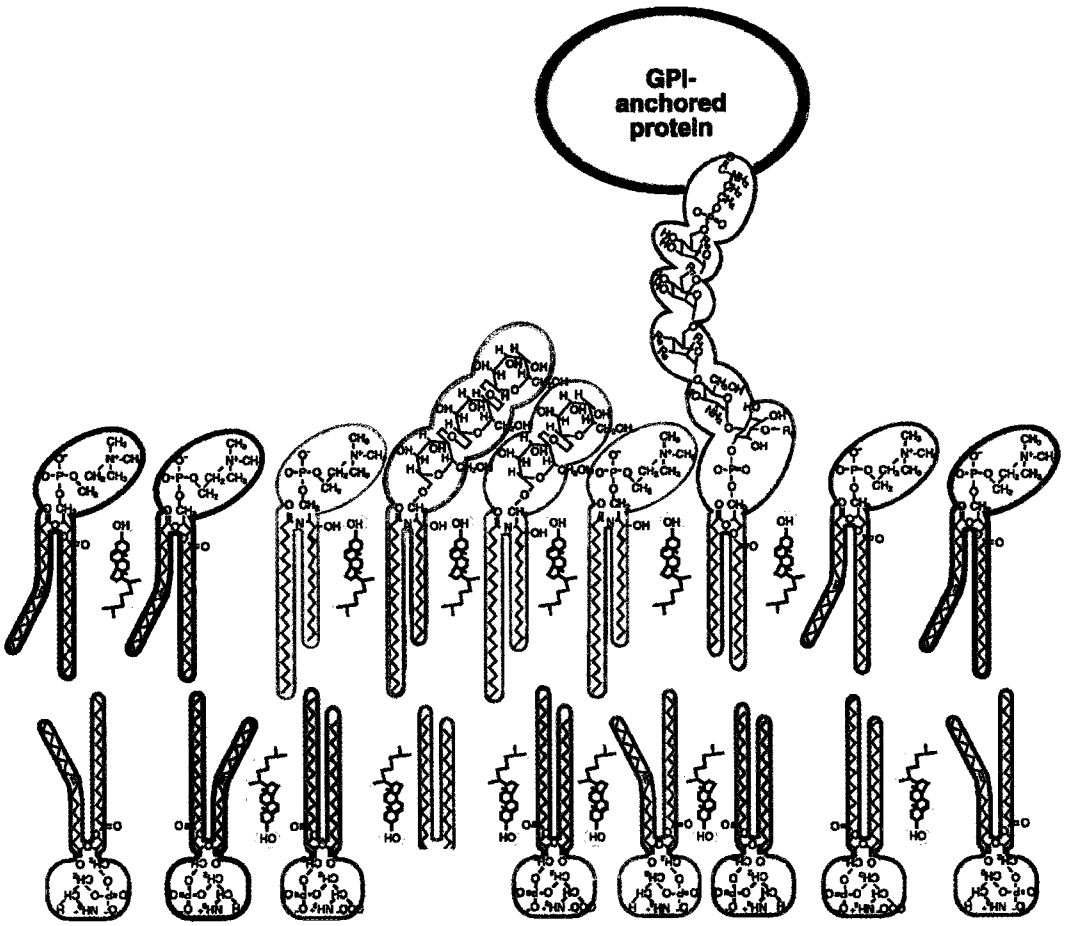
GPI-
anchored
protein
Src-
kinase

The hypothesis of lipid rafts originally came from studies of the plasma membrane of epithelial cells. These cells have a macroscopic organization dividing the cell into apical and basal-lateral regions that can be easily observed by optical microscopy. In the membrane of these epithelial cells, specific lipids and proteins segregate at the apical and basal-lateral membrane domains (Hansson et al., 1986; Lisanti et al., 1988; Salas et al., 1988; van Meer and Simons, 1986; Vega-Salas et al., 1988). For example, newly synthesized sphingolipid is preferentially transported to the apical membrane of the MDCK cells (van Meer et al., 1987), and glycosylphosphatidylinositol (GPI)-linked proteins are also found in the polarized apical region of epithelial cells (Brown and Rose, 1992; Lisanti et al., 1988).

Smaller organizations in the plasma membrane such as those flask-shape invaginations with diameters of 50 – 100 nm have also been identified by electron microscopy (Palade, 1953; Yamada, 1955a; Yamada, 1955b; Yamada, 1955c). These small invaginations contain the glycolipid GM1, which can bind and internalize cholera toxin via endocytosis (Montesano et al., 1982). These cave-like structures (or invaginations) in the membrane can be observed in many cells, and are currently known as caveolae. The unique structure of caveolae can be abolished/flattened when cholesterol is removed from the membrane (Rothberg et al., 1990), which suggests that the presence of cholesterol is important to maintain the structure of caveolae. In 1992, Rothberg and company identified a 22 kDa marker protein of caveolae called caveolin (Rothberg et al., 1992). It is now known that there are three members to the caveolin family namely caveolin-1, 2, and 3; these proteins are similar in structure and molecular weight (Parton, 1996). The caveolins play an important role in transporting cholesterol (Smart et al., 1996). Extracting detergent resistant

membranes (DRMs), via Triton X-100, from cells containing caveolae reveal that caveolins are in the DRMs (Sargiacomo et al., 1993) along with other membrane proteins such as GPI-linked proteins (Brown and Rose, 1992; Hooper and Turner, 1988; Sargiacomo et al., 1993), heteromeric G proteins and Src-family tyrosine kinases (Sargiacomo et al., 1993), and other integral membrane proteins such as the neuronal nAChR (Bruses et al., 2001; Marchand et al., 2002; Oshikawa et al., 2003). It should be noted that there are many other membrane proteins are not isolated in DRMs; these observations suggest that DRMs represent specific domains in the membrane (Brown and Rose, 1992; Sargiacomo et al., 1993). Lipid characterization of these extracted DRMs showed that they are enriched in cholesterol, sphingolipid and glycolipid (Brown and Rose, 1992; Simons and Ikonen, 1997). Such lipid composition is consistent with a liquid ordered state for the DRMs. These findings coincide with earlier studies showing that the protein caveolin and glycolipid GM1 mark the presence of caveolae in the cell; cholesterol is important to maintain the structure of caveolae; and sphingolipids are mainly found in the apical region of epithelial cells (where caveolae are mostly found). Therefore, this evidence indicates that caveolae are flask-shaped domains in the membrane that contain caveolins and are enriched in cholesterol, sphingolipid and glycolipid (GM1).

Interestingly, DRMs can be extracted from cells lacking caveolae such as lymphocytes ((Fra et al., 1994), neuroblastoma (Gorodinsky and Harris, 1995), Caco-2 cells (Mirre et al., 1996) and many other cells. The lipid compositions of these DRMs are remarkably similar to those of caveolae, typically enriched in cholesterol and saturated lipids, such as sphingolipid and the glycolipid GM1 (Fra et al., 1994; Gorodinsky and Harris, 1995). Again, such a lipid composition indicates the extracted DRM is in a liquid

ordered state. Additionally, there are many proteins found in the DRMs of these cells similar to those DRMs in the cells containing caveolae, and these proteins colocalize with GM1 in the cell membrane. These proteins include the GPI-anchored proteins (Fra et al., 1994; Gorodinsky and Harris, 1995; Mirre et al., 1996), Src-family tyrosine kinases (Gorodinsky and Harris, 1995), trimeric G proteins (Gorodinsky and Harris, 1995), and other integral proteins. Finally, there are many membrane proteins that are not found in the extracted DRMs and are not co-localized with GM1 in the cell membrane. These findings suggest that the extracted DRMs from these cells may represent some kind of domains in cellular membranes that are not caveolae.

The components in the extracted DRMs support the existence of lipid rafts other than caveolae in cellular membranes. However, the detergent extraction of a specific subset of membrane lipids does not provide direct information on the organization of small domains in a cell membrane, Thus DRMs cannot be equated directly to lipid rafts and we need to understand clearly the difference between lipid rafts and DRMs to avoid confusion. The DRMs are insoluble membranes extracted from cellular membranes via Triton X-100 (Brown and Rose, 1992; Fra et al., 1994; Gorodinsky and Harris, 1995; Hooper and Turner, 1988; Mirre et al., 1996; Sargiacomo et al., 1993), and they can be found in cells with or without caveolae. These detergent insoluble membranes are enriched in sphingolipid and cholesterol, and typically contain the marker glycolipid GM1. Since DRMs are extracted from the cell membrane with detergent at low temperature, it is possible that the cold temperature may induce the aggregation of cholesterol and saturated lipids along with other proteins during extraction. Hence, the extracted DRMs could be artifacts from the detergent

extraction procedure. Therefore, DRMs should not be concluded as lipid rafts, which are lipid domains in the cell membrane.

As the term lipid rafts has been used loosely in the past, a symposium on lipid rafts and cell function was summoned by biophysicists, biochemists, and cell biologists to discuss and define lipid rafts (Pike, 2006). A consensus definition of rafts by this group is: "Membrane rafts are small (10 – 200 nm), heterogenous, highly dynamic, sterol- and sphingolipid-enriched domains that compartmentalize cellular processes. Small rafts can sometimes be stabilized to form larger platforms through protein-protein and protein-lipid interactions" (Pike, 2006). This definition of rafts is specifically restricted to domains in cell membranes, not in model membrane, and of course not DRMs. The definition of rafts emphasizes that the formation of domains in cellular membranes is energetically driven by lipid interactions, and proteins and lipids can both contribute to the formation of domains in the membrane. In addition, rafts are not restricted to the plasma membrane of the cell. Rather, they encompass domains that may be found in the membrane of organelles such as mitochondrion and endoplasmic reticulum. The 200 nm upper limit to the size of rafts is meant to include the surface area of caveolae, which has been unanimously accepted as a subset of rafts in the cell membrane. However, this upper limit for the size of rafts poses a great challenge to identify them in the cell membrane via light microscopy because the optical resolution is limited to about 250 – 300 nm. For this reason, the use of fluorescence microscopy to study rafts in cellular membrane is limited by the resolution power of optical microscopy. Until now, caveolae is the best characterized example of a raft-like domain in cellular membranes.

1.2 Model membranes

It has now been accepted that the cell membrane has a complex and dynamic structural organization, which makes studying it as a whole very difficult. Therefore, we need to break down the cell membrane into its structural components and study them in a more simplified manner. This can be done by studying model membranes of well defined lipid or lipid-protein composition. We will first examine the properties of lipid alone membranes. We will then advance further to examine lipid-protein membranes to understand how lipid and protein interact with each other in a membrane, and the effect of their interaction.

1.2.1 The lipid bilayer

Lipids are amphipathic molecules, which have a polar head group and non-polar tail(s) (Figure 1.3). A lipid membrane is formed by the spontaneous arrangement of lipids in water into two continuous layers, also known as a bilayer (Figure 1.4). The non-polar tail(s) of lipids are driven by the hydrophobic effect to interact with each other and form a hydrophobic core, while the polar head groups interact with the surrounding water and shield the non-polar tail from the solvent. The establishment of the hydrophobic core gives the lipid bilayer the ability to function as a physical barrier against polar or charged molecules, whereas non-polar molecules can diffuse relatively easily through the bilayer.

The two main types of model membranes that have been studied extensively are liposomes and planar bilayers. A liposome is an enclosed lipid bilayer in the shape of a sphere that contains an aqueous core. Hence, a liposome is also known as a lipid vesicle. On the other hand, a planar bilayer is a flat and continuous lipid membrane, which typically sits on top of

Figure 1.3. The stick and space filling structures of some biologically relevant lipids. The lipids shown here are steroyl-sphingomyelin (C18-SM), dipalmitoyl-phosphatidylcholine (DPPC), palmitoyl-oleoyl-phosphatidylcholine (POPC), palmitoyl-oleoyl-phosphatidate (POPA), and cholesterol. All lipids have a polar head group (gold dashed-box) and non-polar tail(s) (gray dashed-box). The space filling structures highlight the potential of the acyl chains to rotate about the C – C bond of lipids. The lipid structures were obtained from Avanti Polar Lipids.

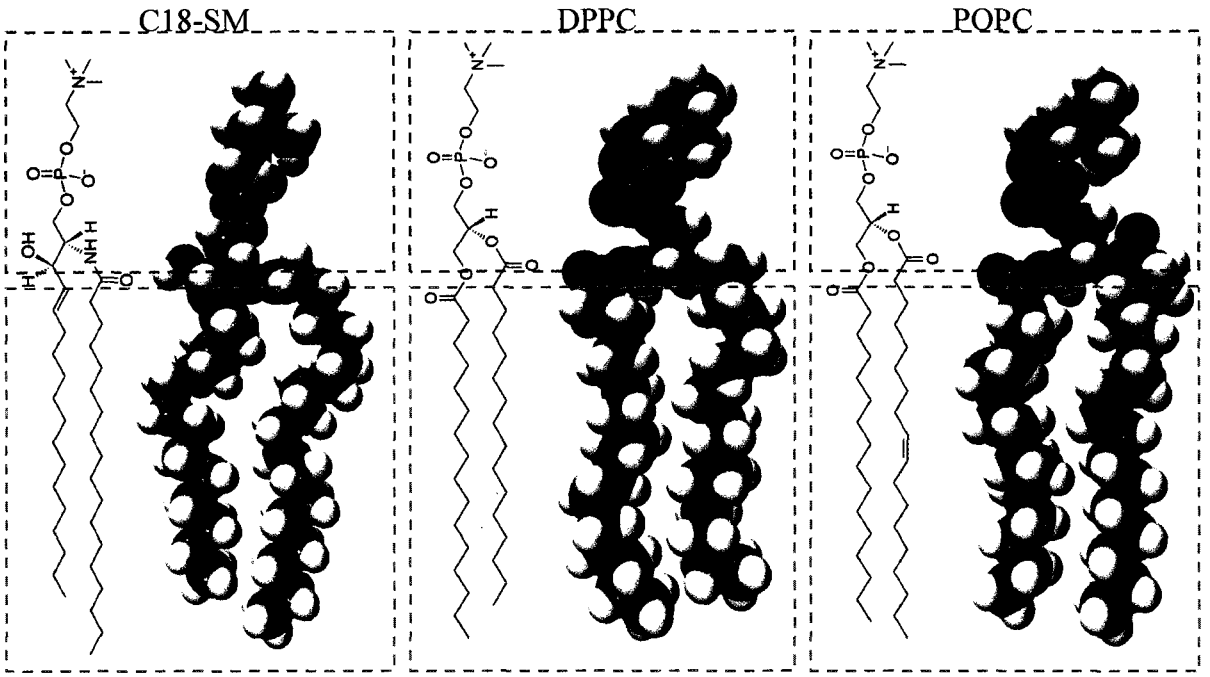
C18-SM
DPPC
POPC

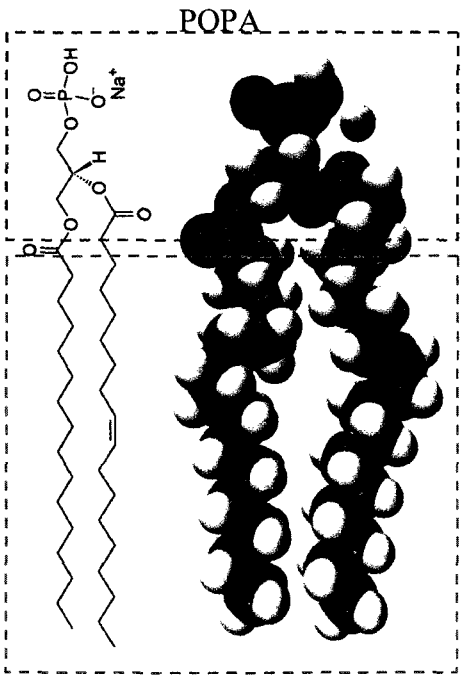
POPA

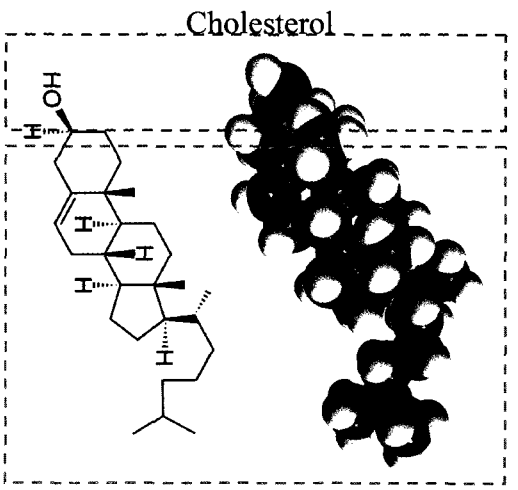
Cholesterol

Figure 1.4. Different models for a lipid bilayer. (A) A typical cartoon of a lipid bilayer. (B) Molecular dynamics simulations of a DPPC bilayer in the liquid disordered state (i.e., at 50°C) by (Feller et al., 1997). Atoms and atom groups are colored as follows: yellow, chain terminal methyl; gray, chain methylene; red, carbonyl and ester oxygen; brown, glycerol carbon; green, phosphate; pink, choline; dark blue, water oxygen; and light blue, water hydrogen.

A)

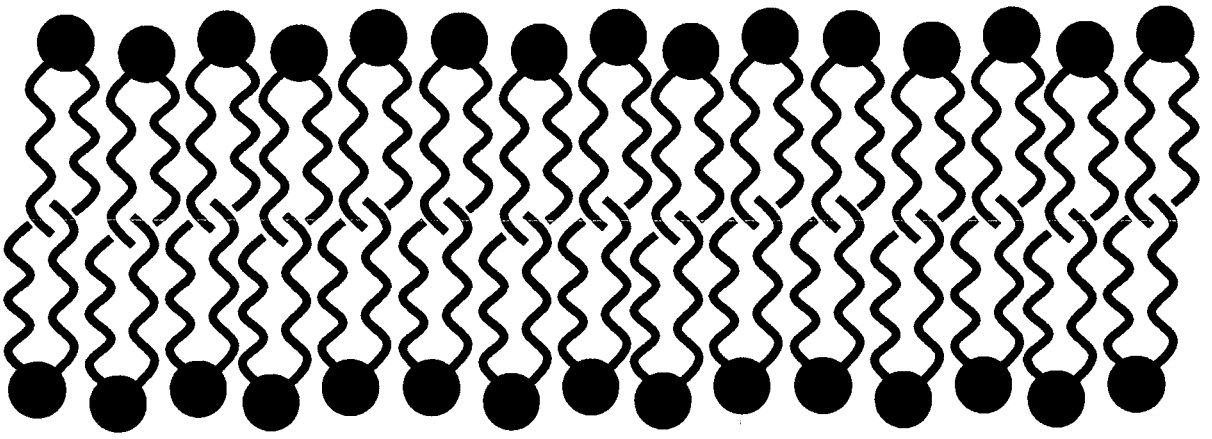

B)

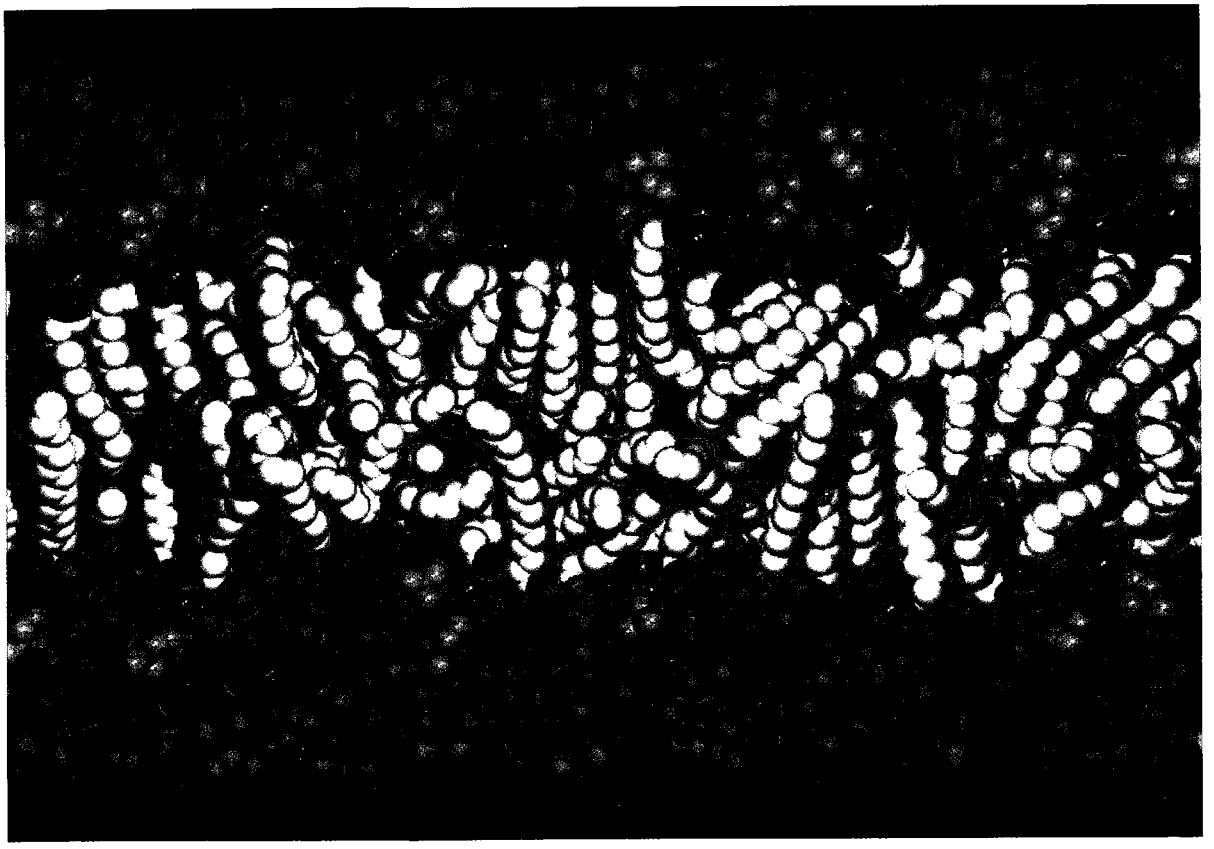

a solid support. Examining the properties of these bilayers has allowed us to understand some of the fundamental characteristics of cellular membranes.

The physical properties of a bilayer depend highly on its lipid composition. The lipid composition and the temperature of the environment dictate whether a bilayer will adopt the following phases: 1) liquid disordered (also known as liquid crystalline), 2) gel or 3) liquid ordered phase (Figure 1.5). These phases describe the order and mobility of lipid molecules in the lateral dimension of a bilayer.

1.2.2 The liquid disordered phase

In the liquid disordered phase (also known as liquid crystalline phase), the lipid molecules are highly disordered and mobile such that they can diffuse rapidly in the lateral dimension of the bilayer. A liquid disordered bilayer is typically formed from those lipids with unsaturated and/or short acyl chain(s). For example, both dilauroyl-phosphatidyl-choline and dioleoyl-phosphatidylcholine (DOPC) form a liquid disordered bilayer at physiological temperature. The high degree of disorder and mobility of lipids in the liquid disordered phase is due to the constant motion of the acyl chains, which includes the trans-gauche isomerization around the C – C bond (Yellin and Levin, 1977). The isomerization allows the acyl chains to curve and wiggle extensively (disorder) in the hydrophobic core of the bilayer (Figure 1.4) (Feller et al., 1997). Thus, the lipids pack very loosely in the liquid disordered phase, which creates lots of space for the lipids to diffuse rapidly in the lateral dimension of the bilayer; the liquid disordered phase is also known as the fluid phase. The lateral diffusion rate of lipids in the liquid disordered phase is around 10 $\mu m^2/s$ (Filippov et al., 2006). In contrast to cartoon figures that tend to depict the acyl chains being apart from each other (Figure 1.4A), interdigitation of the acyl chains in the bilayer is also possible

Figure 1.5. The three phases of a lipid bilayer: A) liquid disordered, B) gel and C) liquid ordered.

Liquid disordered

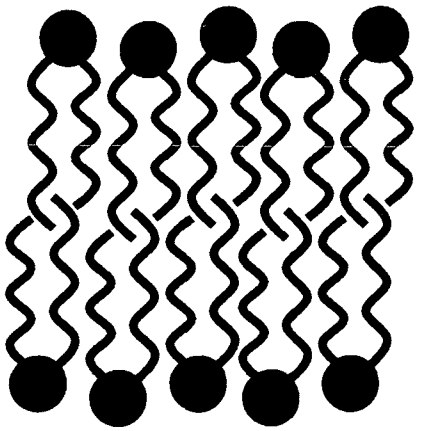

Gel

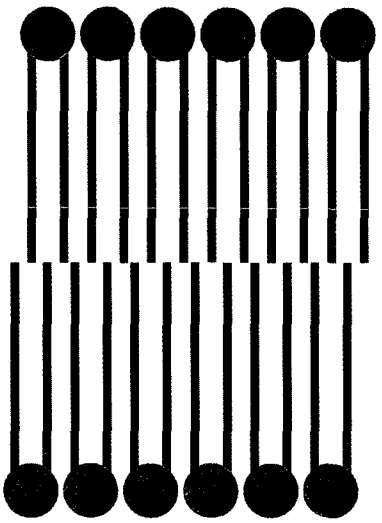

Liquid ordered

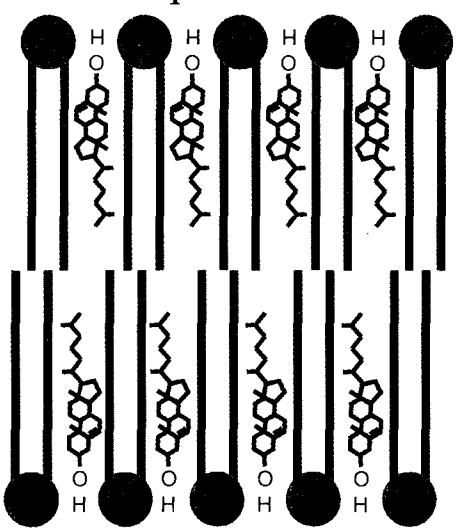

(Figure 1.4B). With the interdigitation and curvature of the acyl chains, the thickness of a bilayer in the liquid disordered state is typically shorter than expected for a bilayer with fully stretched acyl chains. The measured thickness of a bilayer composed of DOPC in the liquid disordered phase is about 4 nm (Leonenko et al., 2000; Tristram-Nagle et al., 1998). In addition, the liquid disordered phase has been reported to be relatively leaky to small charged or polar molecules (Paula et al., 1998; Paula et al., 1996; Xiang and Anderson, 1998). In summary, the lipids in the liquid disordered phase are highly mobile and disordered, which makes the bilayer relatively thin and leaky.

1.2.3 The gel phase

In contrast to the liquid disordered phase is the gel phase, where the lipid molecules are highly ordered and immobile such that their diffusion in the lateral dimension of the bilayer is highly restricted. Generally, those lipids with saturated and/or long acyl chains tend to form bilayers at room temperature in the gel phase. For example, a bilayer consisting of dipalmitoyl-phosphatidylcholine (DPPC) is in the gel phase at physiological temperature. In the gel phase, the acyl chains of lipid molecules in the bilayer are highly ordered, where the frequency of trans-gauche isomerization around the C – C bond in the acyl chains of the lipids is low. The acyl chains are fully stretched and the lipid molecules can be packed tightly against each other, which restricts the lateral diffusion of lipids in the bilayer (i.e., the lipids are less mobile than in the fluid phase). Fluorescence microscopy suggests that the lateral diffusion rate of lipids in the gel phase is about 1.5 $\mu m^2/s$ (Filippov et al., 2006); the diffusion rate in this case is about 7 times slower than the lipids in the liquid disordered phase. Additionally, since the acyl chains are nearly fully stretched, the thickness of a bilayer in the gel phase approaches its expected value. The thickness of a

DPPC bilayer in the gel phase is about 5 nm (Nagle et al., 1996). As the lipids are packed tightly in the gel phase and the hydrophobic core of the bilayer increases, the transverse diffusion of polar and charged molecules across the bilayer becomes much more challenging as compared to the liquid disordered phase. In brief, a bilayer in the gel phase is relatively impermeable to polar and charged molecules, where the constituent lipids in the bilayer are highly ordered and immobile.

1.2.4 The liquid ordered phase

The most physiologically relevant phase which a bilayer can adopt is the liquid ordered phase, which is typically formed by a mixture of lipid(s) and cholesterol. In a liquid ordered phase, the lipid molecules are relatively ordered but still can diffuse quickly in the lateral dimension of the bilayer. In this phase, the lipids are in an ordered state such that the frequency of trans-gauche isomerization around the C – C bond in the acyl chains is relatively low and the acyl chains are nearly fully stretched. The main difference between the gel and liquid ordered phase is the presence of cholesterol in the bilayer, which allows the lipid molecules to move easily. Cholesterol has a rigid and bulky steroid ring system that can intercalate between the acyl chains of other lipids, and prevents the tight packing of the ordered lipids in the bilayer. As a consequence, lipid molecules can diffuse readily in the lateral dimension of the bilayer while they still remain in an ordered state. The lateral diffusion of lipid in the liquid ordered phase is reportedly about 5 $\mu m^2/s$ (Filippov et al., 2006). Thus, the lipids in a liquid ordered phase are more ordered than the liquid disordered phase, while the mobility of the lipid approaches the liquid crystalline phase.

1.2.5 Phase transition temperature

As the lipid composition influences the phase adopted by a lipid bilayer, the temperature of the environment also exerts an equally important effect on the bilayer physical properties. For example, a bilayer in the gel phase is transformed into the liquid disordered phase by raising the temperature of the lipid environment, and vice versa. The temperature at which the bilayer undergoes the gel to liquid disordered phase transition is known as the melting temperature (Tm). Unsaturated lipids such as POPC have a low gel to liquid crystalline phase transition temperatures (Tm = -2°C, value obtained from Avanti Polar Lipids), and form liquid disordered bilayers at physiological temperature. On the other hand, saturated lipids such as DPPC have a high transition temperatures (Tm = 41°C, value obtained from Avanti Polar Lipids), and form bilayers in the gel phase at physiological temperature. The gel to liquid disordered phase transition of a lipid typically follows a sigmoidal curve with a sharp change in the curve at the Tm. However, if cholesterol is present in a bilayer, the transition becomes broader. This is because cholesterol prevents the tight packing of lipid in the gel phase, while its presence in a bilayer in the liquid disordered phase also restricts the diffusion of lipids (due to its bulky and rigid steroid ring). Importantly, whether cholesterol is present or not, all bilayers can be forced into a gel or liquid disordered phase by controlling the temperature of the environment.

1.2.6 Phase separated bilayers

When a bilayer is made from a mixture of both saturated and unsaturated lipids, the gel and liquid crystalline phases may co-exist in the same bilayer (Figure 1.6). This is caused by the differential packing ability of the lipids, with the saturated lipid segregating into domains when it is present in sufficient concentration (Jorgensen and Mouritsen, 1995;

Parasassi et al., 1990; Veatch and Keller, 2003). As a result, the properties of a bilayer can be predicted based on its lipid constituents.

Phase separation can also occur for mixtures of cholesterol, and saturated and unsaturated lipids. In this case, lipid domains in the liquid ordered phase may form when the concentration of cholesterol and saturated lipid are adequate (Ira and Johnston, 2008; Owicki and McConnell, 1980; Veatch and Keller, 2003). Such domains of saturated lipids and cholesterol surrounded by liquid disordered lipids in a bilayer resemble the description of lipid rafts in cellular membranes. For this reason model membranes with such ternary (or more) lipid mixtures have been extensively studied in attempts to elucidate the complex and dynamic organization of the cell membrane. In fact, the formation of domains in bilayers of some ternary lipid mixture can now be accurately predicted from their phase diagrams (Veatch and Keller, 2003).

1.3 The nicotinic acetylcholine receptor

While lipids are important to form the basic bilayer structure of a membrane, proteins are essential to membrane function since they are the machines in biological membranes that carry out many vital biological processes. In fact, ~30 % of the genome encodes for membrane proteins (Wallin and von Heijne, 1998). Therefore, understanding how these membrane proteins work in the lipid environment is essential. This study attempts to investigate the interaction between one integral membrane protein, the nicotinic acetylcholine receptor (nAChR), and its lipid environment. The nAChR is a ligand-gated cation-selective channel that is found in the central and peripheral nervous system. The nAChR is one of the main neurotransmitter-gated cationic channels that are responsible for

Figure 1.6. The co-existence of the lipid phases in a bilayer.

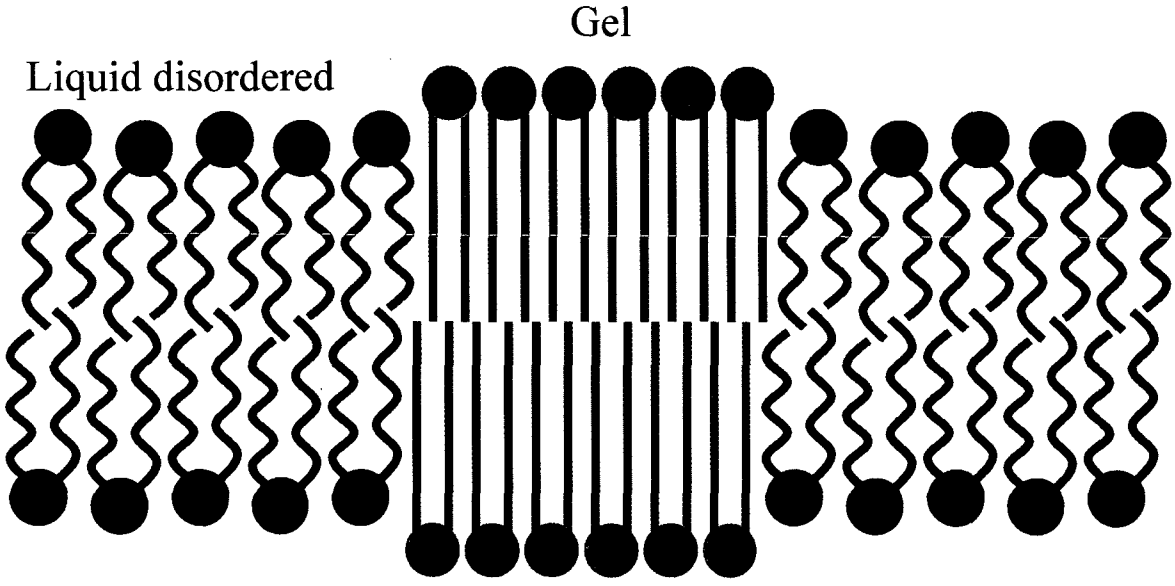
Gel
Liquid disordered

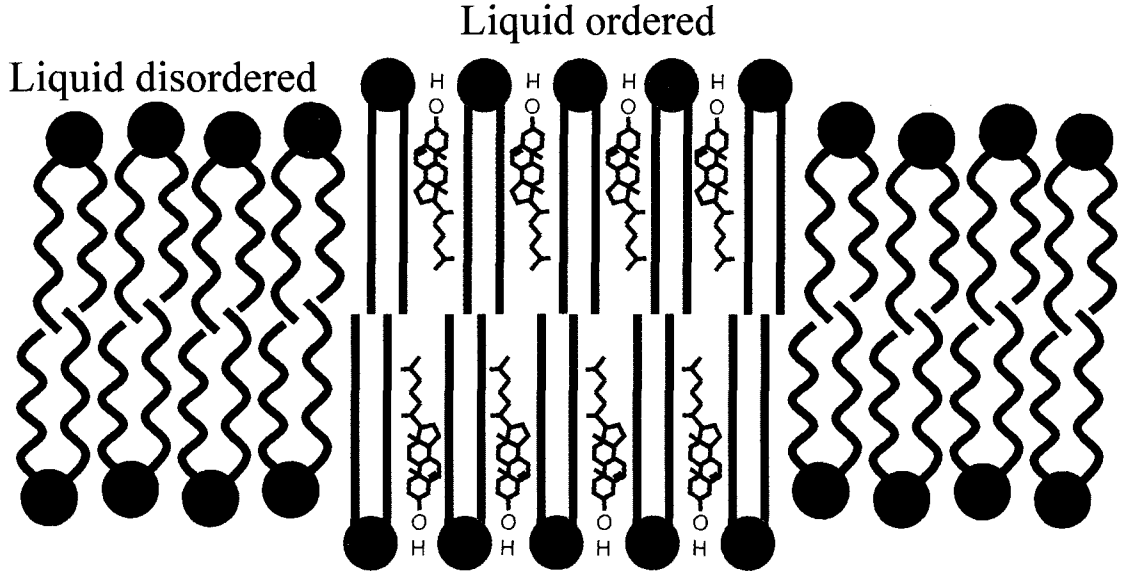
Liquid ordered
Liquid disordered

the transmission of signals from one cell to another. As an integral membrane protein, the nAChR is embedded in a lipid membrane, and the structure and function of the receptor have been suggested to be influenced by the membrane in which it is reconstituted (see below). Interestingly, it has also been suggested that the nAChR can increase the order of the bilayer in which it is reconstituted (daCosta et al., 2002). Maybe it is possible that the nAChR induces the segregation of lipids in the bilayer (i.e., the formation of domains). The ultimate goal of my project was to examine whether the nAChR induces the formation of domains in a bilayer by using atomic force microscopy.

1.3.1 The history of the nAChR

The study of the nAChR actually began in the mid 1800s when Claude Bernard started to investigate the action of the Central American arrow poison *curare*, which is now known to cause paralysis in muscle tissue. In Bernard's experiments, he observed that only the motor nerves become unresponsive to electrical stimulation in different animals treated with the poison, and concluded that *curare* acts mainly on the motor nerve as opposed to the muscle cell itself (Bernard, 1865).

Bernard's conclusion for the action of curare on the nervous tissue was widely accepted for half a decade until John Newport Langley demonstrated in the early 1900's that *curare* actually acts on muscle tissue as opposed to the motor nerve. Langley showed that nicotine stimulates contraction of denervated muscle tissue, and this muscle contraction could be inhibited by pretreating the tissue with *curare*. The inhibition by curare, however, could be overcome by electrical stimulation (Langley, 1907). Langley's observations unequivocally showed that *curare* did not inhibit muscle contraction when the tissue was stimulated electrically, but that the poison blocked the action of nicotine on the muscle

tissue. From his observations, Langley recognized that *curare* can interfere with the access of nicotine to muscle tissue. Langley's observations sparked him to theorize that there must be "receptive substances" for molecules in bodily tissues. His unorthodox theory at that time received many criticisms but subsequently became the foundation of modern pharmacology (Maehle, 2004). Furthermore, his studies also suggested that nerve and muscle cells communicate with each other via a chemical molecule. This theory was supported by the work of Sir Henry Hallet Dale who subsequently showed that acetylcholine is a predominant neurotransmitter in the peripheral nervous system (Dale and Dudley, 1929). Nevertheless, Langley's theory did not explain how the binding of a molecule causes changes inside the cell. It was not until the 1950's that Alan Hodgkin and Andrew Huxley explained the ionic mechanisms behind nerve conduction, and introduced the concept of ion channels (Hodgkin and Huxley, 1952a; Hodgkin and Huxley, 1952b; Hodgkin and Huxley, 1952c).

The picture of the nAChR started to form in the 1960's when Jacques Monod, Jeffries Wyman and Jean-Pierre Changeux postulated the allosteric protein model (Monod et al., 1965), which explains the change in protein conformation upon binding of a ligand. Changeux recognized that the allosteric protein model and ion channel concept could be combined to explain how the binding of acetylcholine to its "receptive substance" on the cell membrane causes an intracellular change. Importantly, Changeux managed to identify the nAChR in the *Torpedo* electric fish in 1970 (Changeux et al., 1970) and the nAChR was first isolated in the subsequent year (Miledi et al., 1971). Within a few years, several other groups were able to isolate and purify the nAChR from the electric organ of the *Torpedo* electric fish successfully, and the mystery behind the nAChR began to be solved.

1.3.2 The nAChR up to date

Over 30 years of characterizing the nAChR, many fascinating and fundamental details have been learned about ion channels and signal transmission in the central and peripheral nervous system. However, it would be beyond the scope of this thesis to describe all of the interesting features regarding the nAChR. Therefore, some of the general knowledge about nAChR will be reviewed first, and those details about the receptor that are relevant to the topic of this study will be discussed next.

The nAChR is a ligand-gated ion channel that is found throughout the central and peripheral nervous system. It can be found in many tissues including nerve and muscle. The receptor can be found on the post synaptic membrane of a neuro-muscular synaptic cleft (Figure 1.7). The nAChR is a neurotransmitter-gated ion channel that is responsible for the transmission of chemical signals from one cell to another. As an action potential arrives at the synaptic terminal, it triggers the release of the neural transmitter acetylcholine into the synaptic cleft. Acetylcholine then binds to the nAChR on the post synaptic membrane. The ion channel then gates open and allows the influx of cations into the cell, where the influx may trigger another action potential. Hence, an action potential arriving at the terminus of one cell can be communicated to another cell. Stimulation of the nAChR in muscle cell will lead to muscle contraction. Prolonged exposure to ligand leads to the desensitization of the nAChR, where the ion channel is closed even in the presence of the ligand. In essence, the nAChR can exist in at least three primary conformations: resting, open, and desensitized (Barrantes, 2002; Changeux et al., 1984; Unwin, 1993a; Unwin, 2003; Unwin et al., 1988).

Figure 1.7. A diagram of the synaptic cleft at a neuro-muscular junction.

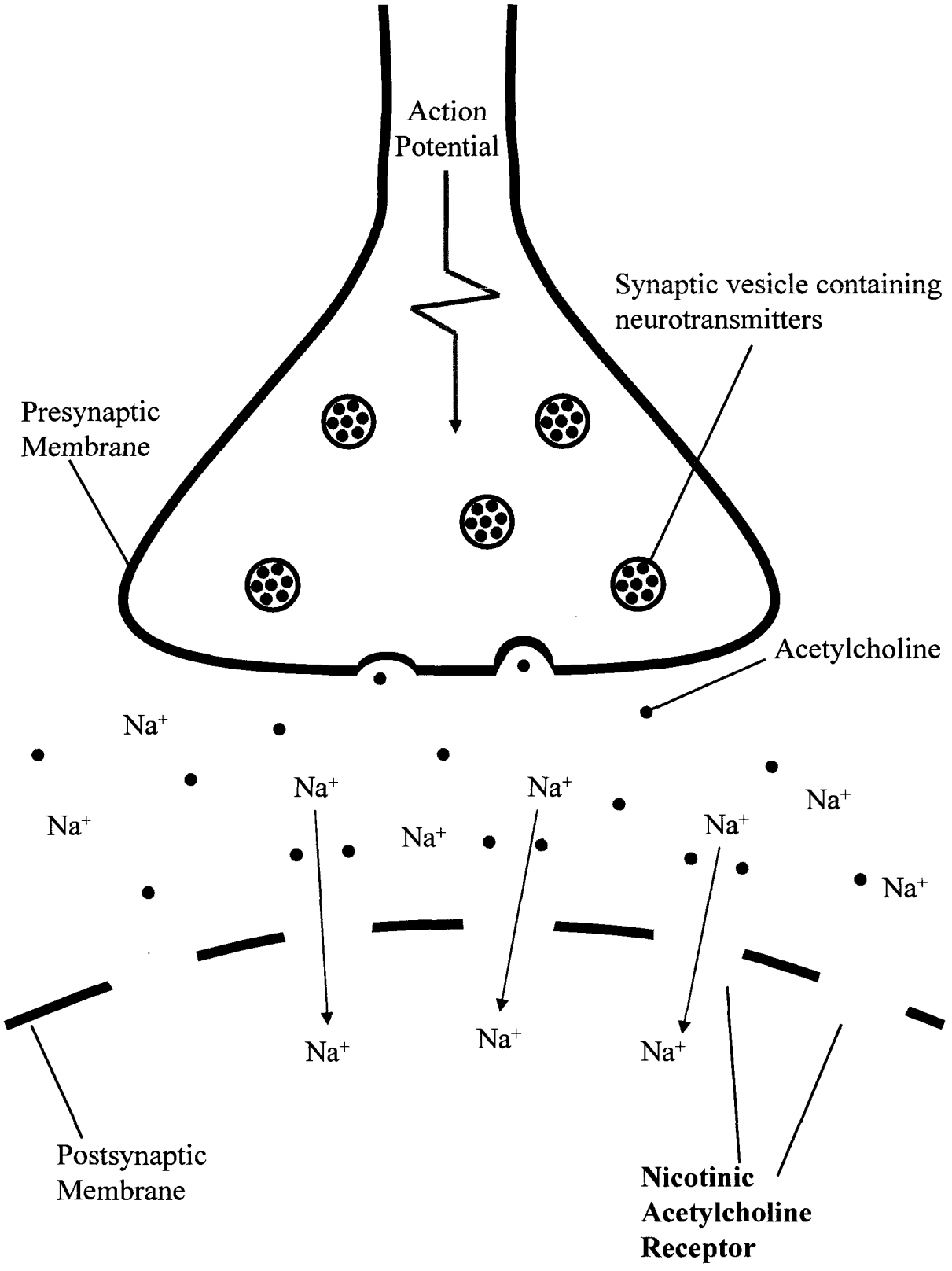
Action
Potential
Synaptic vesicle containing
neurotransmitters
Presynaptic
Membrane
Acetylcholine
Na+
Na+
Na+
Na+
Na+
Na+
Na+
Na+
Na+
Na+
Na+
Postsynaptic
Membrane
Nicotinic
Acetylcholine
Receptor

1.4 The structure of the nAChR

The architecture of a protein dictates how it functions. Understanding the molecular structure of a protein at atomic resolution can be achieved via X-ray crystallography. However, the difficulty in crystallizing membrane proteins, including the nAChR, has challenged researchers to develop alternative biochemical/biophysical methods to characterize the structure of a protein. These methods include mutagenesis, reconstitution, affinity labeling, hydropathy plots, electron spin resonance, cryo-electron microscopy, NMR, infrared spectroscopy and more.

The race to characterize the structure of the *Torpedo* nAChR began quickly after the receptor was discovered in the *Torpedo* electric fish. Early SDS-PAGE identified the nAChR as a multi-subunit protein composed of four different subunits, namely α, β, δ and γ (Weill et al., 1974). The stoichiometry of the whole functional protein, however, is 2α, 1β, 1δ and 1γ (Raftery et al., 1980). Through affinity labeling, it was demonstrated that the α subunits are responsible for ligand binding (Weill et al., 1974). Thus, a receptor binds two ligand molecules. Through peptide sequencing and cDNA screening, the subunits of the *Torpedo* nAChR were found to be homologous, and their peptide length varies from 437 (α) to 501 (δ) amino acids (Claudio et al., 1983; Noda et al., 1982; Noda et al., 1983a; Noda et al., 1983b; Raftery et al., 1980).

As the knowledge of the amino acid sequence of the subunits of the *Torpedo* nAChR became available, it paved the way for the structural characterization of the receptor. The nAChR actually belongs to a superfamily of the Cys-loop receptors because all members of this superfamily contain a pair of disulfide-bonded cysteines flanking thirteen highly

conserved amino acids in the ligand binding domain (see below) (Karlin, 2002). This eponymous Cys-linked loop plays a key role in channel gating. Some examples of other Cys-loop receptors include the glycine, serotonin ($5\text{-}HT_3$), and γ-aminobutyric acid ($GABA_A$) receptors, and neuronal nAChRs. These receptors are all pentameric, ligand-gated ion channels that share a homologous structure, although they have different ion channel selectivity.

The nAChRs can be broadly divided into 2 main types, namely muscle and neuronal. There are 2 known subtypes of muscle receptor, and they are embryonic and adult muscle nAChR. The human embryonic muscle nAChR and the receptor from the *Torpedo* electric fish are composed of $2\alpha_1$, $1\beta_1$, 1δ and 1γ subunits. Adult muscle receptor on the other hand consists of $2\alpha_1$, $1\beta_1$, 1δ and 1ε subunits. The muscle receptors are typically found on the postsynaptic membrane of the neuromuscular junction. Activation of the muscle nAChR can lead to the contraction of muscle cell, and ultimately the physical movement of an organism.

Neuronal nAChRs, on the other hand, have many different subtypes. This is because a neuronal receptor can be assembled from a large pool of homologous α and β subunits. There are 9 α (α_{2-10}) and 3 β (β_{2-4}) subunits from which a neuronal receptor can be assembled. Unlike muscle receptors, which are strictly heteromeric, neuronal nAChRs can be either heteromeric or homomeric. When it is a homomeric protein, the receptor is typically assembled from five α subunits (e.g., α_7, α_8, and α_9) (Anand et al., 1991; Cooper et al., 1991; Elgoyhen et al., 1994; Gotti et al., 1994). Heteromeric receptors are typically assembled from a combination of α and β subunits. When adding different combinations of subunits together to make a pentameric protein, we can get a large number of different

neuronal receptors. Interestingly, neuronal nAChRs can be found on either pre or postsynaptic membranes depending on the subunit composition. All in all, neuronal nAChRs are among the important neurotransmitter-gated cationic channels that are responsible for the propagation of chemical signals/electrical impulses in the central nervous system.

Given its vital role in the central and peripheral nervous system, examining those factors that can influence the molecular behaviour of the nAChR is of pharmacological interest. Inevitably, we need to have a good understanding of the basic structure of the nAChR, and then we will examine how other molecules can affect the structure and function of the protein. Since the *Torpedo* nAChR is the subject of this study, its structure will be reviewed closely.

1.4.1 The early model structure of the nAChR

The first reasonably accurate overall structure of the nAChR was formulated by Unwin in 1993, based on a 9Å resolution cryo-electron microscopy image (Unwin, 1993b) and accumulated biophysical/biochemical data. This model suggested that the receptor is composed of five subunits (2α, 1β, 1δ, and 1γ) arranged in a pseudo-symmetric manner about the central ion channel (Figure 1.8). Hydropathy plots suggest each subunit has three domains, namely the extracellular, transmembrane, and cytoplasmic domain. The extracellular domain consists of ~210 N-terminal amino acids, the M2–M3 loop and a small segment of C-terminal peptide. Since the extracellular domain is responsible for the binding of ligand, it is also known as the ligand binding domain (Changeux, 1993). It is the α subunit that is primarily responsible for the binding of ligand, but it is now known that the binding occurs at the interfaces between the α-γ and α-δ subunits (Blount and Merlie, 1989)

Figure 1.8. The first overall structure of the nAChR. The nAChR is approximately 300 kDa. It is composed of five subunits (2α, 1β, 1δ, and 1γ) arranged in a pseudosymmetric manner about the central opening. Each subunit has three domains namely the extracellular, transmembrane, and cytoplasmic domain. The transmembrane domain composed of 4 transmembrane α-helix (M1-4), where the M2 lines the pore of the channel. The extracellular domains of the two α subunits are responsible for the binding of ligands. The cytoplasmic domain can be linked to the cytoskeleton.

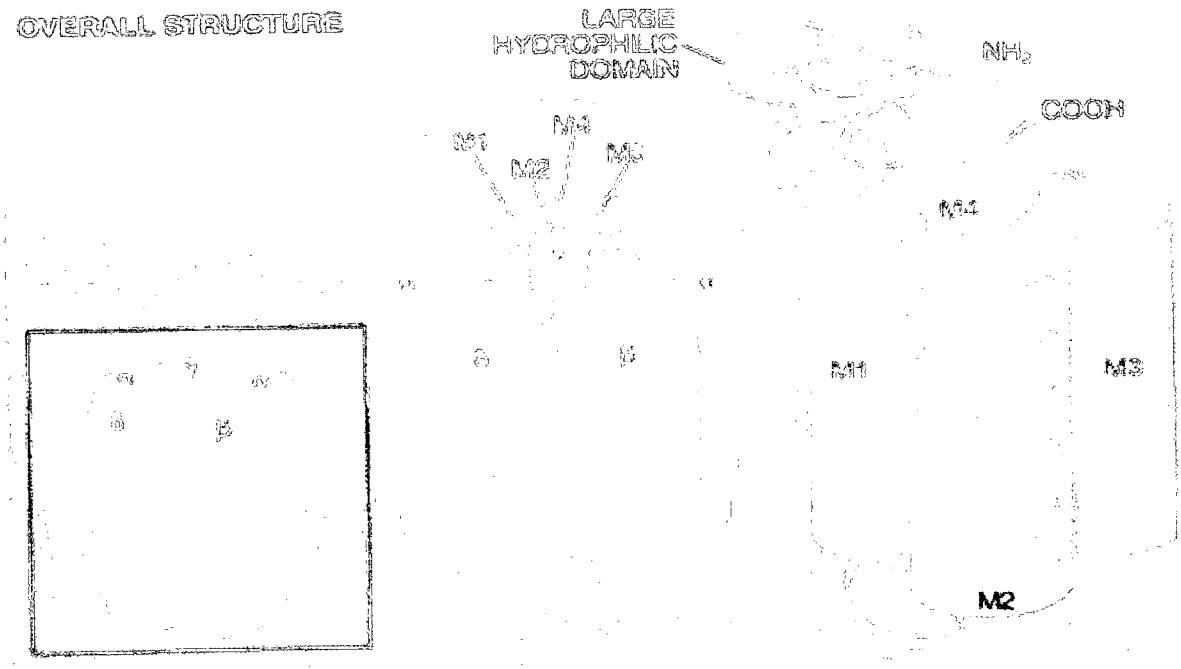

(Changeux 1993. *Scientific American)*

(Pedersen and Cohen, 1990). The transmembrane domain consists of 4 α-helices namely M1, M2, M3 and M4. It is the M2 that lines the pore of the ion channel, which selects for cations only but has no specificity for specific cations. The intracellular domain is made from a short loop connecting the M1 and M2 (M1–M2 loop) and a long loop that connects M3 and M4 (M3–M4 loop).

1.4.2 The crystal structure of the acetylcholine binding protein

Our understanding of the nAChR structure/function took a giant step forward when the crystal structure of the acetylcholine binding protein (AChBP) was solved at 2.7 Å resolution (Brejc et al., 2001). Such resolution allows an atomic structure of the protein to be deduced. The AChBP has an overall dimension of 62 Å tall and 80 Å wide, which is roughly the dimension of the ligand binding domain of the nAChR (Figure 1.9). The AChBP is a soluble homopentameric protein that can bind agonists and antagonists of the nAChR, including acetylcholine, nicotine, α-bungarotoxin, and (+)-tubocurarine (Karlin, 2002). Each subunit of the AChBP is 210 amino acids long, and it is about 20 – 24 % identical to the 210 N-terminal amino acids of the ligand binding domain of the nAChR's subunits. Moreover, those residues directly involved in acetylcholine binding in the AChBP are conserved in the nAChRs. For these reasons, the AChBP is thought to be a homologous protein to the N-terminal domain of the nAChR, so that the high resolution structure of the AChBP (Figure 1.9) can be used to model the ligand binding domain of the nAChR.

1.4.3 The structure of the nAChR approaching the atomic resolution

More recently, the structure of the *Torpedo* nAChR in the resting state has been refined by cryo-electron microscopy to 4Å resolution (Unwin, 2005). The peptide backbone

Figure 1.9. The crystal structure of the acetylcholine binding protein (AChBP) was solved at 2.7 Å resolution (Brejc et al., 2001). Panel (a) is the top view of the AChBP showing the interactions among the subunits (Subunit A is yellow, B is blue, C is red, D is green, and E is magenta). Panel (b) is the side view of the protein that shows the ligand binding site between subunit A (yellow) and B (blue). Panel (c) shows individual loops, beta sheet and a helix in a subunit of the homopentamer protein.

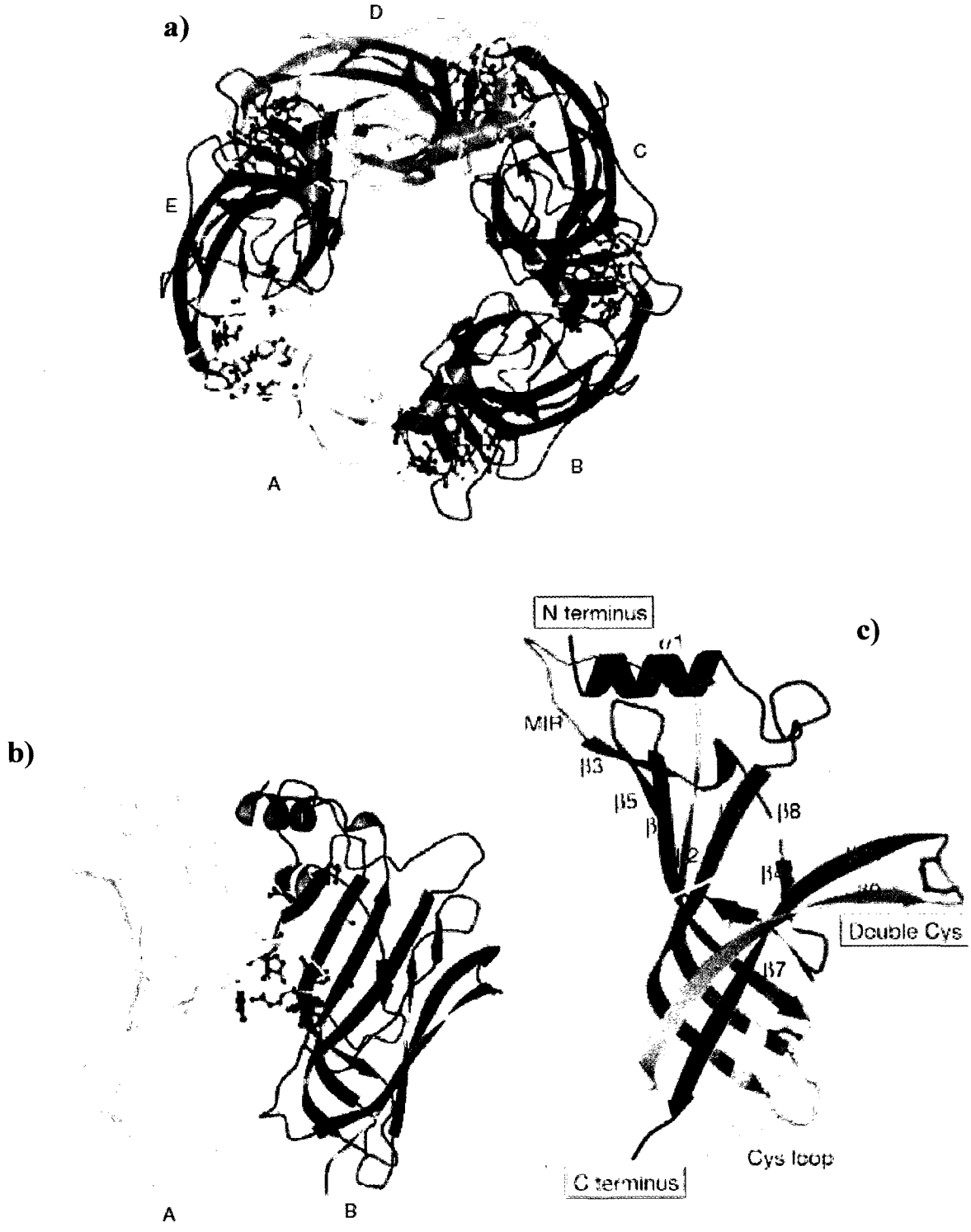
a)
D
C
E
A
B
b)
A
B
c)
N terminus
MIH
β3
β5
β8
Double Cys
β7
Cys loop
C terminus

of the nAChR can be observed fairly clearly in the electron density image with this resolution, but the position of most side chains can not be accurately determined. For this reason the nAChR structure required careful interpretation from this modest resolution image. Fortunately, there exist the crystal structure of the homologous AChBP, a collection of biochemical data over 30 years, and a 9 Å resolution structure in the open state to aid the structure determination of the nAChR. By using his refined electron density image of the nAChR at 4Å resolution in conjunction with other available data, Unwin proposed a new atomic model structure of the receptor.

Consistent with his earlier model, Unwin's atomic model shows that the nAChR is composed of five elongated subunits arranged in a pseudo-symmetric manner around a central ion channel (Figure 1.10). Each subunit has three distinct domains namely the extracellular ligand binding domain, the α-helical transmembrane domain, and the cytoplasmic domain (Figure 1.10). The ligand binding domain is constituted of the first 210 N-terminal amino acids, which is the size of a protomer of the AChBP. The N-terminal peptide folds into a ten strand β-sandwich with a short α-helix packed on top. The C-terminal end of the ligand binding domain leads directly into the first of the four α-helices (M1, M2, M3 and M4) of the transmembrane domain. It is the transmembrane domain that constitutes the ion channel of the receptor, where the M2 lines the pore of the channel. The cytoplasmic domain consists of a short M1–M2 loop and a long M3–M4 loop (roughly 60 to 100 amino acids depending on the subunit). Due to the incomplete electron density in the image, the cytoplasmic domain has not been completely modeled. However, an α-helix (MA) can be observed from the electron density, and this α-helix may be responsible for the interaction of the receptor with the cytoskeleton. Overall, each subunit of the nAChR makes

Figure 1.10. The crystal structure of the nAChR at 4 Å resolution determined by cryo-electron microscopy (Unwin 2005). The top image is the top view of the nAChR (from the extracellular side) showing the organization of the heteropentameric protein, where subunit α is red, β is green, δ is cyan, and γ is blue). The bottom image is the side view of the nAChR by rotating the top image 90 °, where the interaction between the γ subunit and an α subunit can be observed at the front. The bottom image shows the orientation of the cytoplasmic, transmembrane and extracellular domain of the receptor. The extracellular and intracellular side of the membrane is indicated by the letter E and I, respectively. The main immunogenic regions (MIR) of the nAChR is also showed in the figure.

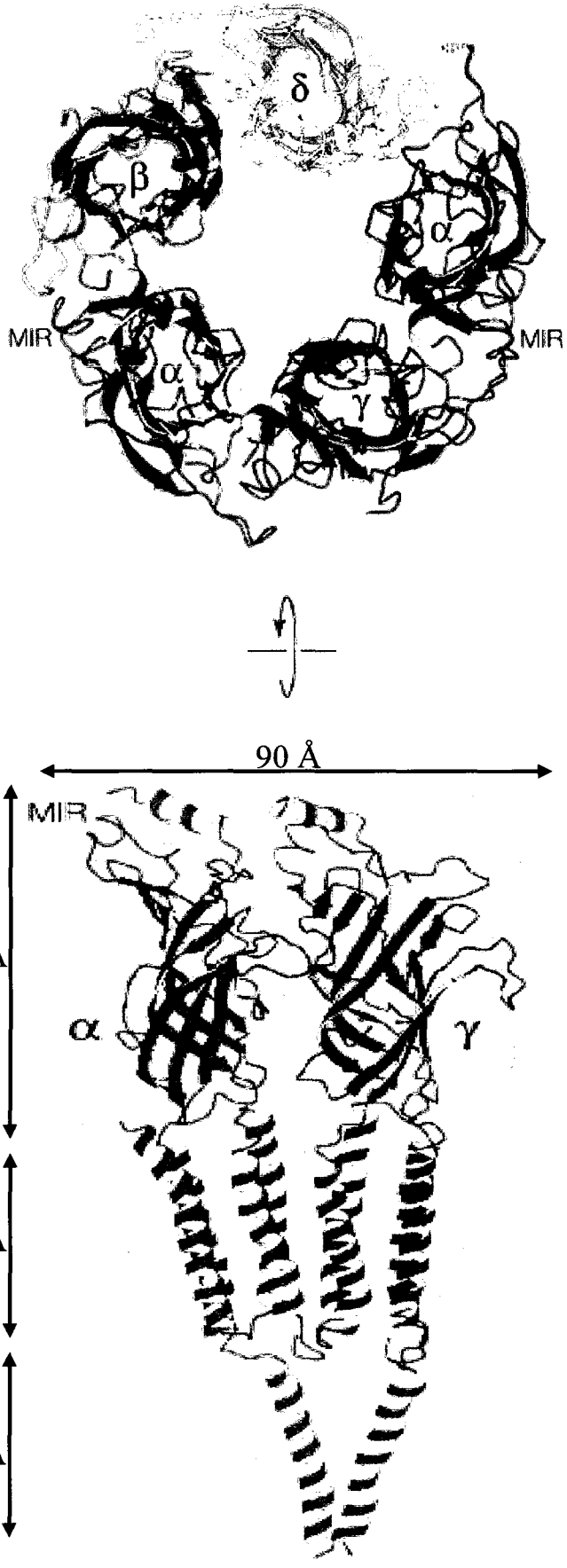
δ
β
α
MIR
MIR
α
γ
90 Å
MIR
70 Å
α
γ
40 Å
40 Å

extensive contacts with its neighbouring subunits throughout the three domains to form a ligand gated ion channel that has a maximum length of 150 Å and width of 90 Å.

1.4.4 The ligand binding domain

Since Unwin's cryo-electron microscopy image of nAChR is at a modest resolution that is not high enough to reveal the exact location of the amino acids in the protein, he modeled the ligand binding domain of the nAChR after the atomic resolution structure of the AChBP. Unwin assumed that these two should share the same overall architecture because they have very similar overall dimensions, amino acid length, sequence homology (20–24 % identical), and agonist and antagonist binding properties. In addition, the AChBP structure confirms over 30 years of mutagenesis and chemical labeling studies which have identified the important residues for the binding of ligands on the nAChR. Based on the information above, Unwin fitted his modest resolution structure of the ligand binding domain of the nAChR to that of the AChBP to estimate an atomic resolution structure of the ligand binding domain.

Unwin's model illustrates the ligand binding domain of each subunit that is composed of a twisted ten strand β-sandwich and an α-helix (α1) at the N-terminal (Figure 1.10). The β-strands twist around each other to form an inner (β1–6 and 8) and outer (β7, 9 and 10) sheet, where the sheets are held together by hydrophobic effect. The interfaces between any two subunits are also hydrophobic which helps to hold the pentamer together. In between the β-strands are connecting loops of variable length, where some of these loops have important function for the binding of ligand and the coupling between ligand binding and gating of the ion pore.

Affinity labeling experiments using various competitive antagonists and agonists showed that the binding of ligand occurs at the interfaces between the α-γ and α-δ subunit (Dennis et al., 1988; Langenbuch-Cachat et al., 1988; Middleton and Cohen, 1991; Oswald and Changeux, 1982; Pedersen and Cohen, 1990). Since chemical labeling studies have demonstrated that the α subunit is more strongly labeled, it is referred to as the principal binding subunit, whereas the γ and δ are called the complementary subunits (Corringer et al., 2000). It was found that most residues involved in the binding of ligand are aromatic. The most notable residues on the α subunits are W86, W149, Y151, Y190, and Y198. These residues are thought to stabilize the ligand through a cation-π interaction mechanism, where the quaternary ammonium portion of the ligand (e.g., acetylcholine) is stabilized by the π electron of the aromatic residues. Other residues in and around the binding site on the δ and γ subunit such as the δW57, δR113, δD1 65, δD180, and δE183, and γW55 and γY111 have also been identified as important for the binding of ligand. The binding of the ligand in the nAChR is very similar to that in the AChBP, which occurs through the long extended C loop of the α subunit. It is hypothesized that the closing of the C loop upon the binding of the ligands would cause the inner and outer β-sheets to rotate which leads to downstream movements in the nAChR that ultimately couples the binding of ligand to the opening of the pore of the ion channel.

Although the subunits make extensive contact with each other, there are gaps or vestibules between subunits in the extracellular and cytoplasmic domains. The wall of these vestibules is lined with negatively charged residues that can effectively repel anions. The diameter of these vestibules is about 20 Å, which is large enough for hydrated cation to enter. As these vestibules partly provide selection for cations, they also raise the local

concentration of cation to increase the efficiency of ion conduction following ligand binding. In particular, the αAsp238, αGlu251 and αGlu262 residues surrounding the entrance of the ion channel are important for cation conduction.

1.4.5 The ion channel of the nAChR

In agreement with his earlier model, Unwin's atomic model shows that the ion channel of the nAChR is composed of the helical transmembrane domain. The transmembrane domain of each subunit consists of 4 α-helices namely M1, M2, M3 and M4. The helices are 20 – 25 amino acids long, which allow them to span the length of the membrane (~40 Å) and extend beyond the membrane surface by about 10Å into the extracellular side. Since the nAChR is a pentameric protein, the ion channel of the receptor is composed of 5 groups of 4 helices. These helices assembled into a near perfect five-fold symmetry, and are arranged into 2 rings of helices designated as the inner and outer ring. The inner ring consists of the M2 of all five subunits which lines the pore of the ion channel, whereas the remaining helices (M1, M3, and M4) form the outer ring that shields the M2 from the surrounding lipid in the membrane. The M4 is the most lipid-exposed helix, and it may be important for the interaction with the surrounding lipids (Figure 1.10).

The five M2 helices tilt inward toward the central axis of the channel to form an ion conducting pore. M1, M3 and M4 of the five subunits also tilt radially toward the central axis of the pore, but they do not make extensive contact with M2. The five M2 helices cross the membrane perfectly in register such that amino acids with similar properties can be aligned as hydrophobic and hydrophilic rings. The rings at the extracellular and cytoplasmic opening of the pore consist of negatively charged amino acids (e.g., αE262 and αE241, respectively). These negatively charged residues only favor the entry of cation in the pore,

and thus exclude anions. The rest of the pore is mainly hydrophobic, and it is not favorable to interact with ions. It was once thought that the highly conserved leucine ring at αLeu251 forms a hydrophobic girdle that gates the conduction of ions (Unwin, 1993b). However, the hydrophobic girdle has now been extended to residues from between αLeu251 and αVal259 (Miyazawa et al., 2003). The hydrophobic girdle is located at the centre of the membrane, where the pore is maximally constricted with the narrowest diameter of approximately 7Å, which is small enough to prevent the passage of a hydrated sodium or potassium (~8Å). Since the wall of the pore is mainly hydrophobic, it would be energetically unfavorable for an ion to shred its hydration shell to pass through the ion channel. Thus, ions can not pass through the pore while the nAChR is in the closed conformation. The gating mechanism is more likely an energetic barrier rather than a physical barrier. Unwin structure confirms that the closed ion pore is hollow and continuous such that there no peptide blocks the pore. In short, the gating mechanism is an energetic barrier, and the binding of a ligand would somehow have to widen the pore to allow hydrated cations to flux through the nAChR.

The defining feature of a ligand gated ion channel such as the nAChR is its ability to couple the binding of a ligand to the opening of the ion pore. The M2–M3 linker of the transmembrane domain has been reported to be the gating element of the nAChR (Campos-Caro et al., 1996; Grosman et al., 2000; Lee and Sine, 2005; Rovira et al., 1998; Rovira et al., 1999). Unwin's model shows the M2–M3 linker is in close proximity to the Cys loop (resting) and A loop (desensitized) of the ligand binding domain (Figure 1.11). It is suggested that the binding of the ligands at the α subunits causes the C loop to close onto the ligands which results in the rotational movement between the inner and outer β-sheets.

Figure 1.11. The α subunit of the Torpedo nAChR at 4 Å resolution determined by cryo-electron microscopy (Unwin 2005). (A) and (B) are two different side views of the subunit to show the coordination of different loops (grey), β-sheets (β4, β7, β9, β10 outer sheets are red and β1, β2, β3, β6, β8 inner sheets are blue), and α-helices (yellow). The main immunogenic regions (MIR) of the nAChR is also showed in the figure.

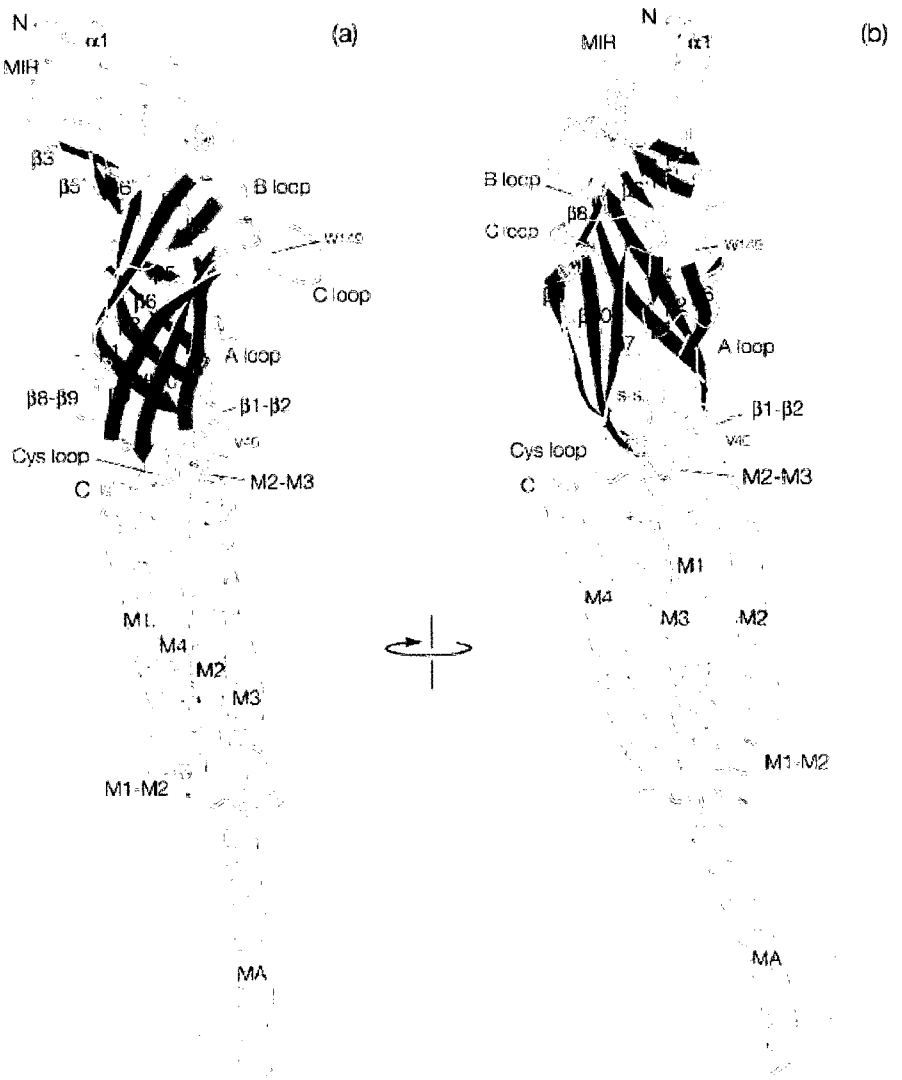
N
α1
(a)
MIR
β3
β5
B loop
C loop
A loop
β8-β9
β1-β2
Cys loop
M2-M3
M1
M4
M2
M3
M1-M2
MA
N
(b)
MIR
α1
B loop
C loop
A loop
β1-β2
Cys loop
M2-M3
M1
M4
M3
M2
M1-M2
MA

Such movement of the β-sheets alters the physical contact between the M2–M3 linker and A & Cys loop. Consequently, the M2 helices undergo a clockwise rotation and collapse back against the M1, M3 and M4 helices, and the ion pore is opened wider to allow hydrated ions to flux through the channel. Clearly, the gating of the nAChR is highly orchestrated, and there must be a tight coupling between the ligand binding domain and the ion channel to maintain the gating function of the receptor. Interestingly, there are data suggesting the structure and function of the nAChR can be altered by the lipid environment in which it is embedded (see below).

1.5 The interaction between the nAChR and its lipid environment

As an integral membrane protein, the nAChR is embedded in a complex and dynamic sea of lipids and proteins, and its structure and function can undoubtedly be influenced by the surrounding lipids and proteins. Given its vital role in the central and peripheral nervous system, examining those factors that can influence the behaviour of the nAChR at the molecular level is of fundamental interest. However, characterizing the structure and function of the receptor in the cell membrane can be very difficult due to the presence of other molecules. One approach we could use is isolating the receptor from its native membrane and studying it in a well defined environment; this can be achieved by reconstituting the nAChR in a well defined lipid bilayer.

A reconstitution procedure involves the removal of the nAChR from its native membrane with a detergent. The isolated receptor can then be integrated into a defined lipid bilayer of interest to examine its behaviour. While the concept of reconstitution is simple to grasp, the procedure involved is rather complicated. Early attempts showed that it is very

difficult to reconstitute a "functional" receptor into a lipid bilayer (Briley and Changeux, 1977; Briley and Changeux, 1978; Hazelbauer and Changeux, 1974; Michaelson and Raftery, 1974). First of all, only a few detergents can be used to remove the nAChR from its native membrane and retain its ability to bind ligand(s). Secondly, those detergents that can maintain the ligand binding ability of the receptor do not always guarantee that the nAChR will retain the ability to flux ions. These problems in the early days clearly reflect the lack of knowledge of the parameters required to achieve successful reconstitution of a functional nAChR that can bind ligands and flux ions.

The first reliable protocol to reconstitute a functional nAChR into a bilayer was not developed until the late 1970's by Epstein and Racker. They found that one of the most important factors to maintain the function of the nAChR is to keep the receptor constantly in contact with lipids throughout the purification procedure (Epstein and Racker, 1978). The detergent-lipid-protein complex will form a reconstituted bilayer as the detergent is removed via dialysis. In their work, the lipid used was asolectin (a mixture of phospholipids from soybean) and the detergent used was cholic acid, which became the most common detergent used in many reconstitution studies of the nAChR.

Interestingly, the receptor was not functional when phosphatidylcholine (PC) was used for the reconstitution of the nAChR (Criado et al., 1984; daCosta et al., 2002; Fong and McNamee, 1986; Ryan et al., 1996). In these circumstances the receptor can still bind ligand but cannot undergo the necessary conformational changes to flux ions, a state which resembles the desensitized conformation of the nAChR. Thus, the ligand binding domain and the ion channel were somehow uncoupled when the receptor was reconstituted with PC.

What exactly happened to the receptor remains unclear, but it is clear that the nAChR requires at least another lipid in a PC bilayer to maintain its structure and function.

The discovery that the lipid environment is important for the reconstitution of the nAChR sparked an interest in finding the specific lipids that are important to support a functional receptor. Since the nAChR is fully functional in its native membrane or when it is reconstituted with asolectin, examining the lipid composition of these two membranes may provide some insight. The work of several groups showed that the native membrane contains approximately 30% cholesterol (Chol) and most of the remaining lipids are phospholipids, which include about 30% phosphatidylcholine (PC), 25% phosphatidylethanolamine (PE), 9% phosphatidylserine (PS), 1% phosphatidylinositol (PI), <5% sphingomyelin (SM), <7% phosphatidic acid (PA), and 1% other lipids (Gonzalez-Ros et al., 1982; Popot et al., 1978; Schiebler and Hucho, 1978). On the other hand, asolectin consists of a mixture of phospholipids including 24% PC, 39% PE, 19% PS, 6% PA, 1% PI, 9% lyso-lipid derivatives, and 2% other phospholipids (Demel et al., 1991). Evidently, the lipid content is fairly different between asolectin and the nAChR native membrane. Interestingly, both seem to contain a relatively high level of anionic lipid (e.g., PA, PI, and PS), and the native nAChR membrane has a significant level of cholesterol.

Early reconstitution studies attempted to investigate the lipid requirements to support a functional nAChR by attempting to reconstitute it into vesicles with a defined lipid mixture and examine the receptor's ability to flux radiolabeled cation. At first, there were controversies as to which lipid mixture is required to support a functional receptor. There were reports claiming that cholesterol is absolutely required in a PC bilayer (Criado et al., 1984; Dalziel et al., 1980; Fong and McNamee, 1986), while others suggested that anionic

lipids in a PC bilayer are sufficient (daCosta et al., 2002; Ochoa et al., 1983; Ryan et al., 1996; Sunshine and McNamee, 1992). The differences in these reports are likely due to the inherent artifacts in the ion flux measurements in the reconstituted vesicles, since it has been shown that the size and permeability of a vesicle depends on its composition (Anholt et al., 1982). However, most of the studies referred to above agreed that a PC bilayer containing a neutral lipid (i.e., Chol) and anionic lipids (e.g., PA, PS and PG) can support a functional nAChR.

Some recent studies have shown that mixtures of PC/PA are particularly good at stabilizing the nAChR in a functional state. For example, it was demonstrated that a lipid mixture containing PC and PA can support a receptor that has similar radiolabeling pattern as a mixture containing PC/PA/Chol and the native membrane (daCosta et al., 2002; McCarthy and Moore, 1992). A FTIR *difference* spectroscopy study suggested that gradual increase in the level of PA in the PC/PA lipid mixture can gradually recover the ability of the reconstituted nAChR to bind ligand and undergo allosteric transition (Baenziger et al., 2000). At an appropriate ratio of PC:PA (i.e., 3:2) the reconstituted nAChR would approach its functional conformational state in the native membrane and reconstituted with a PC/PA/Chol mixture. On the other hand, raising the level of Chol could not fully recover the functional conformation of the nAChR. Thus, it was suggested that Chol is not as effective as PA in stabilizing the resting conformation of the receptor. Interestingly, early electron paramagnetic resonance (EPR) studies suggested there is a strong interaction between PA and the nAChR (Ellena et al., 1983). In fact, EPR studies hypothesized that specific lipids could form a ring, referred to as "annulus" lipid, around the nAChR to support its function. Since PC/PA is the best known binary lipid mixture that can support a

functional nAChR, it may be possible that there is a specific interaction between PA and the nAChR (daCosta et al., 2002; Ryan et al., 1996).

Recent studies have also shown that the incorporation of a functional nAChR in a lipid bilayer can significantly affect the physical properties of the lipid membrane (daCosta et al., 2002). A palmitoyl-oleoyl-PC (POPC) and palmitoyl-oleoyl-PA (POPA) lipid mixture at the molar ratio of 3:2 has a Tm of ~11 °C (daCosta et al., 2002). When the nAChR was reconstituted in a 3:2 POPC/POPA lipid mixture, the receptor appears to be in a resting-like conformation, and the Tm of the reconstituted membrane is about 24 °C (daCosta et al., 2002). The presence of the nAChR evidently increases the order of the bilayer. It could be argued that the presence of a large integral membrane protein in a bilayer can naturally increase the Tm. However, such a large increase in the Tm was not observed when the nAChR was reconstituted with PC alone or PC/Chol and PC/PS lipid mixtures (daCosta et al., 2004). Therefore, there may be a specific interaction between PA and the nAChR such that it increases the order of the reconstituted bilayer. This phenomenon was similarly observed by others using FTIR and fluorescence spectroscopy (Poveda et al., 2002; Wenz and Barrantes, 2005), leading to the suggestion that the nAChR may segregate lipids into domains in the reconstituted bilayer. This hypothesis is plausible because there are reports showing that the neuronal nAChR (α7 receptor) can be found in rafts (Bruses et al., 2001; Marchand et al., 2002; Oshikawa et al., 2003). Moreover, early EPR studies have also suggested that PA has a strong affinity for the nAChR in a bilayer (Ellena et al., 1983). Unfortunately, the lipid to protein ratio of the samples used in the FTIR and fluorescence spectroscopy studies above are relatively low, ranging from 150:1 to 500:1 mol/mol; the highest lipid to protein (500:1) ratio can barely form 4 lipid shells

around an individual nAChR. For this reason, it would be difficult to conclude if the nAChR actually induced domain formation. Thus, it is of interest to examine whether the nAChR forms domain in a POPC/POPA membrane via microscopic techniques that can clearly show the nAChR and lipid domains in a bilayer, which is the purpose of this project.

1.6 Atomic force microscopy (AFM)

In recent years, scanning probe microscopy techniques such as AFM have been very useful for high resolution imaging of biological and model membranes, providing resolutions of a few nanometers in the x and y direction and a few angstroms in the z direction (Fotiadis et al., 2003; Ira and Johnston, 2006; Seelert et al., 2003). Such resolution is far beyond the diffraction limit and cannot be achieved by conventional optical microscopes. Another attractive feature of the AFM, as compared to other high resolution microscopy techniques such as electron microscopy, is its ability to image biological samples in aqueous buffered environments. As a result, AFM may allow one to obtain high resolution details of a biological sample under physiologically relevant conditions.

The AFM is a relatively new microscopy technique which uses a scanning probe for topographic imaging of a surface (Figure 1.12A). The AFM acquires an image by engaging a sharp tip mounted on a cantilever to the surface of the sample. As the tip is brought into full contact with the sample, it experiences a repulsive force from the sample which causes the cantilever to bend upward. The extent of bending can be monitored through a laser beam bouncing off the cantilever into a photodetector, which can be translated into force of interaction between the tip and sample. By maintaining a constant force while scanning the tip across the surface of the sample, tracking the vertical deflection of the tip allows the

Figure 1.12. The mechanics behind an atomic force microscope (AFM). An AFM can operate in contact mode (A) or tapping mode (B) depend on the nature of the experiment. (C) is the piezoelectric tube scanner, where the AFM tip is mounted, which can contract or expand precisely in angstrom length upon an applied voltage. Images A & B were adopted from Agilent web site, C was hand drawn.

A) Contact Mode AFM

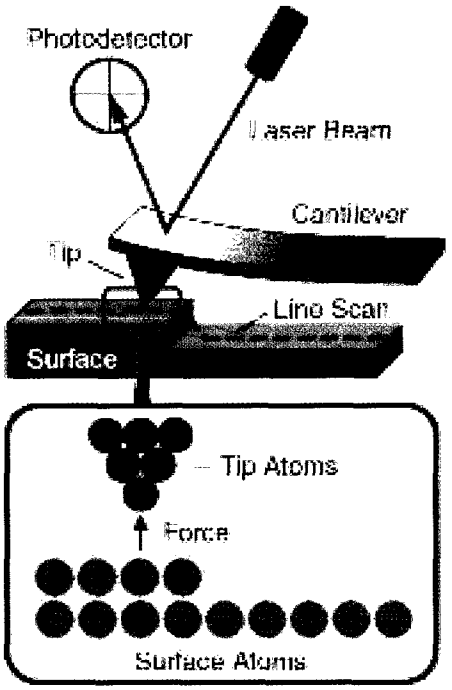

B) Tapping Mode AFM

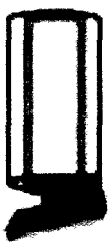

C) Piezoelectric tube scanner

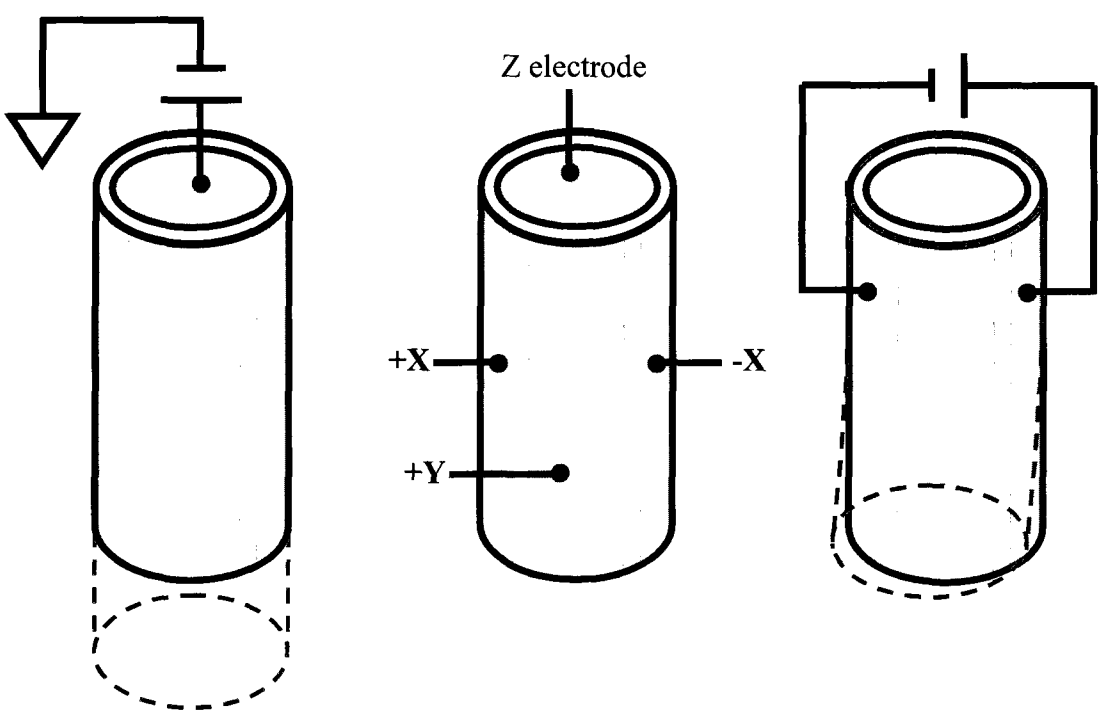

Vertical **No Deflection** **Horizontal**

surface profile of the sample to be probed and recorded as an AFM image.

The essential mechanical device that allows the AFM tip to move precisely in the angstrom range involves the use of a piezoelectric material which contracts or expands proportionally to the applied voltage. Although the property of a piezoelectric material has been known for over a century, the scanning probe microscopy technique was not developed until the early 1980's. The first of its kind, scanning tunneling microscopy (STM), was invented by Binnig and Rohrer in 1982 in response to a semiconductor issue (Baro et al., 1985; Binnig et al., 1985a; Binnig et al., 1985b). They received a Nobel Prize in Physics for their invention in 1986 (Robinson, 1986). In the same year Binnig collaborated with Quate and Gerber to build the first AFM. Within a few years of its invention, the use of AFM began to explode.

The fundamental component of any scanning probe microscope (including the STM and AFM) is the tube scanner, which is a mechanical device consisting of a thin-walled tube of piezoelectric material that is coated with metal on the inner and outer surfaces (Figure 1.12 C). The metal coating on the outer surface has 4 parallel thin gaps that divide the outer surface into four equal quadrants. The inner metal surface is used as the electrode for the vertical movement (i.e., z-direction), whereas the opposing pairs of electrodes on the outer surface are used to control the horizontal movement (i.e., x and y-direction). With this set-up, the length of the tube scanner can be controlled by an applied voltage between the inner and outer electrodes. Hence, the movement in the z-direction is under control. The lateral movements in the x or y-direction can be controlled by applying opposite voltages across the opposing outer electrodes, which will induce one side of the tube to contract and the other to

expand (along with a negligible vertical displacement). By attaching a sharp tip to an end of the tube scanner, it can be used to probe the surface of a sample near the atomic resolution.

Conventional AFM systems operate in contact mode in which the tip is kept in full contact with the surface of the sample when imaging (see above and Figure 1.12A). In this mode, a constant force is applied to the tip as it moves across the sample surface; this mode is not very effective for imaging samples that are loosely attached on a surface (i.e., DNA and RNA on mica) and soft biological samples (i.e., cell membranes). A key improvement to the conventional contact mode AFM was made when tapping mode AFM was invented (Putman et al., 1994), allowing soft and fragile biological samples to be successfully imaged. In tapping mode the AFM tip touches the sample intermittently with a minimal force of contact as it scans across the surface of the sample. In this case, the cantilever is driven to oscillation near its resonance frequency at an amplitude that is typically greater than 10 nm (according to Agilent). As the tip approaches the sample, its oscillation amplitude is dampened by interactions with the sample surface. When imaging a sample, the oscillation amplitude of the cantilever is set to a constant value at which the tip taps on the sample surface with a minimal force of contact. When the tip scans across the surface of a sample, the vertical position of the tip is continuously monitored and adjusted to accommodate the changes in amplitude as the tip encounters obstacles.

The cantilever in most modern AFM systems can be driven to oscillation by a small piezoelectric element mounted in the tip holder. In some AFM systems (and as used in this work), the cantilever is magnetically coated and can be driven by an oscillating magnetic field. In either case, tapping mode AFM is very effective for examining model and cellular membranes in detail at high resolution. For example, lipid domains in model membranes

(Ira and Johnston, 2008; Ira and Johnston, 2006) and rafts extracted from cellular membranes (Mai et al., 2002; Weerachatyanukul et al., 2007) have been clearly observed by AFM. The lipid bilayers/membranes are typically 45Å thick, and the lipid domains/rafts are about 5 – 15Å taller than the surrounding liquid disordered phase. The AFM has also been used to detect complex structural changes in the membrane by the action of a protein such as the restructuring of model raft membranes by sphingomyelinase (Ira and Johnston, 2006). In addition, the organization of integral membrane proteins in cellular membranes has been observed by AFM. For instance, rows of rhodopsin dimers (each rhodopsin is about 3 nm) can be observed from the rod outer segment membrane in bovine retina (Fotiadis et al., 2003), and the subunit organization of the spinach chloroplast ATP synthase was visualized as fourteen symmetrical protomers (Seelert et al., 2003). Since AFM has been proven to be a good tool to examine the structural organization of lipids and proteins in model and cellular membranes, I planned to use AFM to image the nicotinic acetylcholine receptor reconstituted in bilayers.

1.7 Objective of Thesis

The ultimate goal of this study was to use atomic force microscopy (AFM) to investigate whether the nAChR segregates lipid into domains in a bilayer with a 3:2 POPC/POPA mixture. However, my early attempts to image the nAChR in a bilayer reconstituted with a 3:2 POPC/POPA lipid mixture were noisy and irreproducible at best. These early results suggest that the preparation of a reconstituted bilayer that is suitable for AFM imaging can be complicated. Thus, it was essential to develop a method that allows the nAChR to be reconstituted in vesicles with a single lipid (i.e., POPC) and then to use the

proteoliposomes to prepare a bilayer containing reconstituted protein for AFM imaging. Upon success, a similar procedure might be used to prepare and image the nAChR reconstituted in more complex lipid mixtures. Therefore, the main objective of my thesis was to develop a protocol for imaging the nAChR reconstituted in a POPC bilayer by AFM.

Chapter 2: Materials and Methods

2.1 Materials

Frozen *Torpedo californica* electroplax tissue was obtained from either Marinus (Long Beach, California) or Aquatic Research Consultants (San Pedro, California). DOPC, POPC, POPA, and eggSM were from Avanti Polar Lipids, Inc. (Alabaster, Alabama) and both cholesterol and carbamylcholine (Carb) were from Sigma. Alpha-bungarotoxin conjugated to Alexa488 (αBTx-A488) and Texas Red dihexadecanoyl-phosphatidylethanolamine (TR-DHPE) were from Invitrogen. The atomic force microscope in magnetic alternating current mode (MAC mode AFM) and MAC mode AFM tips were purchased from Agilent (Phoenix, Arizona). The TIRF microscope was obtained from Olympus. High grade mica sheets were purchased from Tedpella. The Lipofast mini extruder and 400 nm polycarbonate filters are obtained from Avestin (Ottawa, Ontario).

2.2 The preparation of lipid vesicles

Liposomes were prepared by mixing the desired lipid(s) in chloroform at the appropriate ratio in a clean glass vial. If dye-labeled liposomes were required, a fluorescent lipid (e.g., TR-DHPE), solubilized in 1:1 chloroform/methanol, was added to the lipid mixture to make a final TR-DHPE concentration of 0.2 – 2.0 mole % of total lipid. The lipid mixture was vortexed briefly to mix the lipids. Then the lipid mixture was dried down in the glass vial with a stream of nitrogen gas to remove the solvent (mainly chloroform), and the lipid film was dried further under vacuum for at least 10 hours to remove any remaining solvent residue. The lipid film was then hydrated with Tris dialysis buffer (TDB: 10 mM Tris, 100 mM NaCl, 0.01 mM EDTA, 0.01 % NaN_3, pH 7.3), where the added

buffer volume is adjusted to the desired final lipid concentration. The TDB was chosen because this is a common buffer used for the reconstitution and storage of the nAChR. The hydrated film was vortexed for 1 minute to generate large or multilamellar vesicles, and these vesicles were subjected to sonication or extrusion to produce smaller vesicles.

2.2.1 The preparation of sonicated unilamellar vesicles

In my lab small unilamellar vesicles are typically generated by sonication to prepare lipid bilayers on mica for AFM imaging (Ira and Johnston, 2006). The lipid concentration was normally adjusted to 1 mg/ml when TDB was added to the vial containing the dried lipid film. This solution containing large or multilamellar vesicles generally appeared turbid. The solution was then sonicated in a Branson 1510 (Branson, USA) water bath sonicator at room temperature for 10 minutes or until the solution became transparent, which indicates that multilamellar vesicles have been broken up into small unilamellar vesicles that are less than 100 nm in diameter. These vesicles are also referred to as sonicated unilamellar vesicles (SUVs). The SUV solution were then diluted to 0.1 mg/ml and stored at 4°C. The SUVs were used within 1 week of storage.

2.2.2 The preparation of extruded unilamellar vesicles

Extruded unilamellar vesicles were used in this study in an attempt to reconstitute the nAChR in a bilayer at high L:P ratio by the detergent destabilization method. Liposomes of approximately 400 nm in diameter were prepared by passing large or multilamellar vesicles (prepared at 10 mg/ml) through a pair of 400 nm polycarbonate filters assembled in a Liposofast mini extruder (Avestin, Inc). Twenty passes were made to ensure that the extruded liposomes were homogeneous in size and were about 400 nm in diameter.

2.3 Reconstitution of the nAChR

2.3.1 Low lipid to protein ratio reconstitution

To reconstitute the nAChR in a bilayer I used an established procedure in my lab (Ryan et al., 1996). Briefly, the receptor rich membranes were extracted from the electric organ of the *Torpedo californica* electroplax, and the membranes were solubilized in 1 % cholate at 4 °C for 1 hour. The solubilized extract was then applied to an affinity column containing Affi-Gel 102 conjugated to bromoacetylcholine (Sigma). As the nAChR was bound to the column, the undesired proteins and lipids from the native membrane were replaced with the lipid(s) of interest by four rounds of washes with detergent solubilized lipid(s). Wash I: 4 column volumes of 1 mg/ml of lipid in 1 % cholate in Tris Dialysis buffer (TDB) at pH7.3; Wash II: 4 column volumes of 2.4 mg/ml of lipid in 1 % cholate in TDB; Wash III: 4 column volumes of 0.1 mg/ml of lipid in 0.5 % cholate in TDB; and Wash IV: 3 column volumes of 10 mM of carbamylcholine and 0.1 mg/ml of lipid in 0.5 % cholate in TDB. The Wash IV was used to elute the nAChR out of the affinity column, where the purified receptor remains solubilized in a lipid/detergent complex. Those eluted fractions containing a significant amount of protein were pooled together, and then subjected to dialysis to remove the detergent and reconstitute the protein in a bilayer. The pooled fractions were dialyzed against TDB (200 times sample volume) for 3 days with 6 even periods of buffer changes. The dialyzed sample was then ultra-centrifuged at 100,000xg for 2 hours at 4 °C to pellet the reconstituted sample. The pellet was then homogenized and resuspended in a small volume of TDB to keep the sample concentrated. The lipid and

protein content in the sample were determined by the Phospholipid C and BCA assay, respectively (see below). The lipid to protein (L:P) ratio of a reconstituted sample was typically low, where usual L:P ratio is about 1:2 (w/w). Aliquots of 250 μg of protein (as reconstituted proteoliposomes) were made and stored at – 80 °C. Samples were thawed to room temperature prior to use.

2.3.2 High lipid to protein ratio reconstitution

To reconstitute the nAChR in a bilayer at high L:P ratio, a similar protocol was initially used, but the lipid concentration was increased in all of the washes. Wash I: the lipid concentration was increased to 1.25 mg/ml of lipid and 1% of cholate in TDB; Wash II: 2.5 mg/ml of lipid and 1% of cholate in TDB; Wash III: 1.25 mg/ml of lipid and 1% of cholate in TDB; and Wash IV: 10 mM Carbamylcholine, 1.25 mg/ml of lipid and 1% of cholate in TDB. Following Wash IV, the purified nAChR is eluted out of the column in complex with lipid and detergent. Those fractions containing a significant amount of protein (estimated by A_{280}) were pooled together. The L:P ratio in the pooled fractions depends on the amount of protein eluted since the lipid concentration in Wash IV is fixed, but the usual L:P ratio was approximately 3:1 (w/w). To increase the L:P ratio further, a small volume of the pooled fractions was added to an appropriate volume of 5 mg/ml of lipid in 1% cholate in TDB to make up the desired L:P ratio. The subsequent reconstitution steps were kept the same as in the traditional reconstitution procedure. For example, the sample was dialyzed and then subjected to ultra-centrifugation at 100 000xg for 2 hours at 4 °C to pellet the reconstituted sample. The pellet was then homogenized and resuspended in a small volume to keep the sample concentrated. The sample was aliquoted and stored at – 80 °C. Samples were thawed at room temperature prior to use. In later reconstitutions, the

dialyzed samples were aliquoted and stored at – 80 °C immediately without ultra-centrifugation (see section 2.3.3).

2.3.3 Reconstitution of the nAChR in a POPC membrane via detergent destabilized liposomes

Based on the available literature, an alternative method known as detergent destabilized liposome reconstitution described by Rigaud and collaborators (Paternostre et al., 1988; Rigaud et al., 1988) has been used to reconstitute membrane proteins into lipid bilayers. This method takes advantage of the fact that bilayers are unstable in the presence of a detergent such that an integral membrane protein can be inserted into the bilayer with very little energy required. For successful reconstitution, the liposomes must be optimally destabilized by a detergent. Thus, the stability of the extruded POPC liposomes (see section 2.2.2) in cholate was assessed first. Then a range of destabilized liposomes were selected to test whether a purified and solubilized nAChR can be incorporated into one of these destabilized liposomes.

The stability of the vesicles was tested by mixing the extruded vesicles with various cholate solutions at different concentrations (0.1 – 0.3 % cholate), which was done by taking a small volume of extruded liposome at 10 mg/ml and adding it to a larger volume of cholate solution to get a final lipid concentration of 1.5 mg/ml. Each mixture was gently stirred for 90 minutes at 4°C. Duplicate 200 µl aliquots were taken from each sample and placed in a 96 well plate. The stability of the liposomes in each detergent condition was monitored by measuring the optical density (OD) at 405 nm. According to Rigaud et al (1988), higher OD reading indicates that the vesicle is either larger and/or more stable, whereas lower OD reading signifies that the vesicle is unstable destabilized and/or smaller, and the vesicle

becomes solubilized when the OD approaches that of the blank solution (i.e., the detergent alone solution).

In an attempt to reconstitute the nAChR, extruded POPC liposomes were mixed with an appropriate amount of detergent to destabilize them, and then the purified and solubilized nAChR (in 1% cholate and 1.25 mg/ml POPC) was added to the destabilized liposomes. The final concentrations of lipid and protein were 1.5 mg/ml and 0.03 mg/ml, respectively. Hence, the L:P ratio is 50:1 w/w. Upon mixing, the samples were stirred for 90 minutes at 4°C. Then the sample was subjected to dialysis to remove the detergent to complete the reconstitution procedure. The samples were dialyzed against TDB (200 times sample volume) for 3 days with 6 even periods of buffer change to remove the detergent. It should be noted that the conditions used for the reconstitution attempt with solubilized POPC liposomes at 1.00 % cholate are the same as those in the detergent dialysis method above up to this point, and this sample was intended to be used as a control. To be consistent with the detergent destabilized liposome reconstitution method provided by Rigaud and collaborators (1988), the samples were not pelleted by ultra-centrifugation as in the detergent dialysis method above. The samples were frozen at – 80 °C after reconstitution, and they were thawed to room temperature just before they were characterized by sucrose gradient.

2.4 Protein and lipid assay

Protein was assayed using the Bicinchoninic acid (BCA) kit purchased from Thermal Fisher Scientific, Inc. For improved accuracy, 2 % Triton X-100 (compatible with the BCA assay) was added to the nAChR samples (to solubilize the reconstituted protein) and also to the BSA standards.

Lipid was analyzed using the Phospholipids C kit obtained from Wako Chemical USA, Inc. Again, both the nAChR samples and choline chloride standards were in 2 % Triton X-100 to improve the accuracy of the kit. Again Triton X-100 is compatible with the assay and the detergent is used to solubilize the lipid(s).

2.5 Sucrose Gradient

2.5.1 Analytical sucrose gradient

Following reconstitution, the samples were examined on a discontinuous sucrose gradient (either 0, 5, 10, 20 and 40 % sucrose gradient or 0, 5, 7.5, 10, 20, and 40 % sucrose gradient). The samples were typically loaded on the top of the gradient, and were subjected to ultracentrifugation at 200 000xg for 20 hours at 4 °C. Following ultra-centrifugation, fractions of 250 or 400 µl were drawn from the gradient (starting from the top), and the lipid and protein content of each fraction were analyzed using the Phospholipids C and BCA protein assay.

2.5.2 Preparative sucrose gradient

After characterizing a nAChR sample by analytical sucrose gradient, the relative positions of those bands corresponding to lipid alone, high L:P ratio and low L:P ratio vesicles were determined. High L:P ratio proteoliposomes were prepared by loading reconstituted samples (3 ml) on top of a discontinuous sucrose gradient of 0 % (3 ml, including the sample), 5 % (2.5 ml), 7.5 % (2.5 ml), 10 % (1 ml), 20 % (1 ml) and 40 % sucrose, and the sucrose gradient was subjected to ultracentrifugation at 200 000xg, 20 hours, and 4 °C. Following ultra-centrifugation, those bands containing the vesicles of

interest (i.e. high L:P ratio) were isolated from the sucrose gradient directly by using a sharp needle to puncture through the wall of the sucrose gradient tube and withdraw the fraction of interest. The isolated sample was then dialyzed to remove the sucrose. The sample was dialyzed against TDB (200 times the sample volume) for 3 days with 6 even periods of buffer change. Following dialysis, the samples were diluted to a corresponding concentration of 0.1 mg/ml POPC with TDB (the concentration of the nAChR depends on the L:P ratio), which was then divided into small aliquots, and stored at – 80 °C.

For fluorescence microscopy, the nAChR was labeled with α-*bungarotoxin* conjugated to Alexa488 (αBTx-A488) purchased from Invitrogen, where the toxin binds specifically to the nAChR (Boulter et al., 1987; Changeux et al., 1970). The labeling was accomplished by mixing αBTx-A488 (at 100 times the mole concentration of the receptor) with the nAChR sample immediately after the sample was isolated from the preparative sucrose gradient. The unbound toxin and sucrose in the sample were removed by dialysis as described above.

2.6 Fourier transformed infrared spectroscopy

The structural state of the reconstituted nAChR was examined by Fourier transform infrared (FTIR) spectroscopy. FTIR *difference* spectroscopy was designed to detect very subtle differences in structural conformations of a protein that cannot be otherwise observed by typical FTIR. This technique has been used to assess very subtle changes in conformation of the nAChR as it undergoes a change from the resting to the desensitized conformation in the presence of an agonist such as carbamylcholine (Carb) (Baenziger et al., 1992a; Baenziger et al., 1992b). An FTIR difference spectrum was obtained by subtracting

Figure 2.1. The instrumental set up for FTIR difference spectroscopy. The sample (Green) is applied on a germanium crystal (Yellow), which is an attenuated total internal reflection (ATR) crystal. The sample on the ATR crystal is then sealed in a stainless steel flow cell (Grey). Different buffers (i.e., with or without ligand) can be selected to flow into the cell to interact with the sample via an automated control valve. A FTIR spectrum of the sample can be acquired as the evanescence wave, created by an IR beam directed in the ATR crystal, is interacting with the sample on the crystal. ATR is a common FTIR technique used to examine a sample on a solid surface. When the IR beam is passed through a crystal (typically with high refractive index), the IR beam can be internally reflected when the beam is directed toward the crystal at an appropriate angle. At each point of reflection, an evanescence wave is created (which is a standing wave that decays exponentially away from the surface of the crystal). The FTIR *difference* spectrum of a sample is obtained by subtracting a spectrum of the sample recorded in absence of a ligand from a spectrum of the sample in recorded in the presence of a ligand.

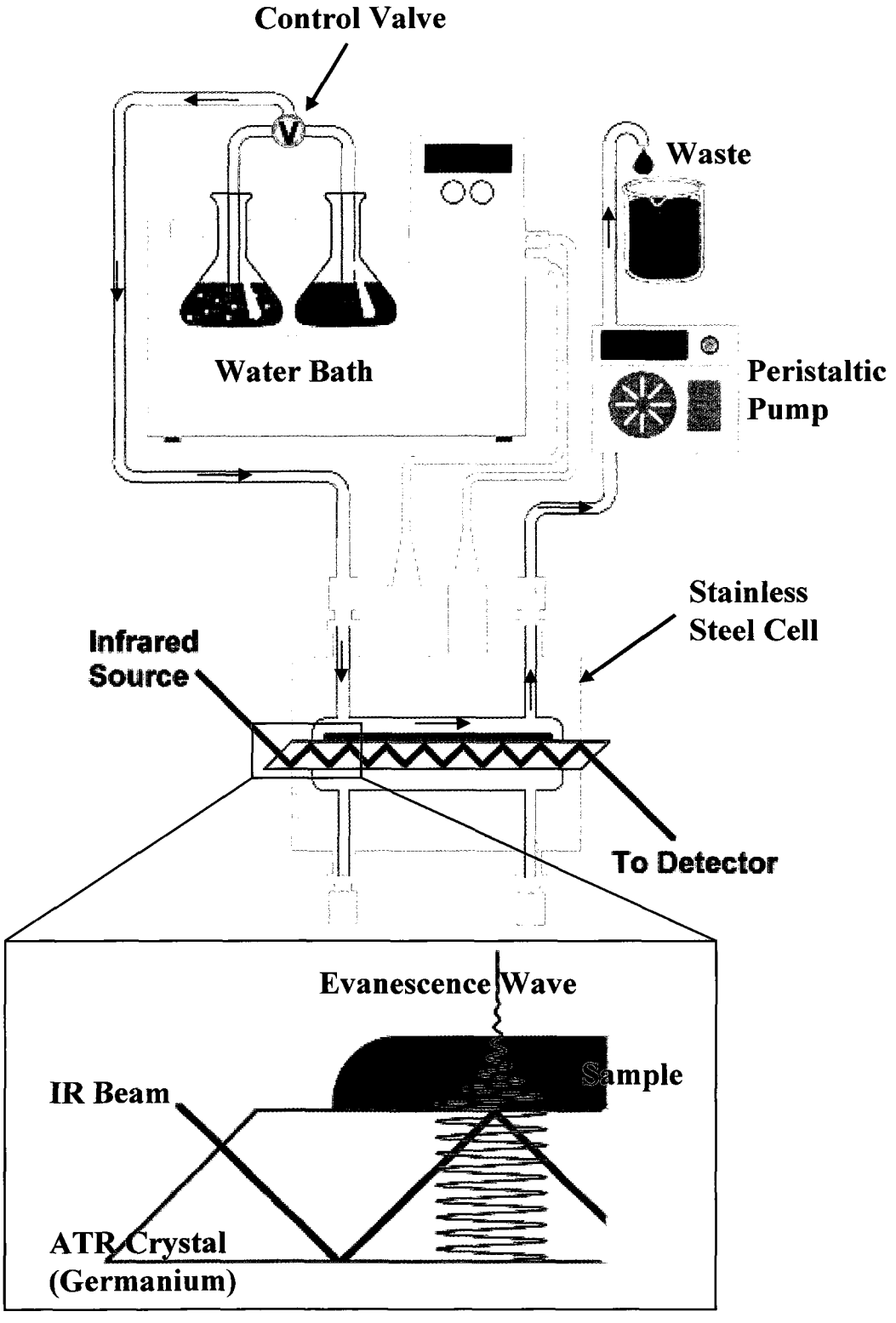
Control Valve
Waste
Water Bath
Peristaltic Pump
Stainless Steel Cell
Infrared Source
To Detector
Evanescence Wave
Sample
IR Beam
ATR Crystal (Germanium)

the nAChR spectrum in the absence of Carb from the nAChR spectrum in the presence of Carb. The set-up for FTIR *difference* spectroscopy is illustrated in Figure 2.1.

To examine the structural state of the reconstituted nAChR by FTIR *difference* spectroscopy, about 250 μg of nAChR protein were spread on the surface of a 50 mm x 20 mm x 2 mm germanium attenuated total reflectance (ATR) crystal (Harrick, Ossining, New York). For consistency, only one germanium crystal was used for all of my experiments. After evaporating the bulk solvent with a gentle stream of N_2 gas, the ATR crystal was installed in an ATR liquid sample cell (also from Harrick) and the nAChR film rehydrated with excess *Torpedo* Ringer buffer (250 mM NaCl, 5 mM KCl, 2 mM $MgCl_2$, 3 mM $CaCl_2$, and 5 mM Na_2HPO_4, pH 7.0). Note that each nAChR film is spread over an equivalent surface area on the ATR crystal, and each expands beyond the effective penetration depth of the infrared beam upon hydration. The absolute intensities of the protein bands in the FTIR spectra are similar from sample to sample.

All FTIR *difference* spectra were acquired using the attenuated total reflectance technique on either a Digi-Lab FTS 575 or a FTS 40 spectrometer (Randolph, Massachusetts). Both spectrometers were equipped with a deuterated triglycine sulfate detector. Spectra were recorded at 8 cm^{-1} resolution using 512 scans, which took roughly 7 min/spectrum. For the difference measurements, two consecutive spectra of the same nAChR film in the absence of Carb were recorded with buffer flowing continuously through the sample compartment of the ATR cell at a rate of ~1.5 ml/min. The flowing solution was then switched to an identical one with 50 μM Carb. After 1 min, a spectrum was recorded of the desensitized state. The difference between both the two resting state spectra (absence of Carb; control spectra) and the consecutive resting and desensitized (presence of Carb)

state spectra were calculated, stored, and the flowing buffer switched back to buffer without Carb. After a 23-min washing period to remove Carb from the film and convert the nAChR back into a resting conformation, the process was repeated many times. The 50 μM Carb solution is sufficient to desensitize the nAChR (Baenziger et al., 1992a), but low enough to allow the rapid washing of Carb from the nAChR film. Each presented *difference* spectrum for each sample was derived from a minimum of 30 *difference* spectra. All presented *difference* spectra were baseline corrected between 1800 and 1000 cm^{-1} and were interpolated to an effective resolution of 4 cm^{-1}.

2.7 Imaging a bilayer by atomic force microscopy (AFM)

A planar bilayer on mica was prepared in an AFM fluid cell, shown in Figure 2.2, in order for the bilayer to be imaged by AFM in a buffer solution. First, the mica was cleaved to obtain a flat and clean surface. The freshly cleaved mica was then assembled in a clean AFM cell, which can hold a maximum volume of approximately 600 – 700 μl. The sample (liposomes or proteoliposomes) was then incubated in a total volume of 500 μl of aqueous buffer; calcium is typically included to assist the formation of the bilayer on mica. For every sample prepared, including the reconstituted nAChR sample, the desired amount of sample used was diluted to 125 μl in TDB and added to 375 μl of the desired calcium concentration in pure water. It must be noted that the final incubation solution contained only one quarter the concentration of the TDB, but the solution can still be buffered above pH 7.2 even after a period of 24 hours. In general, a bilayer was prepared by incubating the liposomes or proteoliposomes in 10 mM $CaCl_2$ for 1 hour, using 7 or 10 μg of lipid to

Figure 2.2. An image of a sample holder for AFM adopted from Agilent. A sheet of freshly cleaved mica is placed on an AFM stage and is held down by an AFM cell. A planar bilayer can be formed on the mica surface by incubating the liposomes or proteoliposomes of interest in a buffer under a specified condition. After incubation, the materials that were not absorbed on the mica surface were washed (or flushed) away by flowing a defined volume of buffer into the cell.

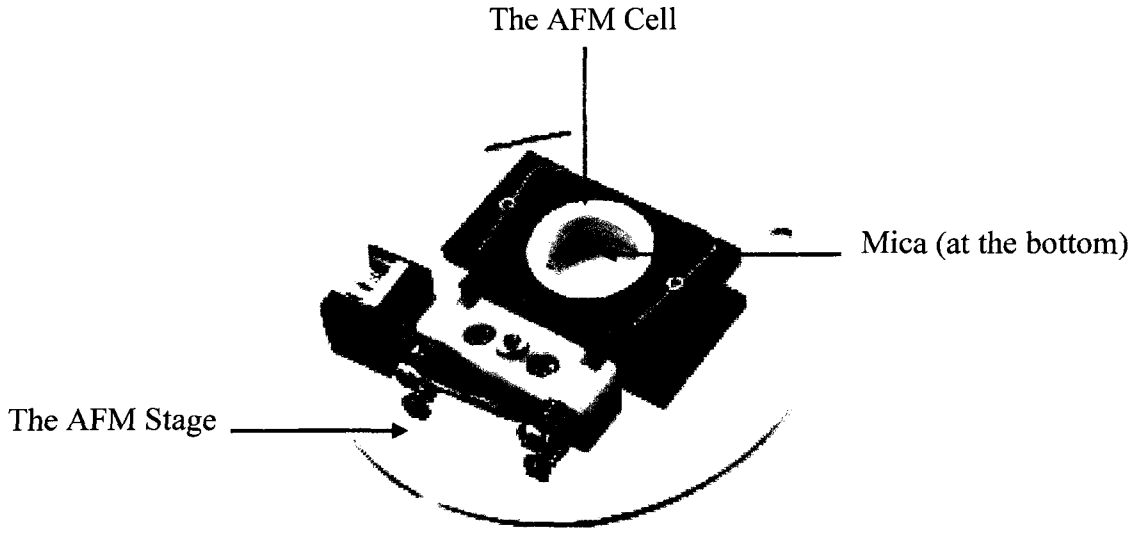
The AFM Cell
Mica (at the bottom)
The AFM Stage

prepare bilayer patches or an intact bilayer on mica, respectively. Alternatively, an intact bilayer was also prepared from 7 μg of lipid by incubating the vesicle sample overnight (i.e., 16 – 20 hours).

Once the sample was incubated on mica over a period of time, the unbound materials were washed away by flowing 100 ml of the imaging buffer into the AFM cell. The sample was allowed to equilibrate for 5 minutes after washing. Prior to AFM imaging, the AFM tip and its holder were washed with ~ 25 ml of 70 % ethanol, followed by 25 ml of water, and 25 ml of the imaging buffer (the same buffer used to wash the sample) to ensure that no contaminant was introduced into the sample. The sample was then imaged by AFM, and the AFM image was subsequently interpreted.

AFM images were obtained on a PicoSPM atomic force microscope (Agilent, Phoenix, Arizona) in magnetic alternating current (MAC)-mode using magnetic coated silicon tips (MAClever Type II) with spring constants of ~0.5 N/m and resonance frequencies between 7 and 35 kHz in aqueous solutions. Either a 30×30 μm^2 or 5×5 μm^2 scanner was used with a scan rate between 0.7 and 1.3 Hz. All images shown are flattened raw data.

2.8 Imaging a bilayer by total internal reflection fluorescence (TIRF) microscopy

TIRF is a fluorescence microscopy technique that has been used to image a bilayer on mica. In order to image a bilayer by TIRF, the presence of a dye labeled lipid is required to visualize a bilayer. Texas Red DHPE (TR-DHPE) is a commercially available

fluorescent lipid that has been commonly used at a very low concentration (i.e., 0.2 - 2 % mole/mole) to visualize the bilayer. Since TR-DHPE has a strong partition coefficient for disordered phase in the bilayer, it is typically used to observe the liquid disordered phase of the bilayer (Veatch and Keller, 2003). For most TIRF microscopy experiments in this study, TR-DHPE is doped in the bilayer to label the liquid disordered phase.

To prepare a planar bilayer for TIRF imaging, the test vesicles were incubated on freshly-cleaved mica assembled in a TIRF cell. In order to achieve the best resolution, the thickness of the mica should be less than 20 μm, based on past experience in my lab. It should be noted that the TIRF cell (17 mm in diameter) is larger than the AFM cell (13 mm in diameter). Hence, the surface area of the mica in the TIRF cell (~230 mm^2) is nearly twice that in the AFM cell (~130 mm^2). Furthermore, the TIRF cell (~1.2 ml) was designed to hold approximately twice the volume of the AFM cell (~0.6 ml). Thus, the quantity of lipid required to prepare a bilayer on mica in these two cells can be correlated. Therefore, a planar bilayer was prepared on mica for TIRF imaging by incubating the vesicle sample in a total volume of 1000 μl, where the desired amount of sample used was made up to 250 μl in TDB and the desired calcium concentration used was made up to 750 μl in water. Upon mixing with a pipette, the mixture was incubated at 20°C for a specified period of time. Following the incubation, the TIRF cell was washed with ~ 150 ml of HEPES buffer to remove the unadsorbed materials, and the bilayer was then imaged.

Fluorescence images of bilayers were taken on an Olympus IX81 total internal reflection fluorescence (TIRF) microscope equipped with a high resolution CCD camera (CoolSNAP, Photometrics, USA) and a 60x/1.45 NA Plan Apochromat objective (Olympus). Alpha *bungarotoxin* conjugated with Alexa-488 was excited at 488 nm and

emission collected at 519 nm (±20) nm, and TR-DHPE was excited at 543 nm and emission collected at 593 (±20) nm.

Chapter 3: Selecting a buffer to image bilayers by AFM

3.1 Introduction

Before imaging the nAChR in a reconstituted bilayer, it was important for me to demonstrate my ability to use AFM to image lipid bilayers. This chapter describes the preparation of two supported lipid bilayers and initial results for AFM imaging in water. The same bilayers were then imaged in several different buffers to screen for a buffer that was suitable to image a bilayer with reconstituted protein. Furthermore, the appearance of the planar bilayers prepared on mica was also examined by total internal reflection fluorescence (TIRF) microscopy to validate AFM images.

3.2 Supported planar bilayer imaged by AFM

To illustrate the ability of the AFM to image lipid bilayers, known domain-forming (i.e., DOPC/eggSM/Chol 2:2:1, DEC221) and non domain-forming (i.e., POPC) bilayers were prepared on mica, and these bilayers were imaged in pure water. The morphological and topographical differences detected between these two bilayers were demonstrated in the resulting AFM images.

3.2.1 Imaging a POPC bilayer in water

A single component POPC bilayer adopts a liquid disordered phase at room temperature, and it is expected to form a flat and featureless bilayer on mica. However, the mica surface is also flat and featureless, and cannot be readily distinguished from a POPC bilayer. Thus, the presence of a continuous POPC planar bilayer on mica must be confirmed. My approach was first to prepare and image bilayer patches on mica by using

small amounts of POPC liposomes, and then to increase the amount of liposomes to form a continuous POPC bilayer on mica.

The POPC bilayer patches on mica were prepared with 7 μg of lipid, incubated for 1 hour in 10 mM $CaCl_2$. Following incubation, the unbound liposomes were washed off with pure water, and the adsorbed bilayer was subsequently imaged by AFM. The AFM image in Figure 3.1A shows POPC bilayer patches adsorbed on the mica surface. The color code bar at the bottom of the image specifies the relative height of the features shown in the AFM image. In Figure 3.1A, the dark brown areas correspond to the mica surface, whereas the light yellow areas correspond to the POPC patches on mica. The graph at the bottom of the AFM image shows a cross section analysis at the position of the green line in the image. Based on this cross section analysis, the thickness/height of a POPC bilayer patch is consistently found to be about 45 Å. This thickness agrees well with the known literature value of a POPC bilayer (Lewis and Engelman, 1983; Tahara and Fujiyoshi, 1994).

An intact POPC bilayer on mica was prepared by incubating 10 μg of lipid in 10 mM $CaCl_2$ for 1 hour. Following incubation, the unbound/excess materials were washed away with pure water. The AFM image in Figure 3.1B shows an intact POPC planar bilayer on mica, imaged in pure water. The image appears featureless and the cross section analysis for the bilayer is flat throughout. These observations are expected for a single component bilayer in the liquid disordered phase at room temperature. Extraction of a POPC bilayer and lipid quantification via the Phospholipids C kit indicated that an individual POPC bilayer prepared in my standard AFM cell contains about 1 – 2 μg of lipid.

The results here demonstrate that a POPC bilayer can be imaged in water by AFM. The POPC bilayer is flat and featureless as expected for a bilayer in the liquid disordered

Figure 3.1. AFM images of lipid bilayers prepared on mica and imaged in water. The lipid bilayers were prepared on mica by incubating sonicated unilamellar vesicles in the AFM cell for 1 hour at 21 °C in the presence of 10 mM $CaCl_2$, and the unabsorbed materials were washed away with 100 ml of water. For every sample prepared, the desired amount of sample used is made up to 125 μl in Tris dialysis buffer (TDB) and the desired calcium concentration used is made up to 375 μl in pure water, which makes the final volume of 500 μl. (A) and (B) are AFM images of bilayer patches and continuous bilayer prepared by loading 7 and 10 μg of POPC vesicle, respectively. Similarly, (C) and (D) are bilayer patches and continuous bilayer prepared with 7 and 10 μg of 2:2:1 DOPC/eggSM/chol (DEC221) vesicles. The relative height of the sample surface detected by the AFM tip is colour coded according to the bar below every image, where taller features are light in colour and shorter features are dark in colour. The green dashed line in the images shows the position for cross section analysis, and blue dashed baselines on the cross sections of (A) and (C) show the position of the surface of the mica. The black arrows in (C) and (D) point out some of the domains detected in the bilayers prepared with DEC221 vesicles.

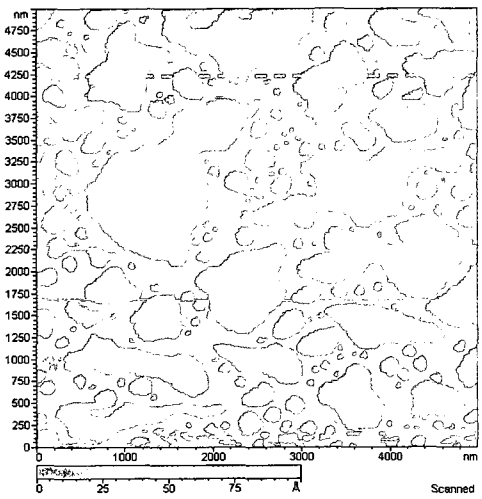

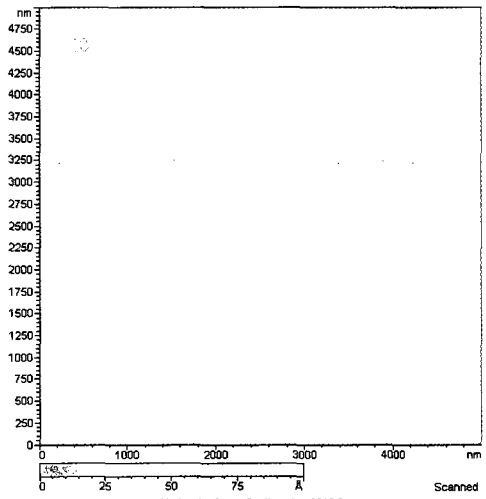

Baseline (mica surface)

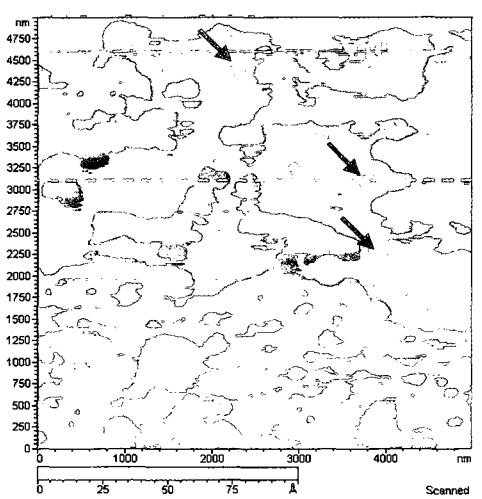

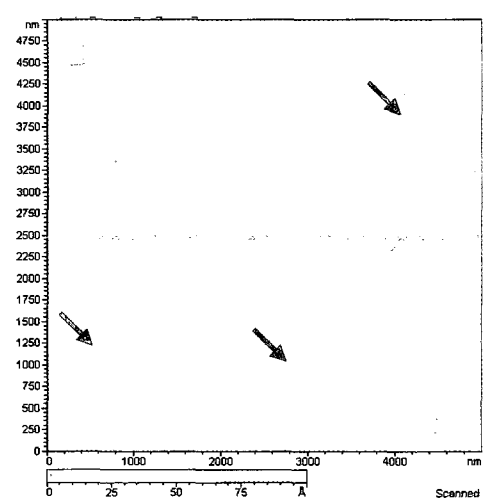

Baseline (mica surface)

phase. Moreover, the POPC bilayer patches measured by AFM are about 45 Å thick, which coincides with the accepted literature value for the thickness of a POPC bilayer.

3.2.2 Imaging a DOPC/eggSM/Chol 2:2:1 bilayer in water

When assessing the DOPC/eggSM/Chol 2:2:1 (DEC221) bilayer, a known lipid domain-forming bilayer, both bilayer patches and an intact bilayer were prepared and imaged in water. The bilayer preparation procedure used for the DEC221 bilayer was the same as that for POPC. The AFM images in Figure 3.1C show the bilayer patches prepared from DEC221 liposomes. In contrast to the featureless POPC patches, the DEC221 patches have small raised regions (light yellow areas). A fluorescence microscopy study of giant unilamellar vesicles of this lipid mixture has previously shown that the domains in the bilayer correspond to the segregation of cholesterol and sphingomyelin into the liquid ordered phase which separates from DOPC in the liquid disordered phase (Veatch and Keller, 2003). The measured thickness of the liquid disordered phase based on the AFM image is about 45 Å, and the domains are approximately 12 Å taller than the liquid disordered phase. Thus, the lipid domains in a bilayer can be clearly distinguished from a bilayer patch based on the height difference.

Figure 3.1D shows a complete and intact DEC221 bilayer imaged in water. Again, the AFM image shows that the DEC221 bilayer has numerous domains of the liquid ordered phase. The liquid ordered phase is about 12 Å taller than the liquid disordered phase. The domains are variable in size, some of them can be as big as 1 μm or more and some are less than 50 nm in diameter. The data is consistent with previously reported AFM data on phase separated bilayers (Choucair et al., 2007; Ira and Johnston, 2008; Weerachatyanukul et al., 2007).

3.3 Imaging planar bilayers in buffers

Up to this point, I have only shown AFM images of lipid bilayers imaged in water, but not in buffers. However, imaging a bilayer containing a protein in pure water is not advisable, because the protein can be denatured if the pH is not controlled. Therefore, I needed to find a buffer that was compatible with imaging both lipid bilayers and protein-containing bilayers. To serve this purpose, lipid bilayers were prepared and imaged in a number of buffers to screen for the best buffer for further experiments.

3.3.1 Imaging a bilayer in the Torpedo Ringer buffer

Initially, the *Torpedo* Ringer buffer (TRB: 250 mM NaCl, 5 mM KCl, 2 mM $MgCl_2$, 3 mM $CaCl_2$, and 5 mM Na_2HPO_4, pH 7.03) was chosen for the purpose of imaging planar bilayers. The TRB was selected because it has been used in many studies to assess the structure and function of the nAChR.

The TRB was tested on the POPC bilayer patches. In this instance, the POPC bilayer patches on mica were first prepared and imaged in pure water (Figure 3.2A), the water was then replaced with TRB (by flowing 50 ml of TRB into the AFM cell), and the POPC bilayer patches in TRB were then imaged by AFM (Figure 3.2B). From Figure 3.2A, the starting POPC bilayer patches in water are the same as observed in previous results in Figure 1A, flat and featureless. However, when the water on the bilayer was replaced with TRB, there were numerous spots in the AFM image (Figure 3.2B). These spots can be found above and around the POPC bilayer patches. These spots correspond to particles that are at least a few nanometers or larger, and they are suspected to be salt precipitation for two

Figure 3.2. AFM images of POPC bilayer patches imaged in pure water and Torpedo Ringer buffer (TRB: 250 mM NaCl, 5 mM KCl, 2 mM $MgCl_2$, 3 mM $CaCl_2$, and 5 mM Na_2HPO_4, pH 7.03). The POPC bilayer patches were prepared with 7 μg of lipid in the AFM cell for 1 hour at 21 °C in the presence of 10 mM $CaCl_2$, and the unabsorbed materials were washed away with 100 ml of water. The POPC bilayer patches were first imaged in pure water (A). Then, the water on the same bilayer was replaced by TRB, and subsequently the bilayer was imaged in TRB (B). In TRB, there are many small features found above and around the bilayer patches. These features are a few nanometers in size, and they are suspected to be the precipitation of salt due to the high salt content in the buffer and the low solubility of calcium phosphate (Ksp of $Ca_3(PO_4)_2 = 1x10^{-26}$).

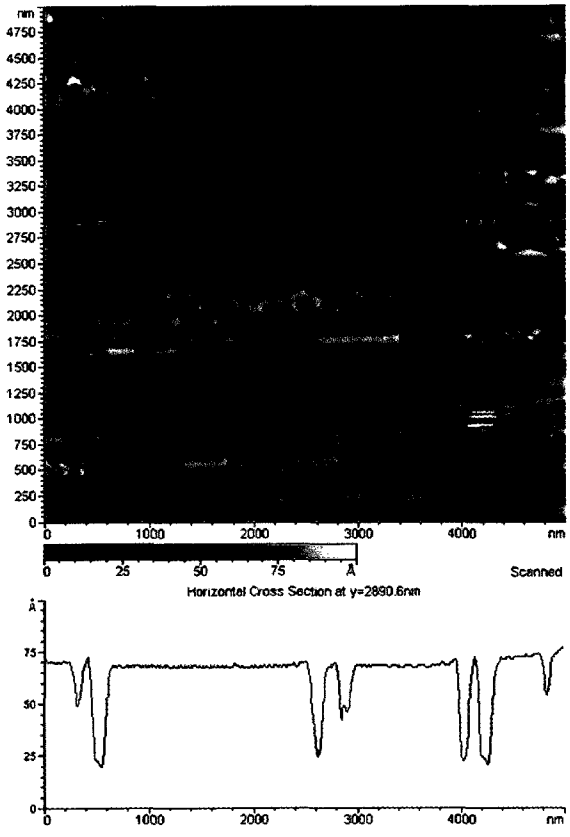
nm
4750
4500
4250
4000
3750
3500
3250
3000
2750
2500
2250
2000
1750
1500
1250
1000
750
500
250
0
0
1000
2000
3000
4000
nm
0
25
50
75
Å
Scanned
Horizontal Cross Section at y=2890.6nm
Å
75
50
25
0
0
1000
2000
3000
4000
nm

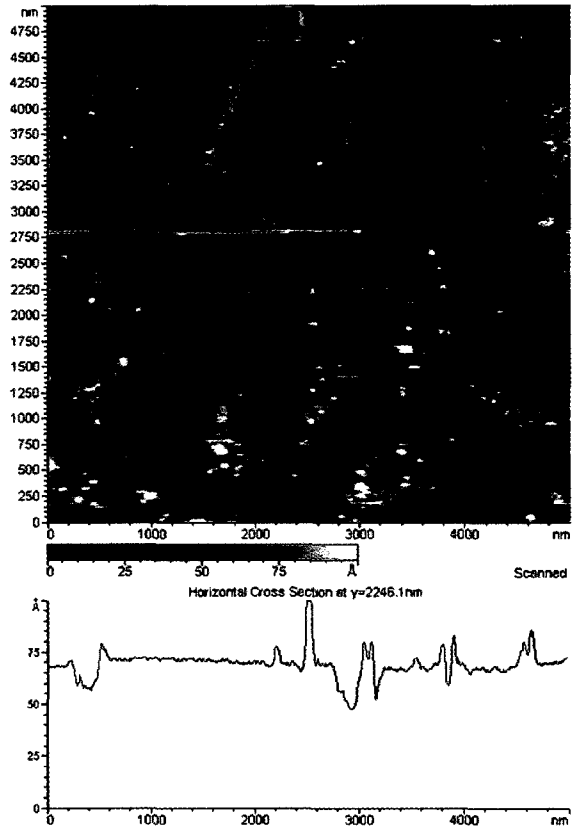
nm
4750
4500
4250
4000
3750
3500
3250
3000
2750
2500
2250
2000
1750
1500
1250
1000
750
500
250
0
0
1000
2000
3000
4000
nm
0
25
50
75
Å
Scanned
Horizontal Cross Section at y=2246.1nm
Å
75
50
25
0
0
1000
2000
3000
4000
nm

reasons. First, the TRB has a high salt content. As the water starts to evaporate from the buffer in the AFM cell, the effective concentration of salt begins to increase. When enough water has evaporated from the AFM cell, salt will start to precipitate. In addition, salt precipitate can be frequently observed at the rim of the bottle containing the TRB buffer. The evaporation of water from the AFM cell is unavoidable due to the fact that the cell is open. Secondly, the TRB contains calcium and phosphate. However, the solubility of calcium phosphate is relatively low, where the solubility of $CaHPO_4$ is about 0.079 mg/ml at pH 6.0 and 0.019 mg/ml at pH 7.5 (Goss et al., 2007). Thus, calcium phosphate salt can be found precipitated in a solution with a pH of 7.03. For these reasons, TRB or any buffer containing high salt concentration and/or calcium and phosphate are not suitable for the "open" AFM imaging system. Consequently, the TRB was quickly eliminated from the list of potential buffers for AFM imaging.

3.3.2 Imaging the bilayers in a Tris dialysis buffer

The next buffer of choice to image a planar bilayer by AFM was Tris dialysis buffer (TDB: 10 mM Tris, 100 mM NaCl, 0.01 mM EDTA, 0.01 % NaN3, pH 7.3). This buffer was selected because it does not contain as high a salt concentration, and has no calcium or phosphate. Furthermore, TDB has been used in the reconstitution procedure and storage of the nAChR.

The potential of the TDB as an imaging buffer, again, was first assessed on an intact POPC bilayer that was prepared by incubating 10 μg of lipid for 1 hour in 10 mM $CaCl_2$. Following incubation, the sample was washed with TDB to remove unbound/excess materials. The morphology of the POPC bilayer imaged in TDB appears very similar to that in water, where the bilayer remains flat and featureless (data not shown). Importantly, no

salt precipitate can be observed. The TDB at this point looked promising for a buffer to image planar bilayers on mica by AFM.

The TDB was then tested on a domain forming bilayer (i.e., DEC221). Again, an intact DEC221 bilayer was prepared on mica by incubating 10 μg of lipid for 1 hour in 10 mM $CaCl_2$. Following incubation, the sample was washed with TDB to remove unbound or excess materials. When the DEC221 bilayer was imaged in TDB, the lipid domains corresponding to the liquid ordered phase could not be observed. The DEC221 bilayer in TDB appears as flat and featureless as the POPC bilayer (Figure 3.3A). However, when the TDB was replaced with pure water on the very same planar bilayer (by flowing 100 ml of water over the original 0.6 ml TDB buffer in the AFM cell), the domains reappeared immediately in the bilayer (Figure 3.3B). Nevertheless, the image looks very messy at this point, with numerous particles ranging from 50 to 200 nm in diameter observed on the bilayer. The observed effects of TDB on the DEC221 bilayer are puzzling, and they still have not been understood clearly. However, a recent ellipsometry study of planar bilayers on mica suggested that Tris may destabilize planar bilayers on the surface of mica (Benes et al., 2004). Perhaps the particles observed in Figure 3.3B are the bilayer debris that has desorbed from the surface of mica due to the action of Tris in the TDB. Additionally, there are other components in the TDB that could have caused problems in the DEC221 bilayer on mica. Therefore, TDB was eliminated from the list of potential buffers to image bilayers on mica by AFM.

Figure 3.3. The DEC221 bilayer was imaged by AFM in TDB and water. The bilayer was prepared by incubating 10 μg of lipid (sonicated unilamellar vesicle) for 1 hour in 10 mM $CaCl_2$ on mica in an AFM cell. The sample was washed with TDB to remove unbound/excess materials following the incubation. The bilayer was subsequently imaged in TDB, where no domains were observed and the bilayer looks flat and featureless (A). The TDB on the bilayer was then replaced with water and imaged in water, where the domains reappear (B). Tris dialysis buffer (TDB): 10 mM Tris, 100 mM NaCl, 0.01 mM EDTA, 0.01 % NaN_3, pH 7.3.

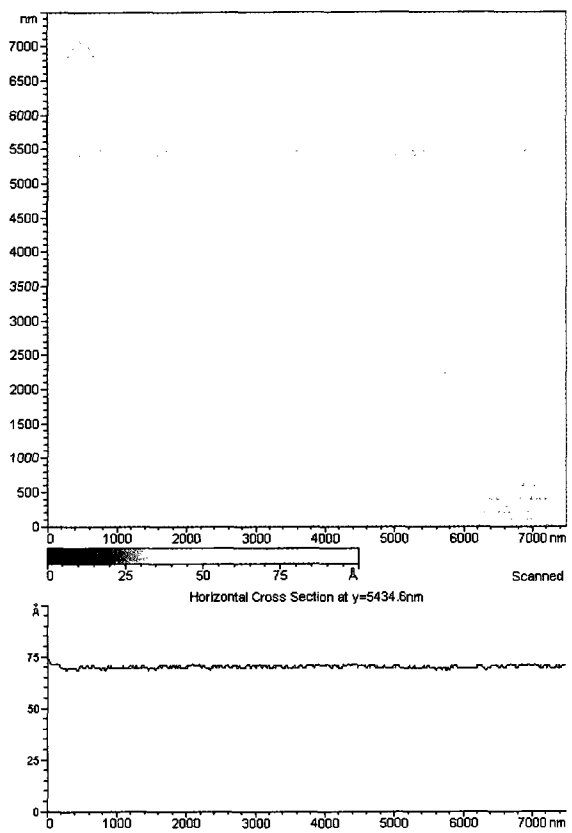
nm
7000
6500
6000
5500
5000
4500
4000
3500
3000
2500
2000
1500
1000
500
0
0 1000 2000 3000 4000 5000 6000 7000 nm
0 25 50 75 Å
Scanned
Horizontal Cross Section at y=5434.6nm
Å
75
50
25
0
0 1000 2000 3000 4000 5000 6000 7000 nm

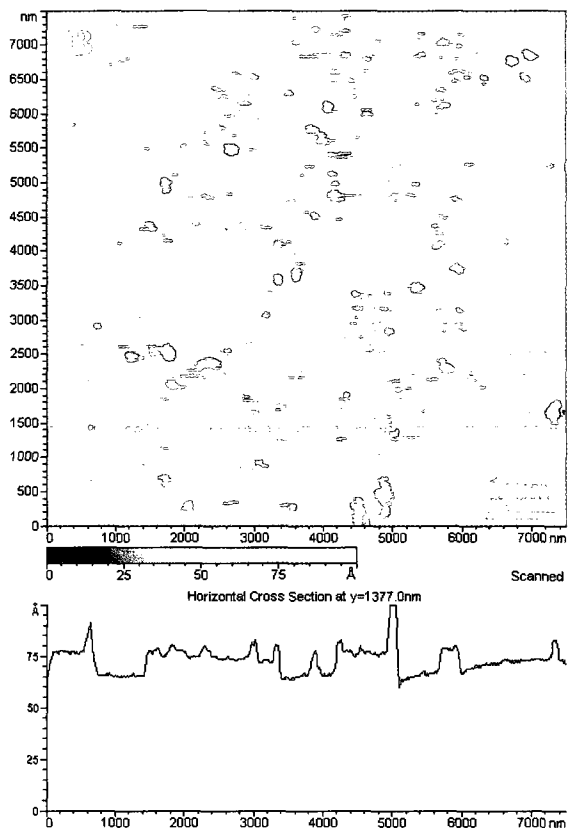
nm
7000
6500
6000
5500
5000
4500
4000
3500
3000
2500
2000
1500
1000
500
0
0 1000 2000 3000 4000 5000 6000 7000 nm
0 25 50 75 Å
Scanned
Horizontal Cross Section at y=1377.0nm
Å
75
50
25
0
0 1000 2000 3000 4000 5000 6000 7000 nm

3.3.3 Imaging a bilayer in HEPES buffers

Based on the available literature, HEPES is one of the most common buffers used to image planar bilayers on mica by AFM. To examine whether HEPES is suitable for my studies, a number of buffer solutions were prepared with several different concentrations of HEPES and NaCl to test whether they can be used to image the DEC221 bilayer on mica.

Five buffers were prepared at pH 7.3: I) 10 mM HEPES and 100 mM NaCl, II) 5 mM HEPES and 100 mM NaCl, III) 5 mM HEPES and 50 mM NaCl, IV) 2.5 mM HEPES and 100 mM NaCl, V) 2.5 mM HEPES and 50 mM NaCl. In all cases, the buffers were adjusted to pH 7.3 with 1 M NaOH and/or HCl. The buffering capacity for each buffer was tested to ensure that each buffer can maintain the pH in a reasonable range for at least one day. The buffering capacity was tested by placing 100 ml of the buffer solution in a 250 ml beaker (open top), and the pH was measured at the beginning and end of a 2 day period. The pH for all of the tested buffers did not deviate by more than 0.1 pH unit after a 2 day period. For AFM imaging purposes, all the buffer solutions were filtered with a 0.2 μm Milli-Pore filter before use to prevent any possible particulate contaminants that could appear in AFM images.

Each of the buffers was tested on an intact DEC221 bilayer on mica. Each DEC221 bilayer was prepared on mica by incubating 10 μg of lipid in 10 mM $CaCl_2$ for 1 hour in an AFM cell. After incubation, the AFM cell was washed with 100 ml of the HEPES buffer in question, and was subsequently imaged. The AFM images in Figure 3.4 compare the DEC221 bilayer imaged in pure water against five other HEPES buffers (I – V). In those buffers with higher concentration of HEPES and NaCl (buffer I & II), the liquid ordered phase was found as large and/or elongated domains. As the concentrations of HEPES and

Figure 3.4. The DEC221 bilayer was imaged by AFM in HEPES buffers at different concentrations of HEPES and NaCl at pH 7.3. The bilayer was prepared on mica by incubating 10 μg of lipid in 10 mM $CaCl_2$ for 1 hour in the AFM cell. After incubation, the AFM cell was washed with 100 ml of the following buffers at pH 7.3: I) 10 mM HEPES and 100 mM NaCl, II) 5 mM HEPES and 100 mM NaCl, III) 5 mM HEPES and 50 mM NaCl, IV) 2.5 mM HEPES and 100 mM NaCl, V) 2.5 mM HEPES and 50 mM NaCl. At all HEPES and NaCl concentrations tested, the lipid domains corresponding to the Lo phase are visible and the domains are approximately 12 Å tall. The domain height in different buffers may vary slightly (1 – 2 Å) due to the variation in the ionic strength.

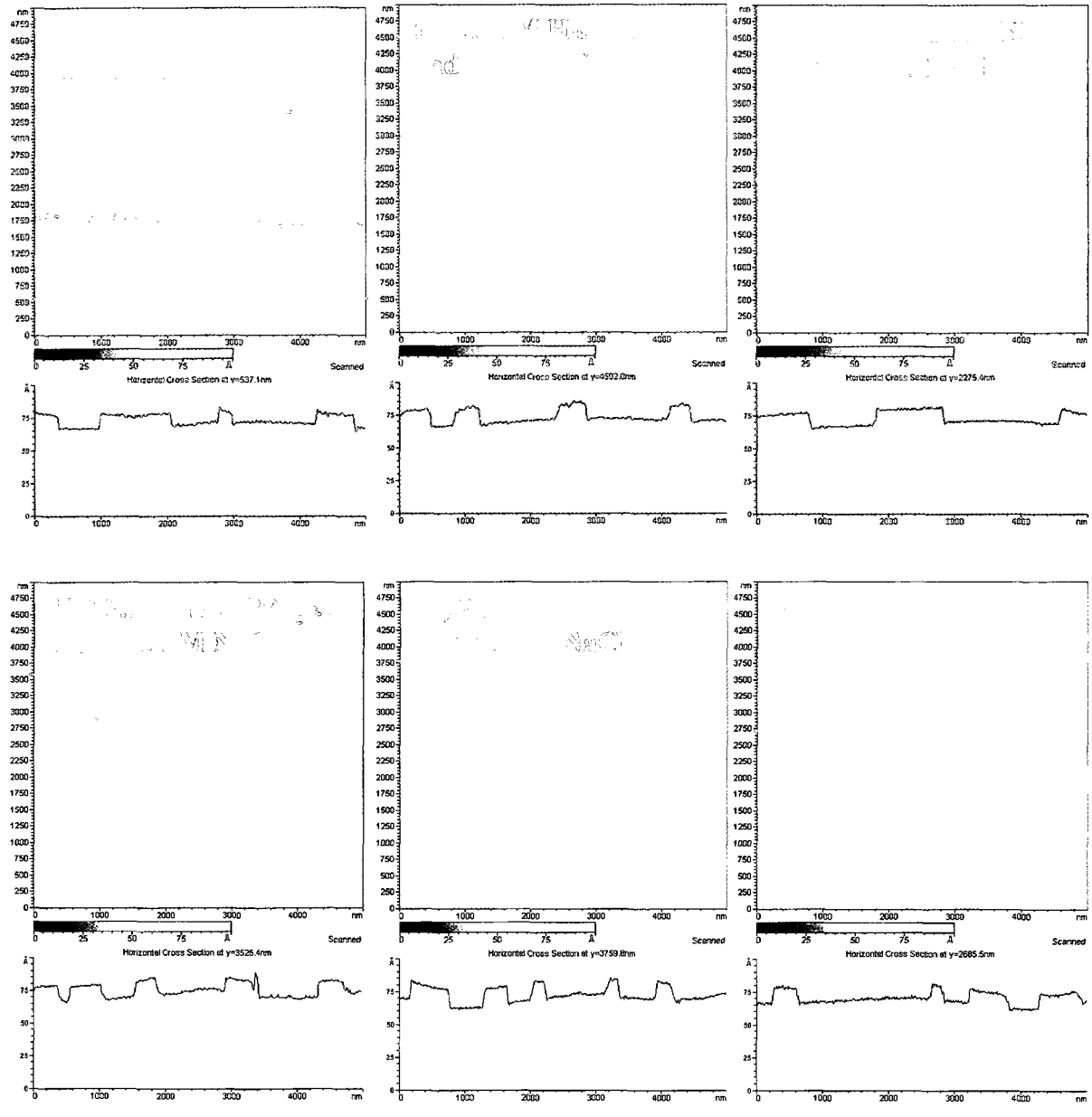
Horizontal Cross Section at y=537.1nm
Horizontal Cross Section at y=4502.0nm
Horizontal Cross Section at y=2275.4nm
Horizontal Cross Section at y=3525.4nm
Horizontal Cross Section at y=3759.8nm
Horizontal Cross Section at y=2685.5nm
Scanned
nm
Å

NaCl were lowered (i.e., buffer V), the domains in the DEC221 bilayer became smaller and somewhat rounder, and started to resemble the domains in pure water. The results suggest that both HEPES and NaCl concentration can affect the morphology of lipid bilayers on mica. The buffer with the lowest HEPES and NaCl concentration (buffer V) was selected as "the imaging buffer" to avoid the possible precipitation of salt due to the evaporation of water from the open AFM cell. Thus, the buffer containing 2.5 mM HEPES and 50 mM NaCl at pH 7.3 can potentially be used as a universal buffer to image all bilayers of interest in this study, including the reconstituted nAChR bilayer.

In summary, domains have been observed with all of the HEPES buffers tested here for the DEC221 bilayer. It appears that the concentration of both HEPES and NaCl can affect the morphology of the bilayer, with the observed effects increasing proportionally with the concentration of HEPES and NaCl. Therefore, the buffer with the lower HEPES (2.5 mM) and NaCl (50 mM) concentration was selected as a potential buffer to image all bilayers of interest. Whether this buffer can be used to image a reconstituted bilayer containing the nAChR remains to be tested. Only a buffer that can maintain the proper structure and function of the receptor can be used to image a reconstituted nAChR bilayer.

3.4 Imaging planar bilayers by TIRF microscopy

To validate the AFM data, the morphology of the bilayers on mica observed by AFM was examined by a different microscopy method. Fluorescence microscopy has been used to examine model bilayers extensively, since it can readily observe microdomains in the bilayer (Ira and Johnston, 2008; Veatch and Keller, 2003). Total internal reflection fluorescence (TIRF) microscopy was used along with AFM to inspect planar bilayers

prepared on mica. TIRF has the advantage of eliminating background fluorescence from fluorophores in the bulk solution.

3.4.1 A comparison between AFM and TIRF imaging

The ability of TIRF microscopy to image a planar bilayer on mica is compared to AFM by imaging POPC and DEC221 bilayers. Figure 3.5A and B are TIRF and AFM images of a POPC bilayer on mica. The bilayer was prepared by incubating sonicated unilamellar vesicles prepared with 0.2 mole% TR-DHPE for 1 hour in 10 mM $CaCl_2$ in an AFM or TIRF cell. To accommodate the size difference between the AFM and TIRF cell, 10 μg of lipid was used for AFM and 20 μg of lipid was used for TIRF. Following incubation, the sample was washed with 100 or 150 ml HEPES buffer for AFM and TIRF imaging, respectively. The observed AFM image shows that a POPC bilayer in the presence of 0.2 % TR-DHPE is still as flat and featureless as a pure POPC bilayer. The AFM image suggests that the presence of TR-DHPE did not alter the morphology of the bilayer. The TIRF image of a POPC bilayer in the presence of 0.2 % TR-DHPE showed a bilayer with reasonably uniform fluorescence, except for variation due to inhomogeneities in the excitation profile from the laser beam, based on visual inspection during alignment of the laser. The uniform fluorescence in the POPC bilayer suggests that the bilayer has only one phase (i.e. liquid disordered), which is characteristic of a POPC bilayer at room temperature. Evidently, the AFM and TIRF images of a POPC bilayer (doped with 0.2 % TR-DHPE) are both consistent with a uniform, fluid bilayer.

Figure 3.5C and D are TIRF and AFM images of a DEC221 bilayer on mica. In the AFM image, lipid domains ranging from 20 nm to 1 μm in diameter can be observed in the bilayer, and these domains are about 1 nm tall. The morphology of the DEC221 bilayer

Figure 3.5. AFM and TIRF images of a POPC (A and B) and DEC221 (C and D) planar bilayer on mica. The bilayer was prepared by incubating the sonicated unilamellar vesicles (doped with 0.2 mole% Texas Red DHPE) for 1 hour in 10 mM $CaCl_2$ in an AFM or TIRF cell. To accommodate the size difference between the AFM and TIRF cell, 10 μg of lipid was used for AFM experiments and 20 μg was used for TIRF. The sample was washed with HEPES buffer to remove unbound/excess materials following the incubation. The bilayers were subsequently imaged in HEPES.

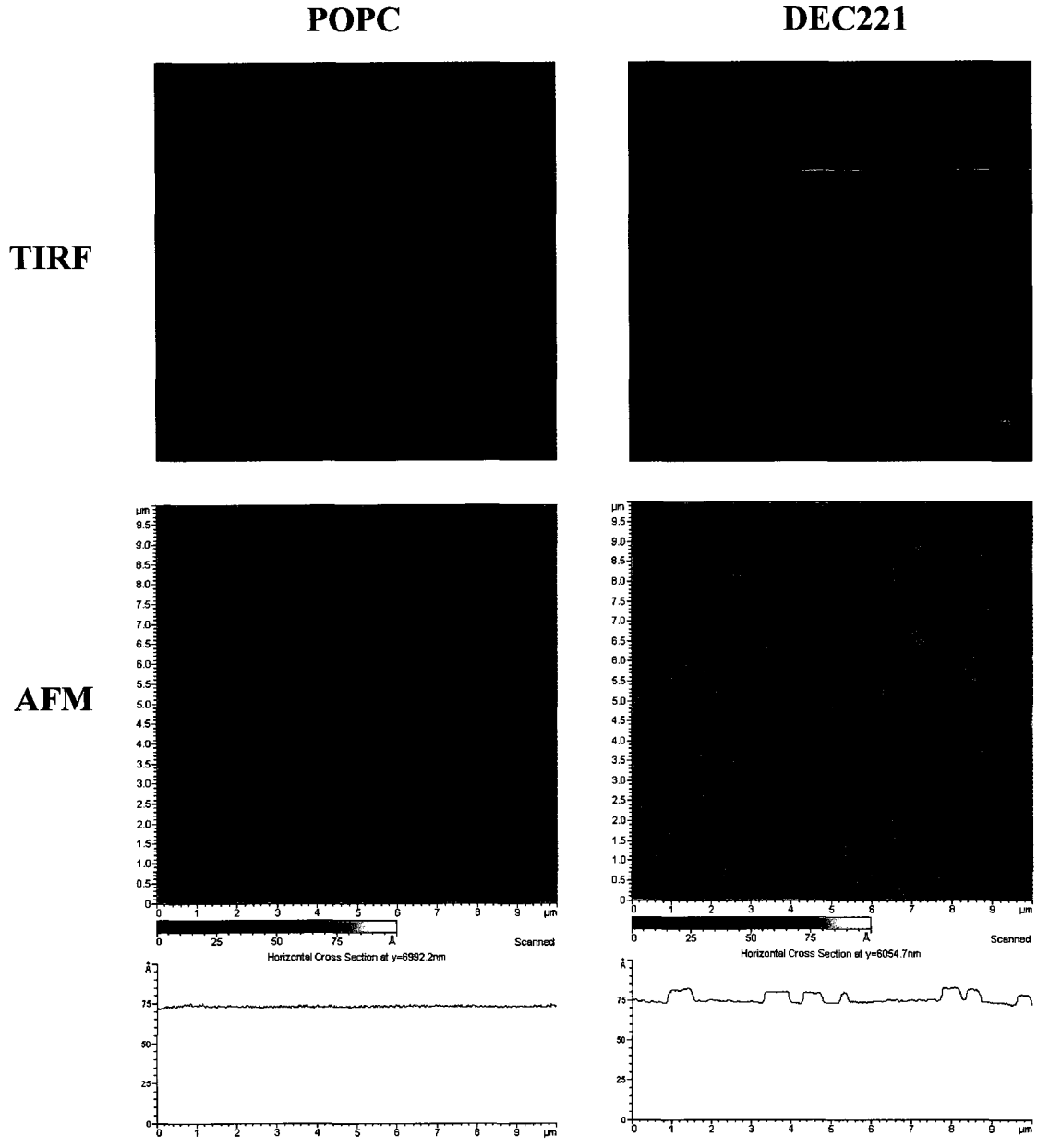
POPC
DEC221
TIRF
AFM
Horizontal Cross Section at y=6992.2nm
Horizontal Cross Section at y=6054.7nm
Scanned
Scanned

essentially remains the same in the presence of 0.2 % TR-DHPE. The DEC221 bilayer was similarly prepared and imaged by TIRF microscopy; Figure 3.5C shows that the bilayer has a number of round dark areas ranging from about 200 nm to 1 μm in diameter. The round dark areas are assigned to liquid-ordered domains based on previous fluorescence microscopy studies on bilayers of similar lipid mixtures (Ira and Johnston, 2008; Veatch and Keller, 2003). The lipid domains correspond to the segregation of cholesterol and sphingomyelin into the liquid ordered phase which separates from DOPC in the liquid disordered phase (Ira and Johnston, 2008; Veatch and Keller, 2003). Due to the limited resolution of TIRF, the perimeters of the lipid domains in the TIRF image are not as sharply defined as those in the AFM image. Moreover, those domains that are less than 200 nm cannot be observed because the optical resolution is limited to about 200 nm. Nevertheless, the AFM and TIRF images of a DEC221 bilayer prepared on mica appear very similar to one another.

3.5 Examining the reconstituted nAChR

The results thus far have demonstrated the successful preparation of lipid bilayers for TIRF and AFM imaging. However, not all buffers can be used to image bilayers on mica (i.e., TRB and TDB are not suitable to image bilayers on mica). It appears that HEPES is the most suitable buffer to image lipid bilayers on mica by AFM. Contradictorily, TRB and TDB are common buffers used in nAChR studies while HEPES had not been examined. Because the structure and function of the nAChR in a HEPES buffer was unknown, the functional capabilities of the nAChR in the HEPES buffer chosen for AFM and TIRF

imaging had to be examined. Thus, the next step was to reconstitute the nAChR in a bilayer, and determine if its structure or function was modified by the use of HEPES buffer.

3.5.1 Lipid and protein characterization for the reconstituted nAChR

The nAChR was reconstituted in a POPC bilayer at a L:P ratio of 1:2 (w/w) (see Material and Methods), and the protein and lipid profile of the reconstituted sample was characterized by SDS-PAGE and thin layer chromatography (TLC). According to the SDS-PAGE in Figure 3.6A, there were four bands of protein in the sample, which corresponded to the α, β, γ, and δ subunits of the *torpedo californica* nAChR (daCosta et al., 2002; Raftery et al., 1980; Weill et al., 1974). The purity of the reconstituted protein was greater than 95 % and all subsequent reconstitutions had similar purity, confirming the successful purification and reconstitution of the nAChR.

To characterize the lipid content of the POPC/nAChR sample reconstituted at a L:P ratio of 1:2 (w/w), lipid was extracted from the proteoliposomes according to the Bligh and Dyer method of lipid extraction (Bligh and Dyer, 1959), and the extracted lipid was then examined by TLC. The TLC result showed that the reconstituted POPC/nAChR proteoliposome contained mainly POPC (Figure 3.6B). Therefore, the combined results suggested that the nAChR was reconstituted in the desired bilayer.

3.5.2. Comparing the functional state of the nAChR reconstituted with POPC/POPC/Chol (3:1:1) and POPC lipids

The ability of the nAChR to bind its ligand and undergo allosteric transition, which reflects the ion channel functionality, was examined by FTIR *difference* spectroscopy. This technique can detect minute conformational changes in the reconstituted protein after ligand

Figure 3.6. Protein and lipid characterization of the reconstituted POPC/nAChR sample by SDS-PAGE (A) and thin layer chromatography (B), respectively.

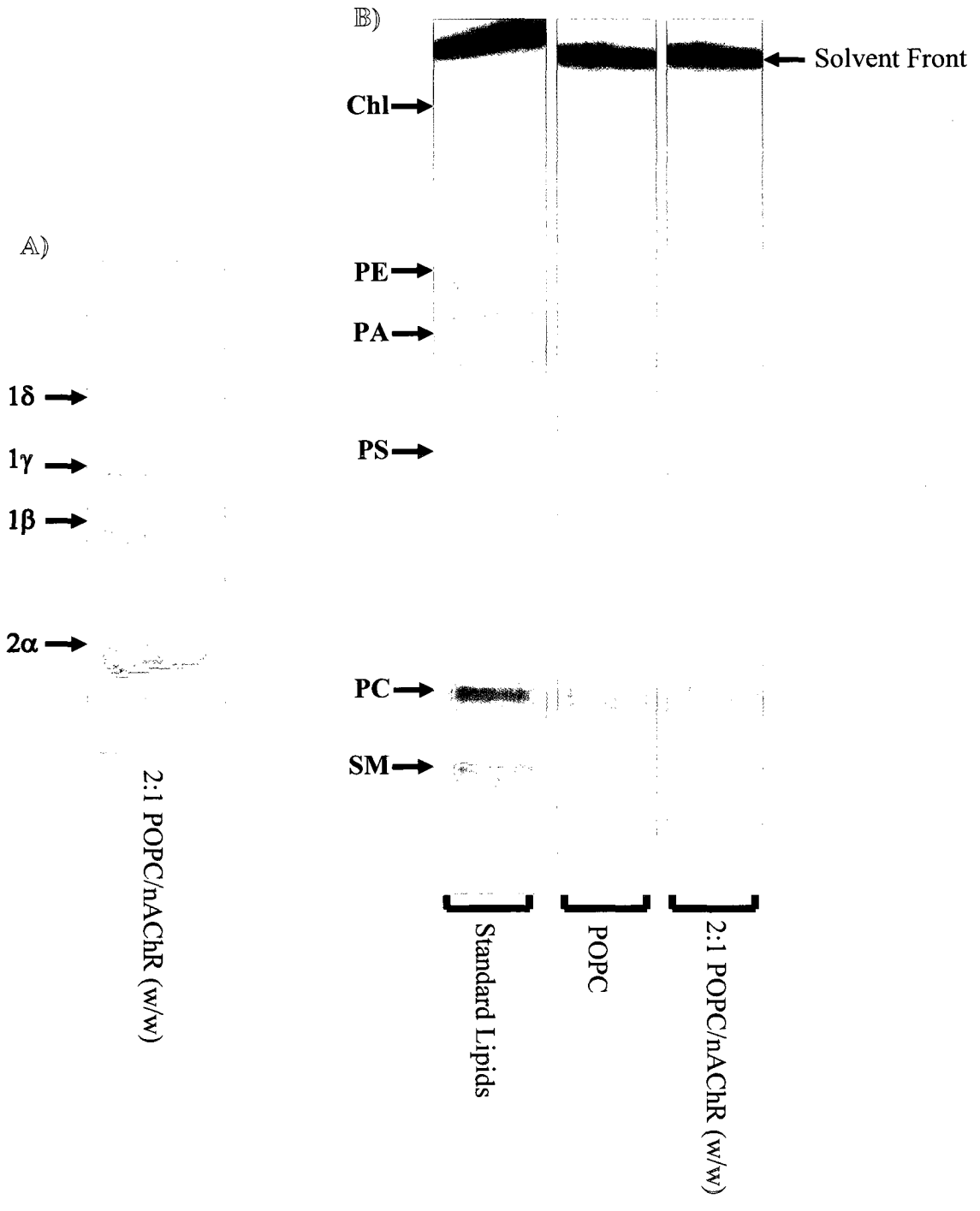
A)
1δ
1γ
1β
2α
2:1 POPC/nAChR (w/w)
B)
Chl
PE
PA
PS
PC
SM
Solvent Front
Standard Lipids
POPC
2:1 POPC/nAChR (w/w)

Figure 3.7. The FTIR difference spectra of the nAChR reconstituted with POPC (bottom) and POPC/POPA/Chol (3:1:1 mol/mol) (top) lipids at a L:P ratio of about 1:2 (w/w), and was examined in *Torpedo* Ringer (TRB) buffer. The two medium positive intensity bands found at 1720 and 1530 cm^{-1} respectively indicate that carbamylcholine (a ligand) has bound to the protein (Beanziger et al., 2000) and the ligand is interacting with the receptor via a tyrosine residue at the ligand binding site (Osaka et al., 1998). The presence of two strong positive intensity bands at 1655 and 1547 cm^{-1} indicate that a shift in the peptide backbone of the reconstituted nAChR has occurred upon the binding of the ligand, which implies the reconstituted nAChR can undergo conformational change (i.e., from resting to desensitized).

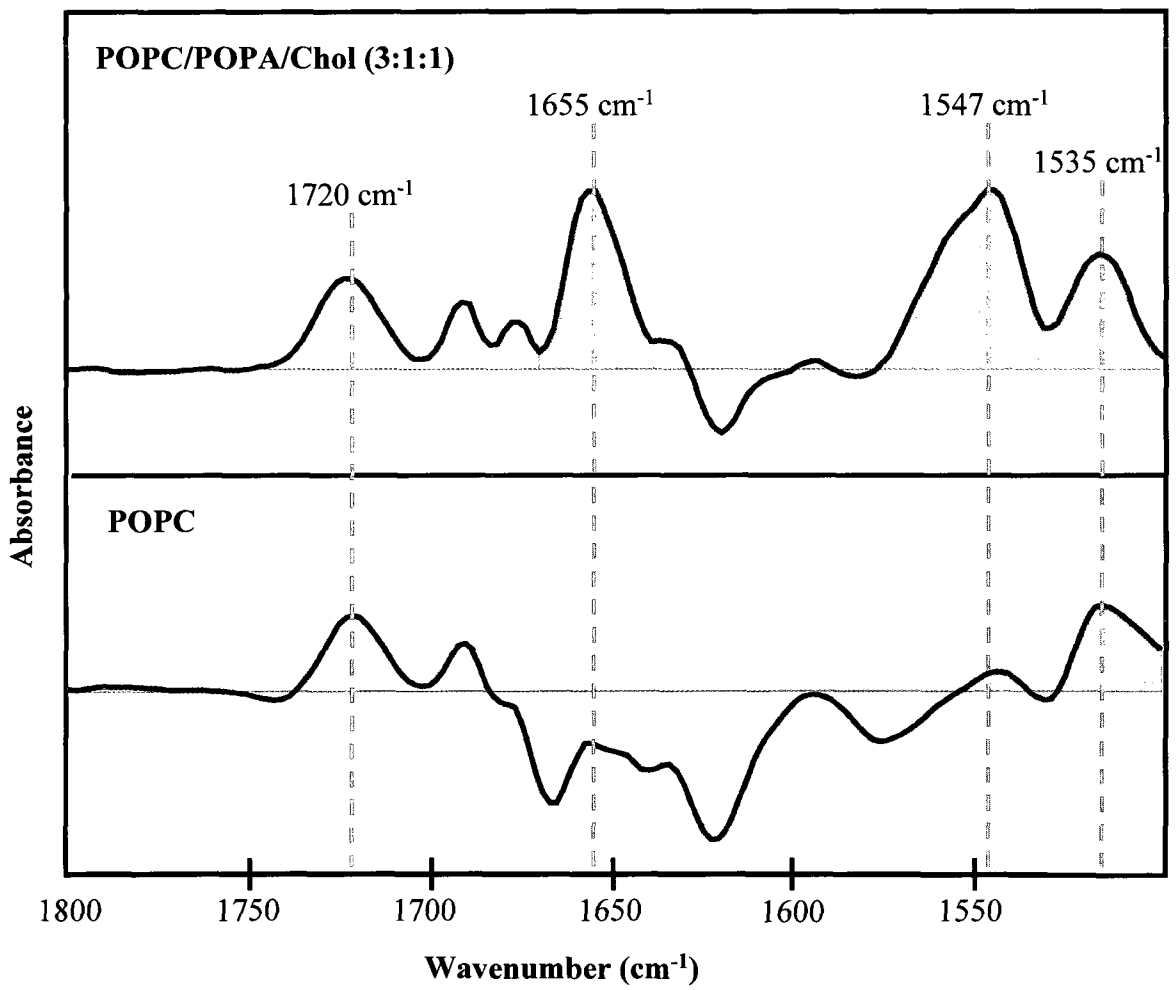
POPC/POPA/Chol (3:1:1)
1655 cm-1
1547 cm-1
1535 cm-1
1720 cm-1
POPC
Absorbance
1800
1750
1700
1650
1600
1550
Wavenumber (cm-1)

binding (Baenziger et al., 1992a; Baenziger et al., 1992b). The top spectrum in Figure 3.7 is a FTIR *difference* spectrum of the nAChR reconstituted with the POPC/POPA/Chol (3:1:1) lipid mixture at the L:P ratio of 1:2 (w/w). This spectrum contains a pattern of positive and negative bands indicative of a conformational change of the nAChR upon exposure to the agonist carbamylcholine (Carb). The medium positive intensity bands at 1720 cm^{-1} indicate Carb has bound to the protein (Baenziger et al., 2000) and the ligand is interacting with the receptor via a tyrosine residue at the ligand binding site (Osaka et al., 1998). The two strong positive intensity bands at 1655 and 1547 cm^{-1} reflect a shift in the amide I and II vibration of the protein backbone, which implies a conformational change (from resting to desensitized) in the nAChR upon the binding of Carb. This result agrees well with previous studies showing that the ability of the receptor to undergo conformational change when reconstituted with a lipid mixture of POPC/POPA/Chol (3:1:1) is similar to the nAChR in its native membrane (Ryan et al., 1996). Hence, the receptor is mainly in the resting state when it is reconstituted with the POPC/POPA/Chol (3:1:1) lipid mixture (daCosta et al., 2002; Ryan et al., 1996).

The FTIR *difference* spectrum at the bottom of Figure 3.7 corresponds to the nAChR reconstituted in a POPC bilayer at the L:P ratio of 1:2 (w/w). The two medium bands observed at 1720 and 1530 cm^{-1} indicate the receptor can bind Carb when reconstituted in a POPC membrane. However, the lack of two strong positive bands at 1655 and 1547 cm^{-1} implies the receptor did not undergo conformational change upon the binding of ligand. The *difference* spectrum here is consistent with previous data in my lab for the nAChR reconstituted in a POPC membrane (Baenziger et al., 2000; daCosta et al., 2002; Ryan et al., 1996), where the receptor is expected to be in an uncoupled conformation (Dacosta and

Baenziger, 2009). Based on the results, the nAChR that I reconstituted with POPC/POPA/Chol (3:1:1) and POPC has similar structural conformation with previous studies.

3.5.3. Comparing the functional state of the reconstituted nAChR in the selected HEPES buffer for AFM imaging and TRB

After screening a number of buffers for AFM imaging earlier in this chapter, the buffer which contains 2.5 mM HEPES and 50 mM NaCl at pH7.3 was selected as a potential buffer for imaging both lipid alone and lipid-protein bilayers on mica. Whether this buffer can provide a satisfactory environment to maintain the proper structure and function of a reconstituted nAChR was yet to be determined. Hence, the functional state of the nAChR in the HEPES buffer was compared against a buffer that has been used to study the receptor (i.e., *Torpedo* Ringer buffer).

The top FTIR *difference* spectrum in Figure 3.8 belongs to the nAChR reconstituted with a lipid mixture of POPC/POPA/Chol (3:1:1) and was examined in TRB. This spectrum shows the presence of two strong positive intensity bands at 1655 and 1547 cm^{-1}, indicating that the nAChR can undergo conformational change in the presence of Carb; hence the receptor is in the resting state. This agrees well with the previous results. When the *difference* spectrum of the nAChR was recorded in the HEPES buffer (second spectrum from the top in Figure 3.8), it was very similar to that of TRB. This observation suggested that the nAChR reconstituted with the lipid mixture POPC/POPA/Chol has a similar structural conformation whether it is in TRB or HEPES buffer.

On the other hand, the nAChR is known to be in an uncoupled conformation when reconstituted in a POPC bilayer (daCosta and Baenziger, 2009; daCosta et al., 2002). The

Figure 3.8. A comparison of the structural state of the reconstituted nAChR in a HEPES buffer against the Torpedo Ringer buffer. FTIR *difference* spectra of the nAChR reconstituted with POPC/POPA/Chol (3:1:1), POPC and DOPC/eggSM/Chol (2:2:1) lipids mixture at an approximate L:P of 1:2 (w/w) examined in a HEPES (2.5 mM HEPES, 50 mM NaCl, pH 7.03) and *Torpedo* Ringer buffer (20 mM Tris, 250 mM NaCl, 5 mM KCl, 2 mM $MgCl_2$, 3 mM $CaCl_2$, 0.001% NaN_3, pH 7.03).

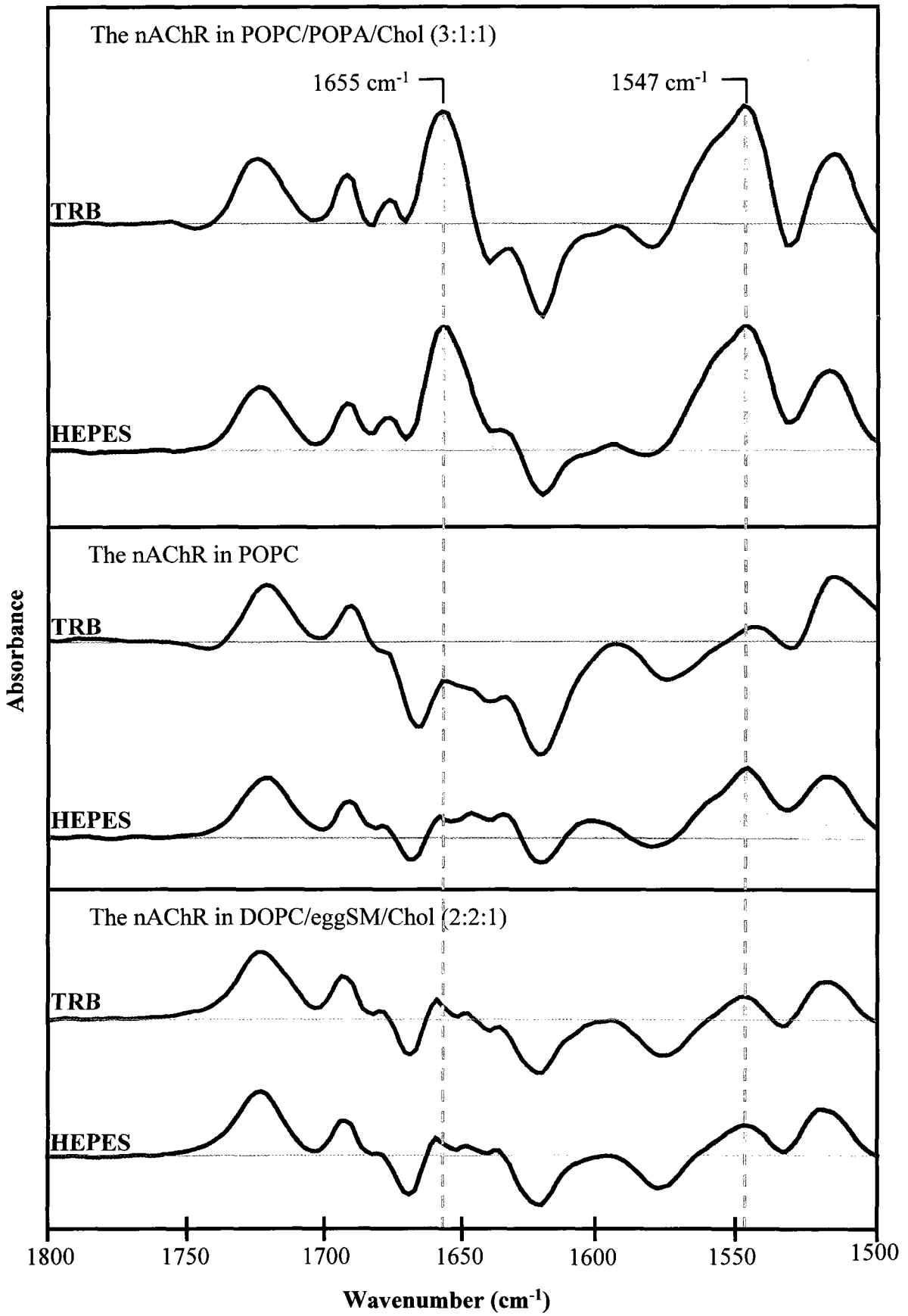
The nAChR in POPC/POPA/Chol (3:1:1)
1655 cm-1
1547 cm-1
TRB
HEPES
The nAChR in POPC
TRB
HEPES
The nAChR in DOPC/eggSM/Chol (2:2:1)
TRB
HEPES
Absorbance
1800
1750
1700
1650
1600
1550
1500
Wavenumber (cm-1)

two middle spectra in Figure 3.8 correspond to the nAChR reconstituted in POPC and examined in TRB and HEPES buffer, respectively. The two spectra are similar, but a slight difference (due to baseline distortions) can be observed in the 1550 and 1650 cm^{-1} region, and the distortions were not corrected. Previous experiences in my laboratory on FTIR *difference* spectroscopy found that baseline distortion is a typical phenomenon that can arise from artifacts such as minute temperature variation and/or loss of sample in the flowing buffer. The spectrum recorded in HEPES buffer showed a small band at 1547 cm^{-1} and there is a dip in the TRB spectrum at 1655 cm^{-1}. It can be debated if there is a difference in the conformational state of the receptor in TRB and HEPES buffer or the observed difference in the spectra may be due to baseline distortions. However, the absence of two strong positive bands at 1655 and 1547 cm^{-1} in the *difference* spectra in both TRB and HEPES buffer, suggested that the receptor is uncoupled in a POPC membrane regardless of the buffer used. The presence of the 1720 and 1530 cm^{-1} positive band in both buffers suggested that the receptor could still bind Carb but it can not undergo conformational change (Baenziger et al., 2000; daCosta et al., 2002; Ryan et al., 1996). Therefore, the conformational state of the nAChR reconstituted into a POPC membrane appears similar in TRB and HEPES buffer (i.e., the receptor is in an uncoupled conformation).

The structural state of the nAChR was also examined when reconstituted with a DOPC/eggSM/Chol (2:2:1) lipid mixture, which is known to form a phase-separated bilayer with liquid-ordered domains (Veatch and Keller, 2003). Although the functional state of the nAChR reconstituted with this lipid mixture has never been studied, the observed *difference* spectrum suggested that the receptor can not undergo conformational change upon the binding of Carb whether it was in TRB or HEPES buffer (two bottom spectra in Figure 3.8).

Positive intensity bands at 1655 and 1547 cm^{-1} were not observed in either buffer, and the *difference* spectra of the protein are almost identical in both buffers. These results suggested that the conformational state of the nAChR when reconstituted with a DOPC/eggSM/Chol (2:1:1) lipid mixture is similar in TRB or HEPES buffer.

In summary, the nAChR is in the resting conformation when it is reconstituted with a POPC/POPA/Chol (3:1:1) lipid mixture in either TRB or HEPES buffers. In contrast, the receptor is in a desensitized-like conformation when reconstituted with POPC or DOPC/eggSM/Chol (2:2:1), regardless of the buffer used. Such results suggest that the structural state of the nAChR is unaffected by the buffer. Therefore, the 2.5 mM HEPES and 50 mM NaCl buffer at pH 7.3 can be used to study the nAChR.

3.5.4. Initial attempts to image the reconstituted nAChR by AFM

For AFM imaging, the reconstituted sample was prepared on mica in a manner similar to that of the lipid alone sample, as described earlier. Briefly, 10 μg of lipid from the reconstituted sample was incubated on freshly cleaved mica in an AFM cell for 1 hour at room temperature in TDB buffer in the presence of 10 mM $CaCl_2$. Following the incubation period the AFM cell was washed with 50 ml of buffer to remove the unbound material on the mica, and the prepared sample was subsequently imaged.

The AFM images from Figure 3.9 show a sample prepared from a reconstituted nAChR sample using the lipid mixture of POPC/POPA (3:2 mol/mol) at the lipid to protein ratio of 1:2 (w/w). The AFM images show a number of particles ranging from 60 to 500 nm in size. These observed particles are much larger than expected for the size of a nAChR, which is about 9 nm in diameter. Moreover, the AFM images are rather fuzzy and the observed particles have identical shadows beside them. These shadows indicate a double tip

Figure 3.9. Imaging a sample on mica prepared from a reconstituted nAChR sample using the lipid mixture of POPC/POPA (3:2 mol/mol) at the lipid to protein ratio of 1:2 (w/w). The sample was prepared on mica by incubating 10 μg of lipid for 1 hour in 10 mM $CaCl_2$. Following incubation, the unabsorbed materials are washed off with water.

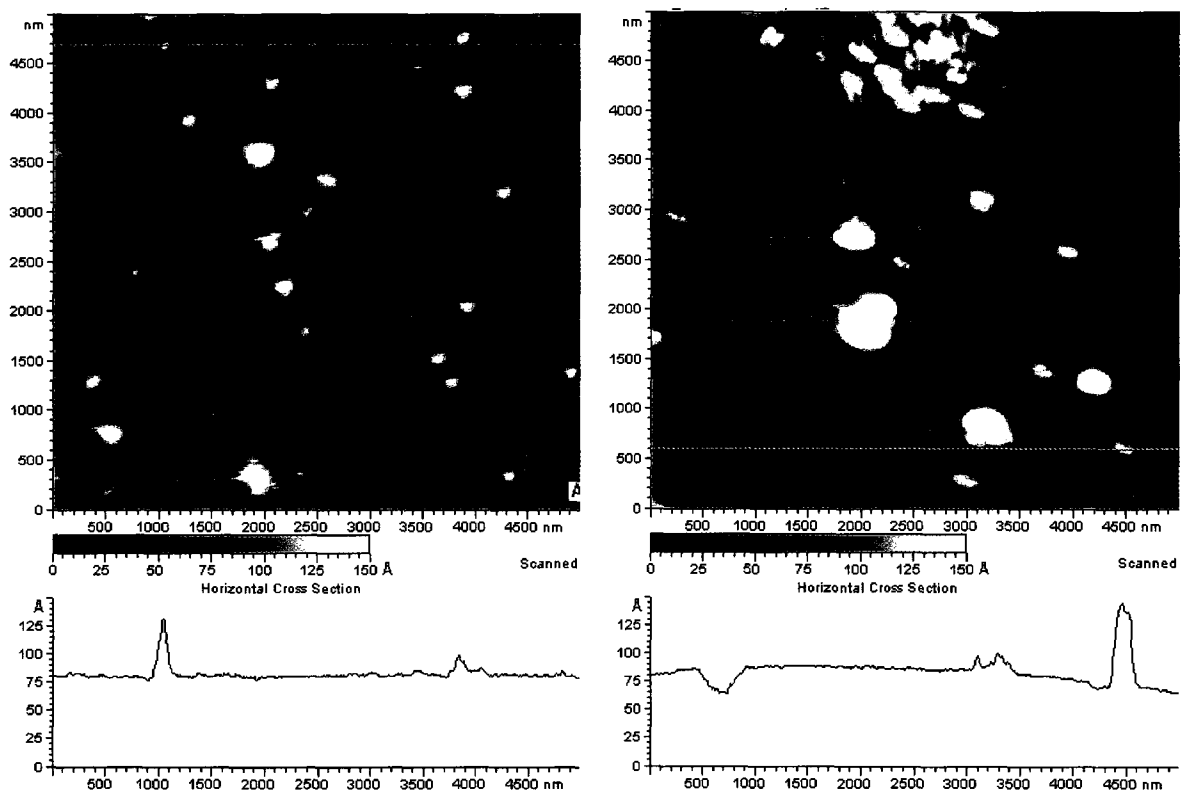
nm
4500
4000
3500
3000
2500
2000
1500
1000
500
0
500 1000 1500 2000 2500 3000 3500 4000 4500 nm
0 25 50 75 100 125 150 Å
Scanned
Horizontal Cross Section
Å
125
100
75
50
25
0
500 1000 1500 2000 2500 3000 3500 4000 4500 nm

image, which is an artifact that arises from contamination of the AFM tip; the extent of the shadow reflects the size of the contaminant particle stuck to the tip. Note also that the similar orientation of the double features is characteristic of an artifact. It is not possible to identify the nAChR in these images. These poor quality images implied that the sample was not optimally prepared for AFM imaging. However, these were the best images that could be acquired from repeated trials. Cleaning the AFM tip (by extensive washing with 70 % ethanol, water and HEPES buffer) or replacing the contaminated tip with a new AFM tip did not result in better images because the tip was immediately contaminated as soon as it contacted the sample. Consequently, the prepared samples can not be interpreted by AFM imaging. These early results indicate that the preparation of a proper reconstituted nAChR bilayer on mica for AFM imaging can be difficult. This is not too surprising due to the lack of information in the literature on the parameters required to prepare a bilayer containing a reconstituted integral membrane protein. For this reason, a more systematic approach was devised to prepare a reconstituted nAChR bilayer on mica for AFM imaging. At this point I decided to develop a method to reconstitute the nAChR in a simple, one-component lipid bilayer (i.e., POPC) that was suitable for AFM imaging. Upon success, the same protocol may be used to image the nAChR reconstituted in more complex lipid mixtures. Therefore, the main objective of this study became imaging the nAChR reconstituted in a POPC bilayer by AFM.

3.6 Discussion and Conclusions

The results in this chapter have demonstrated that planar bilayers such as POPC (non-domain-forming) and DEC221 (domain forming) can be prepared on mica for AFM

imaging. When a POPC bilayer was imaged in water, it is about 45 Å thick and it appears as a flat and featureless bilayer by AFM. These observations are expected for a single lipid component bilayer in the liquid disordered phase. In contrast, when the DEC221 bilayer was imaged in water, lipid domains that are about 12 Å can be found protruding out of the bilayer. These domains correspond to the liquid ordered phase (composed mainly of cholesterol and sphingomyelin) in the bilayer. The remaining area of the DEC221 bilayer corresponds to the liquid disordered phase, which is composed mainly of disordered lipid (DOPC in this case) and it is ~45 Å thick. The results demonstrated that the AFM can image and distinguish clearly the difference between raft and non-raft bilayers in water.

The main objective was to image a reconstituted nAChR bilayer by AFM, and the bilayer should be imaged in a buffer that can maintain the proper structure and function of the protein. The TRB was initially chosen because it has been used extensively to examine the structure of the nAChR. However, the presence of calcium and phosphate and the high NaCl content in the buffer appear to cause precipitation of salt on the planar bilayer (Figure 3.2). Consequently, the TRB was eliminated from my list of potential buffers for AFM imaging.

The next buffer selected was TDB because it is one of the buffers that has been used to store reconstituted nAChR. However, the lipid domains in the DEC221 bilayer could not be observed when the bilayer was imaged in TDB (Figure 3.3). In addition, there were defects and debris on the bilayer after it was exposed to TDB. In a recent ellipsometry study of lipid bilayer formation, the authors suggested that the Tris buffer they used (50 mM Tris and 100 mM NaCl at pH 7.4) destabilized planar bilayers on mica (Benes et al., 2004). As my findings coincided with their results indicating that Tris buffers are not suitable for

forming stable bilayers on mica, I had to search for alternate buffers to image bilayers on mica.

Based on the available literature, HEPES is one of the most common buffers used to image planar bilayers on mica by AFM. The results showed that the liquid ordered phase/domains of the DEC221 bilayer can be observed by AFM in HEPES buffers (Figure 3.4). The results also showed that high concentrations of HEPES or NaCl elongate the shape of the domains. However, the domains appear similar to those in water when the HEPES and NaCl concentrations are low. For this project, I decided to use the buffer with a low concentration of HEPES (2.5 mM) and NaCl (50 mM) at pH 7.03 to avoid any potential side effect from the salt or buffer.

Examining how Tris and HEPES affect the formation and morphology of supported bilayers on mica, however, could be interesting for future studies. In this regard, one could compare the physical and chemical differences between Tris and HEPES to determine how these two buffers affected a supported planar bilayer on mica. Tris and HEPES are very different in size, shape, pKa and charge at pH 7 (see Figure 3.10). The molecular weight of Tris (121 g/mole) is almost half of HEPES (238 g/mole). The shape of Tris is tetrahedral, whereas HEPES is slightly planar and elongated. The pKa of Tris is about 8.0 and HEPES is 7.5. Finally, Tris is positively charged at pH 7, whereas HEPES is negatively charged at the same pH.

The structure of the nAChR was normally examined in TRB in my lab, but TRB was unsuitable for AFM imaging. Fortunately, HEPES buffers can be used for AFM imaging, but switching from TRB to HEPES buffer was a concern regarding the protein structure/function because the ionic strength in TRB is much greater than HEPES buffer. I

Figure 3.10. The structural and chemical differences between HEPES and Tris buffer provided by Sigma Aldrich.

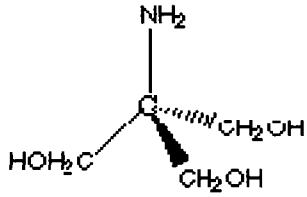

Trizma
Molecular weight: 121 g/mole
pKa: 8.06 (buffer range: pH 7.5 – 9.0)
Net charge at pH 7.3: positive

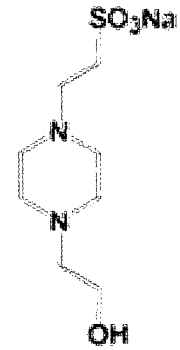

HEPES
Molecular weight: 238 g/mol
pKa: 7.48 (buffer range: pH 6.8 – 8.2)
Net charge at pH 7.3: negative

was not certain whether the decrease in the ionic strength of the buffer would alter the conformation of the nAChR, and the change needed to be assessed. The FTIR *difference* spectra of the nAChR (reconstituted in three different bilayers) are similar in TRB and HEPES buffers. The low ionic strength HEPES buffer does not appear to alter the conformation of the reconstituted nAChR. Thus, the result from FTIR *difference* spectroscopy suggested that the buffer with 2.5 mM HEPES and 50 mM NaCl at pH 7.3 can be used to image a bilayer containing the nAChR without affecting the receptor structure.

To validate the observation of a membrane by AFM, TIRF microscopy was used to image the POPC and DOPC/eggSM/Chol (2:2:1) bilayers prepared on mica. These two bilayers can be imaged by TIRF microscopy by doping a small amount of fluorescent lipid (e.g., 0.2 % TR-DHPE) into the vesicles used to prepare the bilayer. A POPC alone bilayer appears flat and featureless by AFM (Figure 3.5C) and the TIRF image (Figure 3.5D) shows that the TR-DHPE dye is evenly distributed in a POPC bilayer. Thus, both microscopy techniques confirm that a POPC bilayer has only one phase. When imaging the DOPC/eggSM/Chol 2:2:1 bilayer by either AFM or TIRF (Figure 3.5B and A), lipid domains that are depleted in TR-DHPE can be observed in the bilayer. However, the resolution of the TIRF image is much poorer than that of AFM. Importantly, these results show that fluorescent-labeled molecules in a planar bilayer on mica can be reliably detected by TIRF. Therefore, TIRF microscopy should be useful to validate later studies involving the nAChR reconstituted in a bilayer, where the presence of the nAChR in a bilayer can be detected if the receptor is fluorescently labeled.

Chapter 4: Reconstituting the nAChR in a POPC bilayer for AFM imaging

4.1 Introduction

With the goal of preparing a reconstituted nAChR bilayer amenable for AFM imaging, I planned to reconstitute the nAChR in a simple POPC bilayer at a high lipid to protein (L:P) ratio. I have two reasons to reconstitute the receptor at high L:P ratio. First, I have demonstrated that a bilayer can be prepared on mica from pure lipid vesicles and that the bilayer can be subsequently imaged by AFM. Thus, preparation and imaging of a reconstituted nAChR bilayer is more likely to be successful if the receptor is reconstituted in a liposome that has similar properties to a lipid-alone liposome (i.e., a proteoliposome with low protein density). Another reason to reconstitute the nAChR at high L:P ratio is to ensure that the AFM will be able to clearly distinguish protein from the surrounding lipid bilayer. This factor is important for later experiments to determine if the nAChR can segregate lipid into domains in a membrane. To resolve the lipid and protein molecules in the plane of a bilayer, the size of the AFM tip and the distance between 2 proteins in the bilayer must be considered. I made a rough calculation to estimate the spacing distance between 2 receptors in a POPC planar bilayer reconstituted at a given L:P ratio (see Figure 4.1); the nAChR is about 280 000 Da in molecular weight and has a diameter of about 9 nm based on electron microscopy data (Unwin, 2005), and POPC is 760 Da with a diameter of about 0.9 nm (Lewis and Engelman, 1983). Based on my rough calculation which assumes equal spacing between individual proteins, when the L:P ratio is 100:1 (w/w), the expected distance between two nAChR (edge to edge) in a POPC bilayer is about 110 nm in the X or Y direction. Considering that the AFM tip (MAC mode Type II) is about 10 – 14 nm in diameter and has a cone angle of 20° at the apex of the tip, reconstituting the nAChR at a L:P ratio of 100:1 (w/w) or greater should allow observation of individual reconstituted

Figure 4.1. A rough calculation for the spacing of the nAChR in a POPC planar bilayer. The nAChR (MW = 280, 000 Da) is about 90 Å wide in diameter based on the cryoEM structure of Unwin 2005, and the POPC (MW = 760 Da) is about 9Å in diameter (Lewis and Engelman, 1983). I drew a scaled cartoon of the nAChR in a POPC bilayer to estimate the spacing distance between 2 receptors at a given L:P ratio (top). An equation (bottom) is then derived to predict the relationship between the reconstituted L:P ratio and the spacing distance between 2 nAChR in the X or Y direction, assuming the receptor is evenly spread in the bilayer.

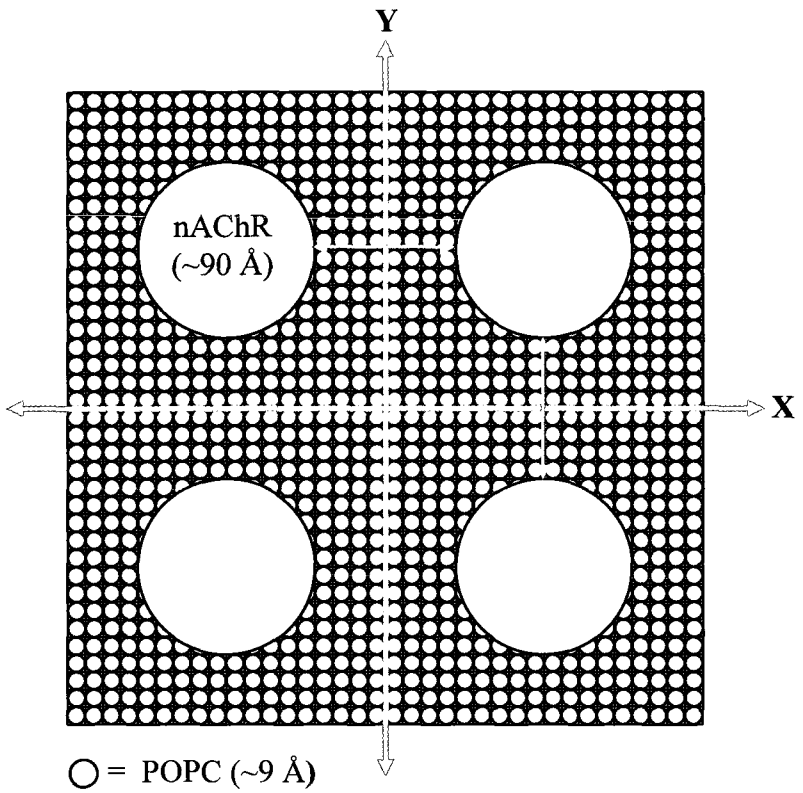
Y
nAChR
(~90 Å)
X
○ = POPC (~9 Å)

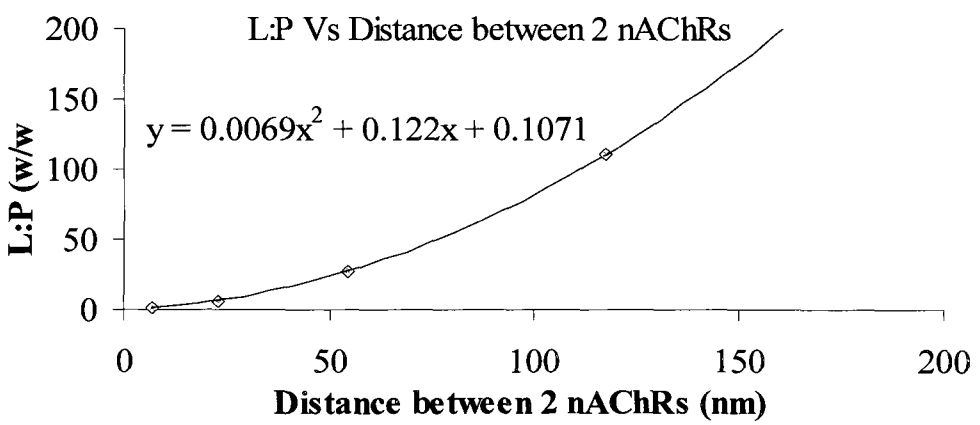
L:P Vs Distance between 2 nAChRs
y = 0.0069x2 + 0.122x + 0.1071
L:P (w/w
200
150
100
50
0
0
50
100
150
200
Distance between 2 nAChRs (nm)

proteins. Thus, I attempted to increase the L:P ratio of the reconstituted sample.

4.2. An attempt to prepare a POPC/nAChR bilayer for AFM imaging

The L:P ratio of the reconstituted sample was initially increased by simply increasing the lipid concentration of the solution used to elute the protein from the affinity column as described in Materials and Methods. In theory, the increase in the lipid content used in the reconstitution should not affect the structure or function of the nAChR, but confirmation was needed before attempting to prepare a bilayer at high L:P ratio on mica for AFM imaging.

4.2.1. Examining the function of the nAChR reconstituted at a higher L:P ratio

The structural conformation of the receptor reconstituted at a higher L:P ratio was compared to a sample reconstituted at low L:P ratio by FTIR *difference* spectroscopy. The top and middle spectrum in Figure 4.2 belongs to the nAChR reconstituted at the L:P ratio of 1:2 and 10:1, respectively. The intensity of all bands in the spectrum was very weak in the 10:1 L:P ratio reconstitution. This is not a surprise because the reconstitution at a L:P ratio of 10:1 contains 20 times more lipid than the reconstitution at a L:P ratio of 1:2 with an equal protein loading. Thus, the effective amount of protein near the surface of the germanium crystal to absorb the evanescence wave (which decays exponentially from the crystal's surface) in the higher L:P ratio reconstitution is much less than that of the lower L:P ratio. Consequently the signal from the protein becomes inversely proportional to the L:P ratio of the reconstituted sample. To better compare the *difference* spectrum between the low and high L:P ratio sample, the spectrum was normalized; this was done by stretching

Figure 4.2. The function of the nAChR reconstituted at 20 times higher lipid concentration than normal was examined by FTIR *difference* spectroscopy. The nAChR was reconstituted with a lipid mixture of POPC/POPA/Chol (3:1:1) at the L:P ratio of 1:2 (top spectrum) and 10:1 w/w (bottom two spectra). The spectral signal from the protein is very weak in the 10:1 L:P ratio reconstitution (middle spectrum), and the protein signal was normalized by expanding the spectrum until the ligand binding band at 1720 cm^{-1} of the 10:1 is equivalent to the 1:2 L:P ratio reconstitution (bottom spectrum).

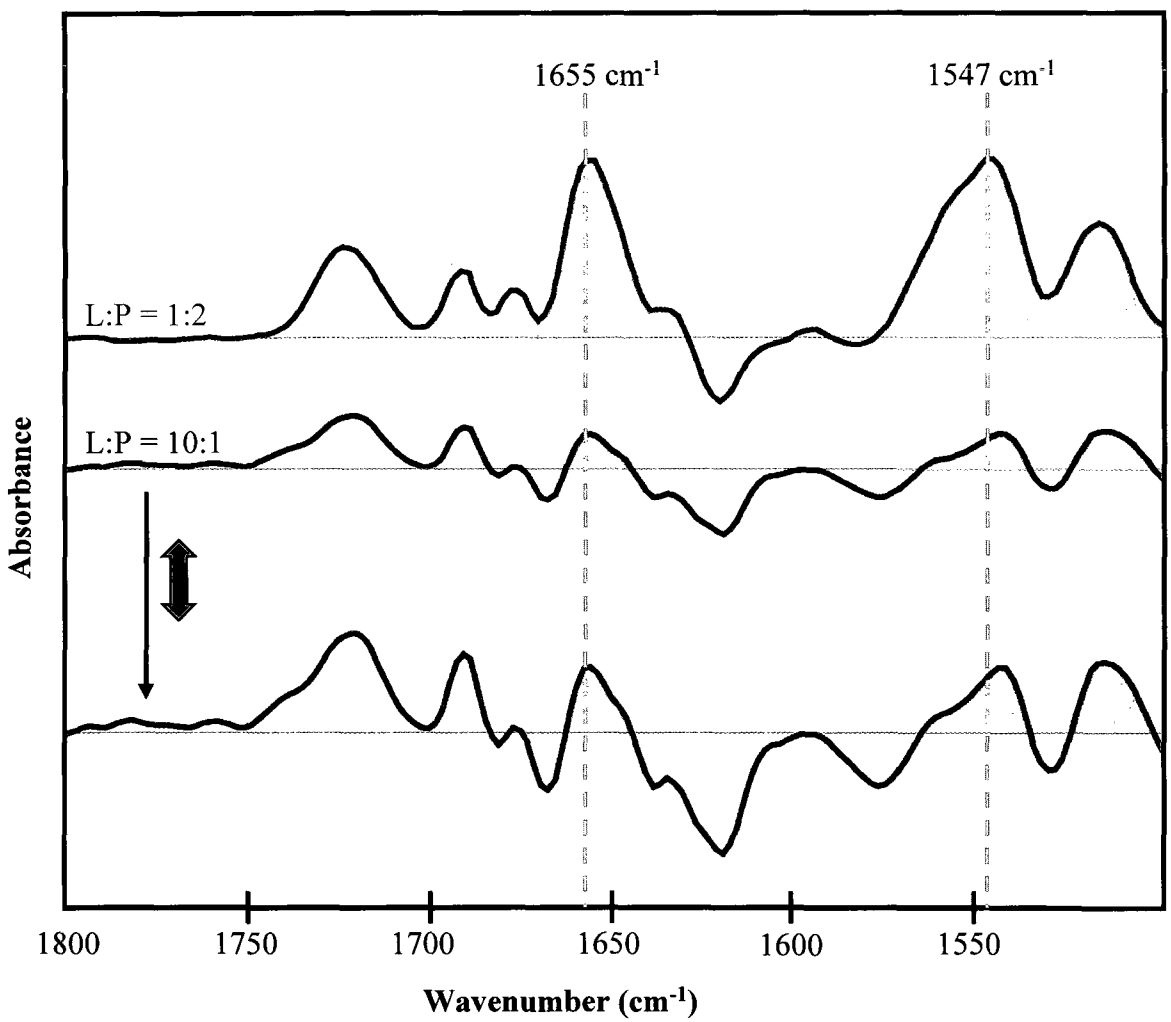
1655 cm-1
1547 cm-1
L:P = 1:2
L:P = 10:1
Absorbance
1800
1750
1700
1650
1600
1550
Wavenumber (cm-1)

out the Carb band at 1720 cm^{-1} for the 10:1 L:P ratio reconstitution until the intensity of the Carb band is similar to that of the 1:2 L:P ratio reconstitution. The bottom spectrum in Figure 4.2 is the stretched *difference* spectrum for the 10:1 L:P ratio reconstitution. This spectrum has a slight negative distortion near the 1600 cm^{-1} region, but two positive bands at 1655 and 1547 cm^{-1} can be definitely observed. The presence of these two positive bands indicates that the structural state of the nAChR remains similar, if not the same, when its density in the membrane decreases by an order of magnitude.

To summarize, the signal from FTIR *difference* spectroscopy is weak at a L:P ratio of 10:1 (w/w), which is about 20 times the lipid concentration for a typical reconstitution done in my lab. However, the FTIR spectra are similar for both concentrations. Based on this observation, I assumed that the receptor conformation would not change at higher L:P ratio (i.e., 100:1 or more). Furthermore, the FTIR *difference* spectroscopy technique cannot be used on a sample reconstituted with a significantly higher L:P ratio (i.e. 100:1); this experiment was attempted but the spectrum was highly distorted and noisy (data not shown) and could not be interpreted.

4.2.2. AFM imaging of a sample reconstituted at a L:P ratio of 100:1 (w/w)

The nAChR was reconstituted in a POPC bilayer at a L:P ratio of 100:1 (w/w) by increasing the concentration of lipid as described in Materials and Methods. Following the reconstitution, a planar bilayer was prepared on mica for AFM imaging. The sample was prepared with 10 μg of lipid (and 0.1 μg protein assuming protein is uniformly distributed), incubated for 1 hour in 10 mM $CaCl_2$ on freshly cleaved mica. Following incubation, the unabsorbed material was washed off with the imaging HEPES buffer, and the adsorbed bilayer was subsequently imaged by AFM. The AFM images in Figure 4.3A and B show

Figure 4.3. An attempted reconstitution of the nAChR in a POPC bilayer at a L:P ratio of 100:1 (w/w). A planar bilayer was prepared on mica from the sample with 10 μg of lipid, incubated for 1 hour in 10 mM $CaCl_2$. Following incubation, the unabsorbed materials were washed away with the imaging HEPES buffer, and the adsorbed bilayer was subsequently imaged by AFM (A and B). To characterize the reconstituted sample, the attempted reconstitution at the L:P ratio of 100:1 (w/w) was loaded on a step sucrose gradient of 0, 5, 10, 20 and 40 % sucrose (2 ml each step). The sample was loaded in the 0 % step, and was subsequently ultra-centrifuged at 200000g, 20 hr, and 4°C. Following ultra-centrifugation, 400 μl fractions were drawn from the gradient (starting from the top) and the lipid and protein content from each fraction was measured (C) as described in section 2.5.1.

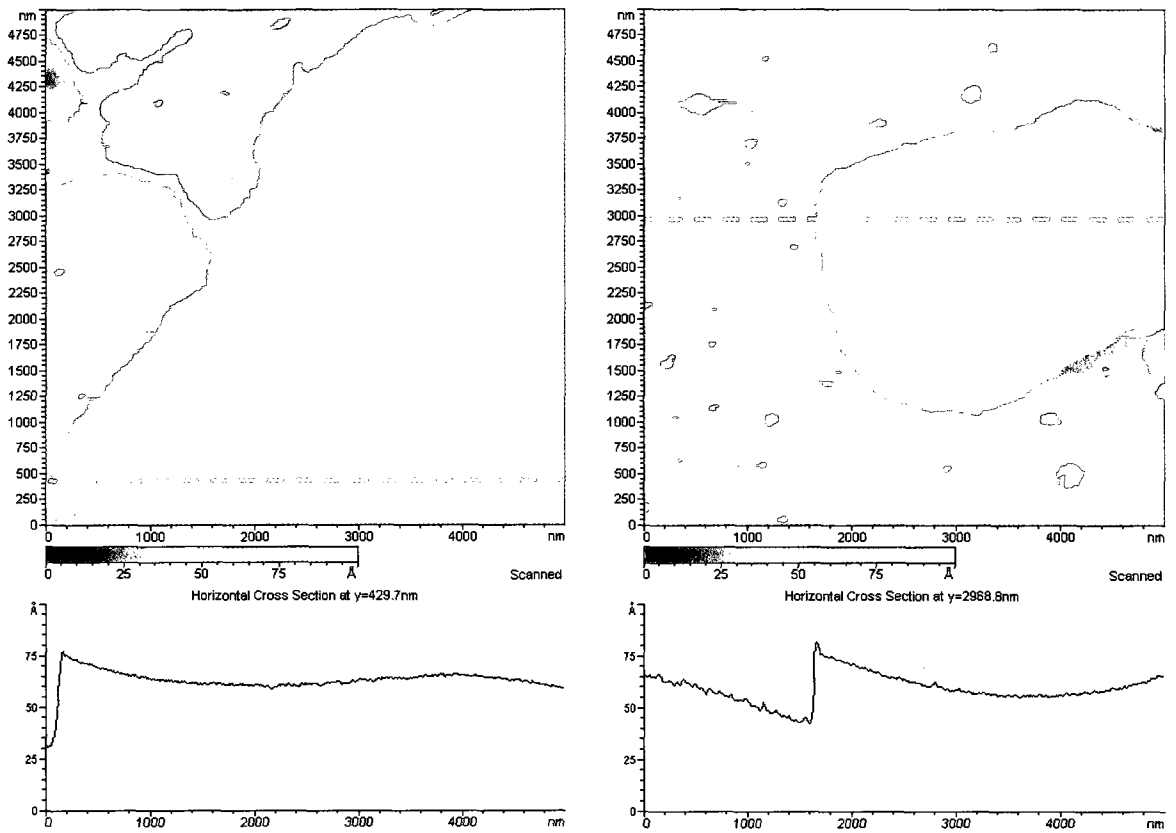
nm
Scanned
Horizontal Cross Section at y=429.7nm
Horizontal Cross Section at y=2968.8nm
Å

C

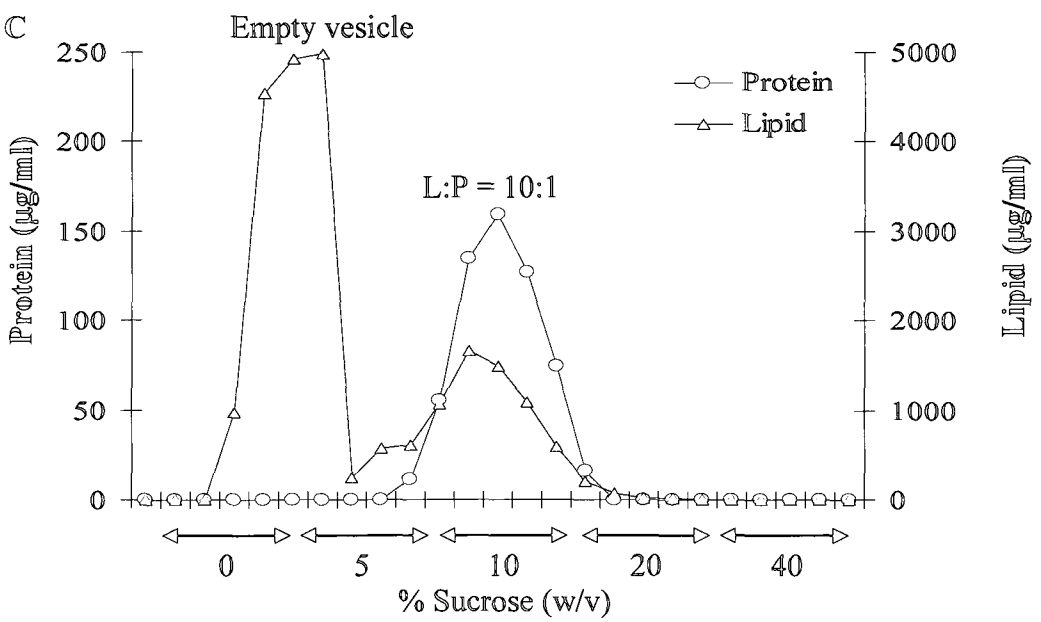
Empty vesicle
Protein
Lipid
L:P = 10:1
Protein (µg/ml)
Lipid (µg/ml)
% Sucrose (w/v)
0
5
10
20
40

patches of planar bilayer that was prepared from the reconstitution in a POPC bilayer at a L:P ratio of 100:1 (w/w). Assuming that the nAChR is evenly spaced in the bilayer upon reconstitution, I would expect to see a feature corresponding to the nAChR dimensions at every 100 nm on average with a bilayer at a L:P ratio of 100:1 (w/w) based on my rough calculation. However, the AFM images of the bilayers on mica were contrary to this prediction; the images were very similar to those for POPC bilayers and there were no features consistent with reconstituted protein. This experiment was repeated many times but features corresponding to the nAChR were never observed. Perhaps the protein was not reconstituted in the bilayer as expected, or maybe it was reconstituted but the proteoliposomes did not form a planar bilayer on the mica surface for some reason. Thus, the reconstituted sample was characterized in more detail.

4.2.3. Characterization of the reconstitution attempted at the L:P ratio of 100:1 (w/w) via sucrose gradient

To investigate whether the nAChR was properly reconstituted in a POPC membrane at high L:P ratio, the reconstituted sample was characterized on a sucrose gradient. The sucrose gradient method has been used to separate empty liposomes, proteoliposomes and protein aggregates from each other according to their differences in density in many studies for the nAChR (Anholt et al., 1982; Anholt et al., 1981; Fong and McNamee, 1986). Empty liposomes are typically found at low sucrose density (i.e., 5 % sucrose), protein aggregates are found in high sucrose density (i.e., 50 % sucrose), and proteoliposomes can be found anywhere from low to high sucrose density depending on the L:P ratio.

The reconstitution attempted at the L:P ratio of 100:1 (w/w) was characterized on a discontinuous gradient of 0, 5, 10, 20 and 40 % sucrose. According to the plot in Figure

4.3C, the reconstituted sample has two peaks. The first peak was found at 5 % sucrose and it contained only lipid. The other peak was found at 10 % sucrose and it contained both lipid and protein, but the L:P ratio was 10 times lower than expected (about 10:1 w/w). This observation showed that the reconstitution at a L:P ratio of 100:1 (w/w) did not yield the expected L:P ratio. Rather, the reconstitution contains two populations of vesicle, one corresponding to empty vesicles, and the other to protein-rich vesicles (with an estimated L:P ratio of about 10:1 w/w).

In summary, the current reconstitution method was not successful in generating proteoliposomes at the expected high L:P ratio. Rather, the reconstitution yields empty and protein-rich vesicles. In addition, AFM data shows that the sample containing both empty and protein-rich vesicles generated only a protein-free planar bilayer on mica. The combined AFM and sucrose gradient results suggested that the empty liposomes in the reconstituted sample form a bilayer on mica much faster than the proteoliposomes at low L:P ratio. Therefore, it may not be possible to prepare a POPC/nAChR bilayer on mica for AFM imaging with a reconstituted sample containing a mixture of liposomes and proteoliposomes.

4.2.4 An attempt to image POPC/nAChR fractions at a low L:P ratio

The reconstituted sample at the L:P ratio of 100:1 (w/w) can not be used to prepare a POPC/nAChR bilayer on mica because it contained both empty and protein-rich vesicles. However, the separation of empty and protein-rich vesicles on the sucrose gradient may offer an alternative approach to prepare a POPC/nAChR bilayer on mica for AFM imaging. Therefore, the protein-rich vesicles were isolated and used to prepare a POPC/nAChR bilayer on mica.

The protein-rich vesicles with an approximate L:P ratio of 10:1 (w/w) were isolated by pooling together those fractions containing both protein and lipid on the sucrose gradient shown in Figure 4.3C and removing the sucrose by dialysis (see section 2.5.2). At this point, I also planned to use total internal reflection fluorescence (TIRF) microscopy as a secondary microscopy method to verify that a POPC/nAChR bilayer could be prepared on mica. In order to observe the nAChR by TIRF microscopy, the pooled fractions were labeled with α-bungarotoxin conjugated to Alexa488 (αBTx-A488) as described in Materials and Methods; the toxin binds specifically to the nAChR (Changeux et al., 1970).

For AFM imaging, 10 μg of lipid from the prepared sample was incubated on mica in an AFM cell at 10 mM $CaCl_2$ for 1 hour at room temperature. The cell was washed with 100 ml of HEPES buffer to remove the unbound vesicles following incubation. The sample was then imaged by AFM (Figure 4.4A). There were patches of bilayer found in this image. There were some features found protruding out of these membrane patches. Those particles that protruded out of the bilayer are in the range of 3 nm to greater than 10 nm in height. Assuming these particles correspond to the nAChR, the AFM image indicates that very few proteins are found in the bilayer on mica. The appearance of this membrane is not what was expected since the low L:P ratio (10:1 w/w) should have produced a bilayer with a high density of nAChR. Moreover, the amount of lipid used (10 μg, see Chapter 3) always gave a continuous bilayer, rather than patches, for POPC vesicles.

To investigate why the sample with a 10:1 L:P ratio did not give an intact bilayer with reconstituted protein, a bilayer was similarly prepared on mica for TIRF microscopy with a sample labeled with αBTx-A488. For TIRF imaging, 20 μg of lipid was incubated in a TIRF cell at 10 mM $CaCl_2$ for 1 hour at room temperature; the quantity of sample loaded

Figure 4.4. Imaging a POPC/nAChR sample with a L:P ratio of 10:1 (w/w). Fractions in the 10% sucrose from Figure 4.3 were pooled, labeled with aBTx-A488, and then dialyzed to remove unbound toxin and sucrose. A bilayer was prepared in the AFM (with 10 μg of lipid) and TIRF cell (with 20 μg of lipid) for imaging, and incubated for 1 hour at the specified $CaCl_2$ concentration. Following incubation, the unabsorbed materials were washed off with the imaging HEPES buffer, and the adsorbed bilayers were subsequently imaged by AFM and TIRF. The AFM and TIRF image in A & B were prepared with 10 mM $CaCl_2$, and the images from C & D were prepared with 75 mM $CaCl_2$. A and B are similarly prepared bilayers from the same sample, but not same imaging area; the same applies to C and D

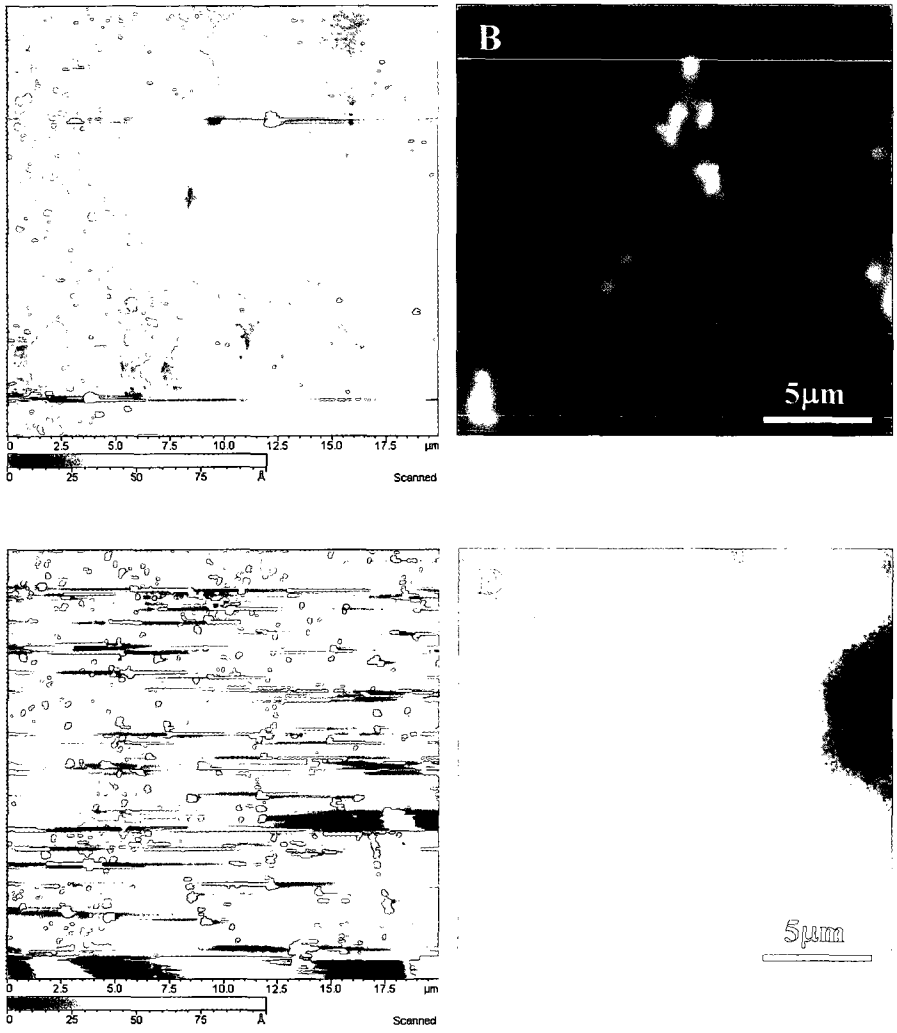
B
5µm
0 2.5 5.0 7.5 10.0 12.5 15.0 17.5 µm
0 25 50 75 Å
Scanned
5µm

was double because the TIRF cell is about twice the size of the AFM cell. Following incubation, the TIRF cell was washed with 150 ml of HEPES buffer to remove the unbound vesicles. The TIRF image for this sample (Figure 4.4B) showed that there were relatively few fluorescence signals from the labeled receptor. The level of fluorescence signals from the αBTx-A488 was apparently less than expected for a labeled POPC/nAChR bilayer with a L:P ratio of 10:1 (w/w), if a continuous bilayer had formed on the mica surface. The low level of fluorescence signal could be due to incomplete bilayer formation and/or little reconstituted protein deposited on the mica surface. The combined AFM and TIRF results suggested that a significant amount of loaded sample did not deposit on the mica surface.

If the majority of the sample did not deposit on the mica surface, where did it go? To answer this question, I need to realize that the mica surface is negatively charged (TedPella) and the nAChR is also negatively charged (so that it could sequester cations and rapidly flux them across the membrane after ligand binding) (Unwin, 2005). Thus, a POPC bilayer containing a significant amount of the reconstituted nAChR (i.e., at a L:P ratio of 10:1) would most likely not be adsorbed on the mica surface unless there is something to bridge the two negatively charged surfaces. This reasoning was based on the fact that the presence of a divalent cation such as calcium is typically used for the deposition of a membrane containing a negatively charged lipid (e.g., GM1) (Yang et al., 1993) and negatively charged molecules such as DNA (Lushnikov et al., 2006; Shlyakhtenko et al., 2003) on mica. Although 10 mM $CaCl_2$ was used to incubate the POPC/nAChR sample at a L:P ratio of 10:1 (w/w), this concentration of calcium may not be enough to adsorb the proteoliposomes on mica. Therefore, I decided to raise the level of calcium in an attempt to increase the deposition of the POPC/nAChR sample reconstituted at a 10:1 (w/w) L:P ratio.

In an attempt to raise the adsorption level of the POPC/nAChR vesicles on mica, the sample at a L:P ratio of 10:1 (w/w) was incubated on mica at higher calcium concentration. The sample was first examined with TIRF microscopy. About 20 μg of lipid were incubated in a TIRF cell at 75 mM $CaCl_2$ for 1 hour at room temperature. Following incubation, the cell was washed with 150 ml of HEPES buffer to remove the unbound vesicles. The sample was then imaged by TIRF microscopy. According to Figure 4.4D, the fluorescence signal in this TIRF image was dramatically increased as compared to the sample incubated at low calcium concentration. The result shows lots of fluorescence signal from αBTx-A488 in the bilayer on mica, which suggested that there was a significant increase in the level of sample deposited on the mica surface. Clearly, increasing the calcium concentration in the incubation media increased the adsorption of the POPC/nAChR proteoliposomes on the mica surface.

For AFM imaging, 10 μg of lipid was incubated in an AFM cell at 75 mM $CaCl_2$ for 1 hour at room temperature. Following incubation, the cell was washed with 100 ml of HEPES buffer to remove the unbound vesicles. The sample was then imaged by AFM (Figure 4.4C). This sample was very difficult to image and analyze. There may be some bilayer patches observed at the top of the AFM image; there are many large particles around these patches, with most of the particles being larger than 100 nm in diameter. These large particles cannot be individual reconstituted nAChR; they are more likely adsorbed protein aggregates or proteoliposomes. The rest of the image is extremely messy and streaky. Such streaks were never present when imaging lipid alone bilayers prepared with 75 mM $CaCl_2$ (data not shown). Hence, these streaks are most likely due to contamination of the tip by some of the large adsorbed particles.

The observation of bilayer patches and large particles for the L:P 10:1 sample at high calcium concentration (Figure 4.4C) suggests that only a fraction of the proteoliposomes that adsorb to the mica surface and rupture to form a bilayer. In order to image this sample successfully by AFM, more effort would be required to optimize the preparation of a POPC/nAChR bilayer at low L:P ratio. However, the low L:P ratio is expected to give a high protein density in the bilayer, which is not compatible with addressing the question of whether the receptor induces domain formation. Thus, I decided to focus on the preparation of a higher L:P ratio bilayer on mica for AFM imaging.

4.2.5. Heterogeneity in vesicle population is a prominent occurrence for the reconstitution of the nAChR in a POPC membrane

Preparation of a bilayer with high L:P ratio for AFM imaging requires reconstitution of the nAChR in vesicles at high L:P ratio. In theory, the L:P ratio of a sample can be controlled by the amount of lipid used to reconstitute the protein. However, the initial attempt to reconstitute the receptor at high L:P ratio was not successful. To address this problem, the L:P ratio of the proteoliposomes was measured for samples reconstituted with varying amounts of lipid. If increasing the amount of lipid can increase the L:P ratio of the reconstituted proteoliposome, then the L:P ratio of the reconstituted proteoliposome should increase proportionally to the amount of lipid used to reconstitute the nAChR, and the desired L:P ratio may be extrapolated or regressed from a "lipid used" Vs "L:P ratio" curve. If the L:P ratio reaches a plateau early, then the current method is not useful to reconstitute the nAChR at high L:P ratio.

The nAChR was reconstituted in a POPC bilayer at L:P ratios of 3:1, 20:1, 50:1, and 100:1 (w/w); lipid alone vesicles (i.e., L:P ratio = ∞:1) were also prepared for comparison.

The reconstituted samples were then examined on a discontinuous sucrose gradient with 0, 5, 10, 20 and 40 % sucrose (2 ml each step), with the samples loaded in the 0 % sucrose. According to the sucrose gradient results in Figure 4.5, all reconstituted samples from low to high L:P ratio consistently gave a heterogeneous vesicle population. Each reconstitution gives a population of empty vesicles and a population of relatively low L:P ratio proteoliposomes. In all cases, there are no vesicles with the desired L:P ratio (i.e., proteoliposome with L:P ratio of 100:1 w/w). The L:P ratio of the reconstituted proteoliposomes seems to level off before 50:1 (w/w). Thus, the current reconstitution method is not ideal to reconstitute the nAChR in vesicles at high L:P ratio. At this point, I investigated an alternate method for reconstitution of the nAChR in a POPC bilayer at high L:P ratio.

4.3 Detergent destabilized liposome reconstitution

Based on the available literature, an alternative method known as detergent destabilized liposome reconstitution described by Rigaud and collaborators (Paternostre et al., 1988; Rigaud et al., 1988) had been used to reconstitute proteins in the bilayer. I planned to test whether this method could be used to reconstitute the nAChR at high L:P ratio. This method requires a preformed liposome to be optimally destabilized by a detergent to allow the incorporation of a detergent solubilized membrane protein. In order to apply this method, the stability of POPC liposomes in the detergent cholate needed to be examined first. Then a range of destabilized liposomes were selected to test whether a purified and solubilized nAChR could be incorporated into one of these destabilized liposomes.

Figure 4.5. Characterization of the reconstituted nAChR in POPC membranes at various L:P ratios. The nAChR was reconstituted using similar conditions as in Figure 4.3 at the L:P ratio of 3:1, 20:1, 50:1, 100:1 and lipid alone, and the samples were examined on a discontinuous sucrose gradient of 0, 5, 10, 20 and 40 % (ultracentrifuged at 200 000xg, 20 h, and 4 °C).

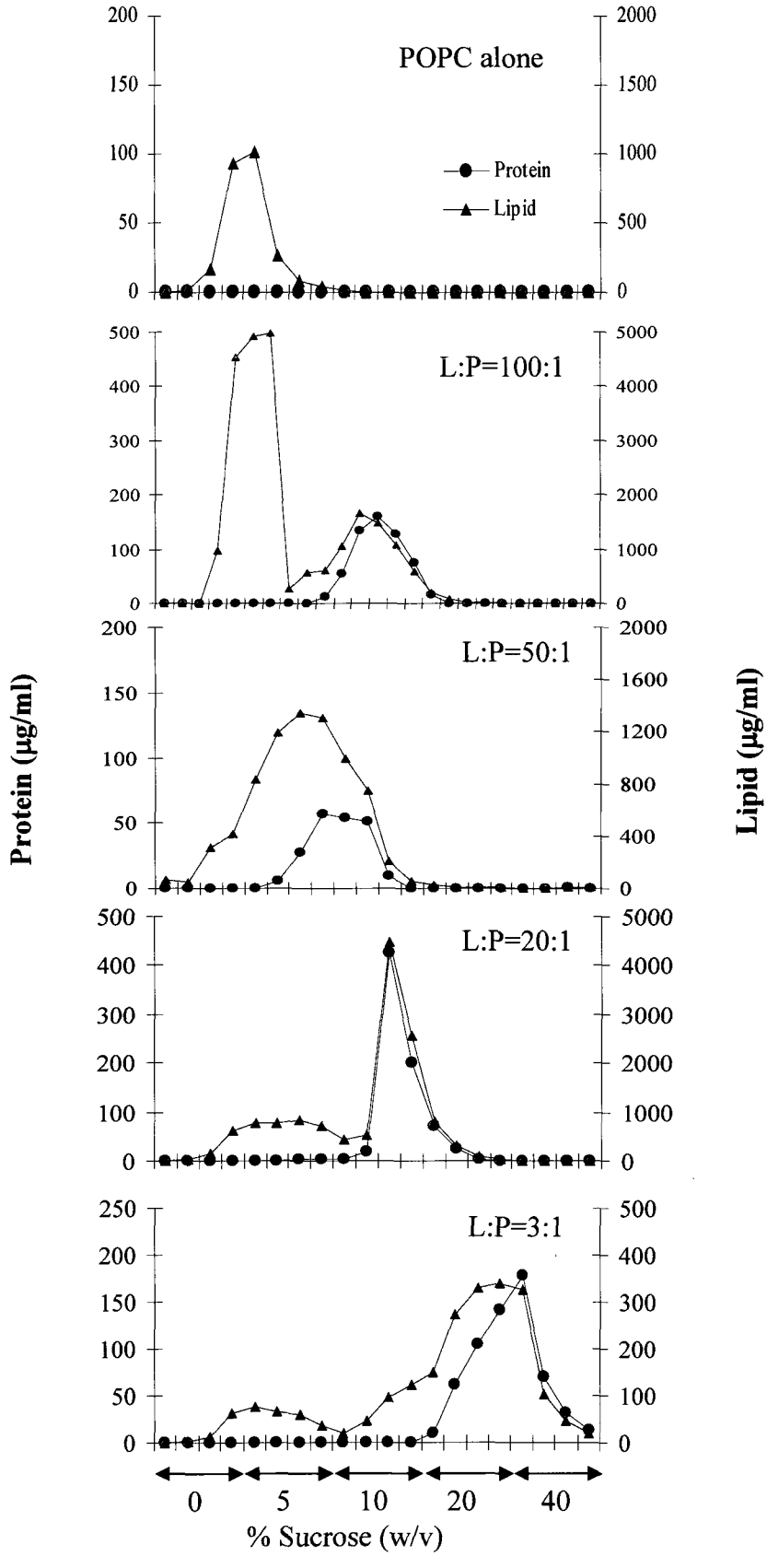
POPC alone
Protein
Lipid
L:P=100:1
L:P=50:1
L:P=20:1
L:P=3:1
Protein (µg/ml)
Lipid (µg/ml)
% Sucrose (w/v)
0
5
10
20
40

4.3.1 The stability of extruded POPC liposomes in cholate

POPC liposomes were prepared by extrusion using a 400 nm polycarbonate filter. The stability of the extruded liposomes in cholate was monitored by measuring the optical density (OD) at 405 nm. A higher OD reading indicates that the vesicle is either larger and/or more stable, whereas a lower OD reading signifies that the vesicle is less stable, destabilized and/or smaller, and the vesicle becomes solubilized when the OD approaches that of the blank solution (Rigaud and Levy, 2003; Rigaud et al., 1988; Rigaud et al., 1995). The graph in Figure 4.6A shows the OD of the extruded POPC liposomes incubated at various concentrations of cholate. The OD of the POPC vesicles dropped significantly when the cholate concentration was above 0.2% (w/v), which suggested the POPC vesicle were unstable at and above this cholate concentration. In addition, it only takes approximately 0.3 % cholate (w/v) to bring the OD down to the baseline, where the POPC vesicles have been solubilized. Thus, the point of solubilization for the extruded POPC vesicles is assumed to be about 0.3 % cholate (w/v), even though the critical micelle concentration of cholate is 0.6 % (w/v). The results here suggest that POPC vesicles can be easily solubilized by cholate.

4.3.2 Characterization of the attempted reconstituted samples via sucrose gradient

In an attempt to reconstitute the nAChR in a bilayer, the receptor was purified and solubilized in a detergent-lipid solution, and then the protein was incubated with extruded POPC liposomes destabilized in a range of detergent concentrations as shown in Figure 4.6 (i.e., from 0.100 to 1.00 % cholate). This was done to examine whether the mildly destabilized, strongly destabilized or completely solubilized POPC liposomes would be effective in reconstituting the nAChR at high L:P ratio. In the case of completely

Figure 4.6. The reconstitution of the nAChR in POPC vesicles was attempted via the detergent destabilized liposome reconstitution method. POPC liposomes (at 10 mg/ml) were prepared by extrusion using a 400 nm polycarbonate filter. The stability of the extruded POPC liposomes in cholate was assessed by reading the OD at 405 nm (A). For each reconstitution trial, an appropriate amount of cholate was added to the extruded POPC liposomes, followed by the addition of the nAChR (solubilized in a detergent/lipid solution composed of 1 % cholate and 1.25 mg/ml of lipid). For all trials, the final concentration of POPC is 1.5 mg/ml and nAChR is 0.03 mg/ml (L:P ratio is about 50:1 w/w), and the concentration of cholate was varied as indicated. As the appropriate contents were mixed, the solution was gently stirred for 90 minutes at 4 °C, and the sample was then subjected to dialysis to remove the detergent. All the samples were frozen immediately after detergent dialysis until further sucrose gradient analysis, and a few samples were thawed at a time for characterization. Each of the reconstitution trials was characterized on a discontinuous sucrose gradient (0, 5, 10, 20 and 40%; ultra-centrifuged at 200000xg, 20 h, and 4 °C). A picture of the sucrose gradient for each sample was recorded for visual inspection (B).

A)

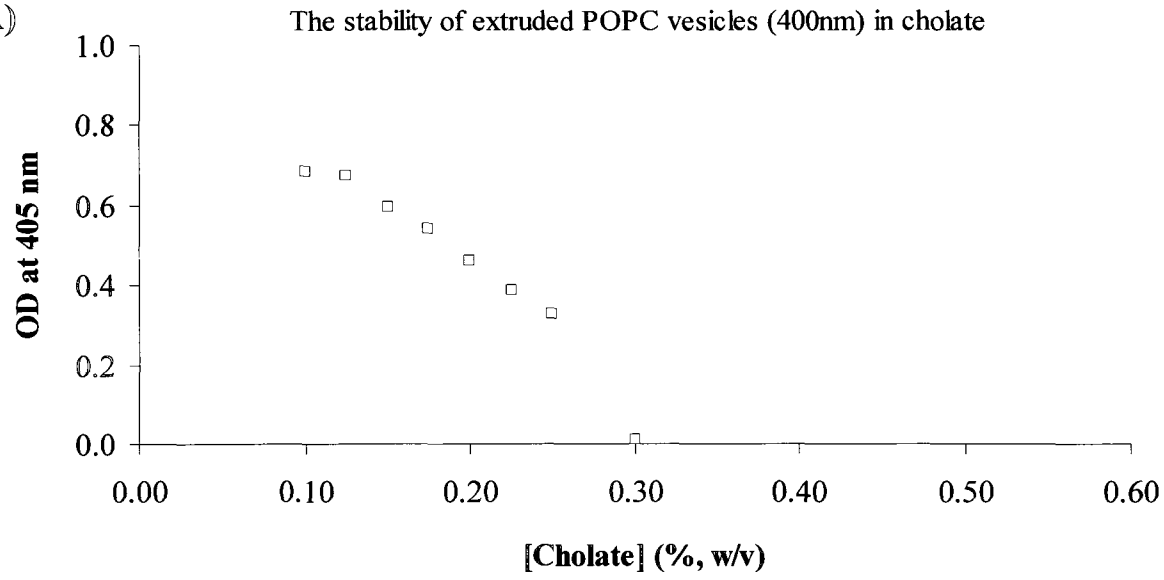
The stability of extruded POPC vesicles (400nm) in cholate
OD at 405 nm
1.0
0.8
0.6
0.4
0.2
0.0
0.00
0.10
0.20
0.30
0.40
0.50
0.60
[Cholate] (%, w/v)

B)

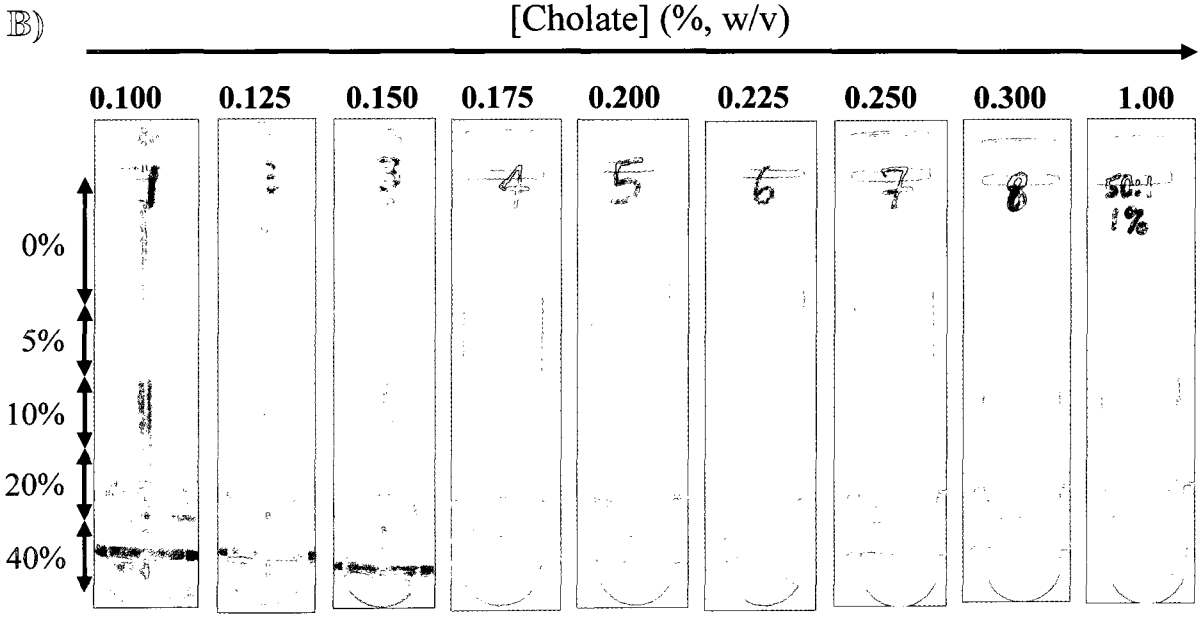
[Cholate] (%, w/v)
0.100
0.125
0.150
0.175
0.200
0.225
0.250
0.300
1.00
0%
5%
10%
20%
40%

solubilized POPC liposomes, the condition would be similar to the original reconstitution method, which will serve as a control. As the appropriate contents were mixed, each solution was gently stirred for 90 minutes at 4 °C, and the sample was then subjected to dialysis to remove the detergent for reconstitution. All the samples were frozen immediately after detergent dialysis until further sucrose gradient analysis; a few samples were thawed at a time for characterization. For more information, see the detergent destabilized liposome reconstitution procedure described in the Materials and Methods section.

Based on visual inspection for the reconstituted samples, there was a notable physical difference if destabilized or solubilized POPC liposomes were used to reconstitute the nAChR. When the nAChR was reconstituted with solubilized liposomes or lipids, the solution appeared transparent before and after detergent dialysis. The sample became cloudy only after it was frozen (to store) and then thawed to room temperature (to use). The change in the level of turbidity suggested a significant change in the morphology of the reconstituted sample following a freeze-thaw cycle. On the other hand, the destabilized liposome reconstitutions were cloudy before and after detergent dialysis, and they remained similarly cloudy after a freeze-thaw cycle. Whether there was any change in the vesicles used in the detergent destabilized liposome reconstitutions would have to be confirmed by other means (e.g., microscopy or dynamic light scattering).

To characterize the attempted reconstitutions, the samples were examined on a discontinuous sucrose gradient of 0, 5, 10, 20 and 40 % sucrose (the sample is in the 0 % sucrose). Based on visual inspection as shown in Figure 4.6B, there was a significant difference between the destabilized (0.100 – 0.250 % cholate) and solubilized (0.300 and 1.00 % cholate) POPC liposome reconstitution trials. However, the difference among the

destabilized liposomes reconstitutions was very subtle; the solubilized liposome reconstitutions were also similar to each other. I can consistently observe the lipid band(s) in the 5 % sucrose in the destabilized POPC liposome trials. The lipid band was noticeably narrower in the 0.100 to 0.150 % cholate samples, whereas in the 0.175 to 0.250 % cholate sample the lipid band was broader and a second minor band appeared between the 0 and 5 % sucrose. In the case of solubilized POPC liposome reconstitution attempts, there was a lipid band found near the bottom of 5 % sucrose. In addition, there was also an observable band in the 10 % sucrose. Clearly, there was a significant difference between the destabilized and solubilized liposome reconstitution trials.

Each sample was characterized by drawing 400 μl fractions from each sucrose gradient (starting from the top), and the lipid and protein content for each fraction was analyzed. The results for the destabilized liposome attempts are shown first; only the results from the 0.150 and 0.250 % cholate trials will be presented because the results for the other trials are similar to these two. In both of these reconstitution trials, a major lipid peak is found in the 5 % sucrose (Figure 4.7). There is no protein in this peak, suggesting that it corresponds to a population of empty liposomes. There also was a minor lipid peak in the 20 % sucrose that was not observed by visual inspection. Overlapping with this minor lipid peak is a protein peak, the 2 peaks combined yielded a very low L:P ratio of about 3:1 (w/w) (Figure 4.7). The presence of the protein at high sucrose density gradient (e.g., 20 %) along with the minor lipid peak suggested that the proteoliposome is high in density, which is characteristic of a low L:P ratio vesicle. The result showed that the nAChR was not successfully incorporated in the POPC liposomes to form vesicles at high L:P ratio with the destabilized liposomes reconstitution method.

On the other hand, the sucrose gradient results for the solubilized POPC liposomes (especially the 1 % cholate trial) reconstitutions were rather unexpectedly successful in the production of a high L:P ratio vesicle population. Figure 4.7 shows the distribution of lipid and protein in the sucrose gradient of the solubilized POPC liposome reconstitution attempts (0.30 and 1 % cholate). There is a small protein peak in both 5 and 10 % sucrose in the solubilized POPC liposome attempts, although the 1 % cholate shows this peak much more clearly. More importantly, there is also a major lipid peak overlapping with these small protein peaks, and the L:P ratio in this peak is high. The 0.30 % cholate trial only shows a protein shoulder in the 5 % sucrose (rather than a peak); the 1.0 % cholate trial clearly shows a small protein peak in the 5 % sucrose that overlaps with a major lipid peak indicated by a star in Figure 4.7. The L:P ratio of this peak is about 150:1 (w/w). Apparently, the cholate solubilized POPC liposomes favor the formation of a vesicle population with high L:P ratio. The conditions used to reconstitute the nAChR with the solubilized POPC in 1 % cholate in this case are very similar to that of the reconstitution procedure described earlier (section 4.2). However, earlier attempts to reconstitute the nAChR at high L:P ratio with solubilized POPC were never successful. Clearly, there must be a difference in the reconstitution procedure used here (as compared to the earlier one) that allowed me to reconstitute the nAChR at high L:P ratio. When the nAChR was reconstituted again with the new procedure, a similar result was observed, where a peak of proteoliposome with high L:P ratio can be observed. Thus, the reconstitution procedure using solubilized POPC can indeed yield a fraction of vesicles with a high L:P ratio. Since I had achieved my goal of reconstituting the nAChR at high L:P ratio, I did not further

Figure 4.7. Sucrose gradient analysis for the attempted reconstitution of the nAChR in POPC vesicles via the detergent destabilized liposomes method from Figure 4.6; a few selected results are shown. Fractions of 400 μl were drawn from each sucrose gradient (starting from the top), and the lipid and protein content in each fraction was analyzed.

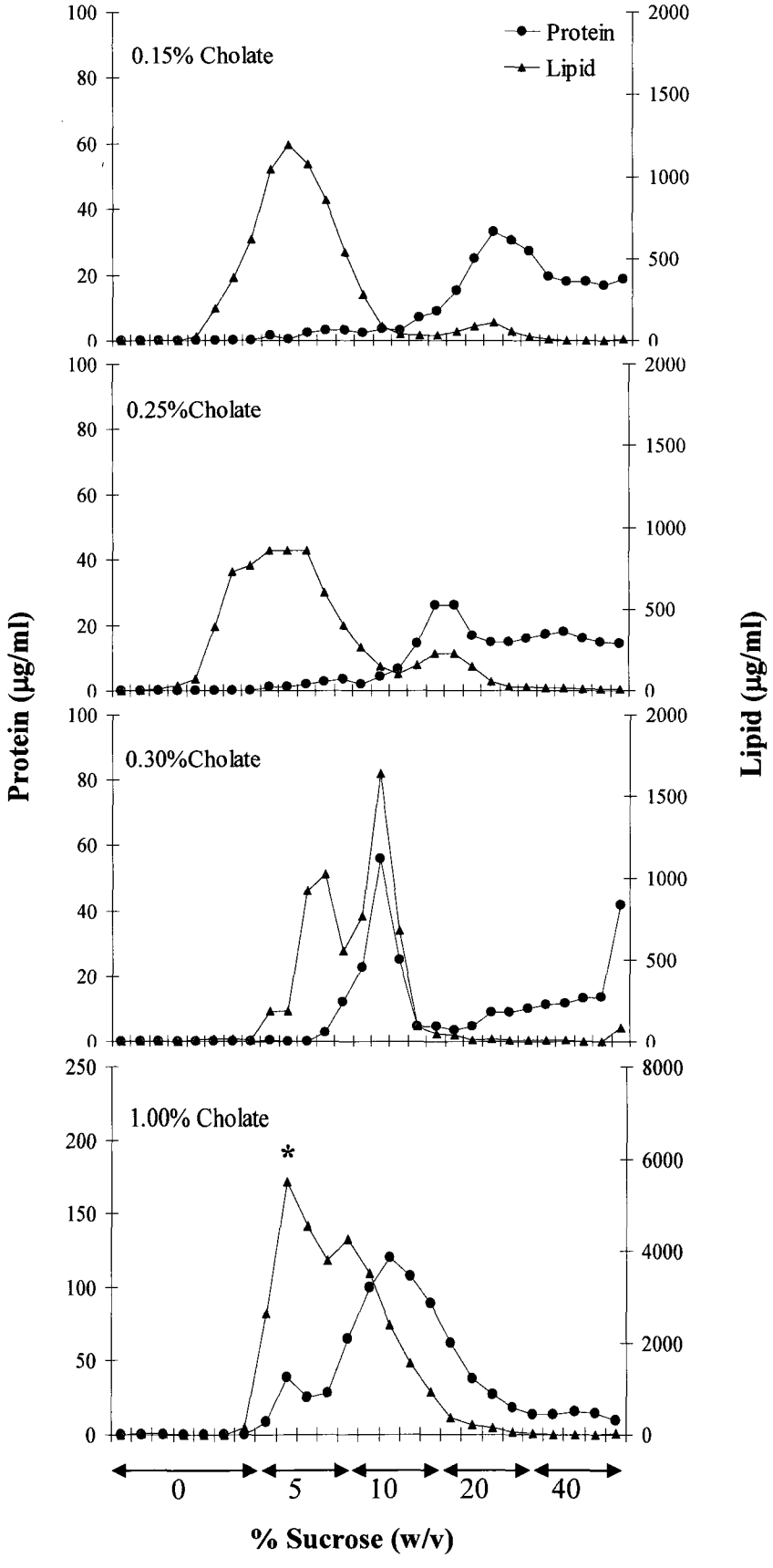
Protein
Lipid
0.15% Cholate
0.25%Cholate
0.30%Cholate
1.00% Cholate
*
Protein (µg/ml)
Lipid (µg/ml)
% Sucrose (w/v)
0
5
10
20
40

investigate the detergent destabilized liposome reconstitution method. Rather, I focused on investigating the mechanism(s) for formation of a fraction of high L:P ratio vesicles.

4.4. A new method to reconstitute the nAChR at high L:P ratio

The procedures used in the earlier and the later methods were identical up to the detergent dialysis point, but there were a few minor differences in the sample treatments after dialysis. In the earlier method, the sample was ultra-centrifuged (100 000xg, 4 °C, 2 hours) to concentrate the reconstituted vesicles. The pellet was then redispersed (with a homogenizer) and diluted to the desired concentration. Then the sample was stored at – 80 °C, and thawed to room temperature prior to use. In the later reconstitution, the dialyzed samples were aliquoted and stored at – 80 °C immediately without ultra-centrifugation. How these differences contribute to the formation of a fraction of vesicles with high L:P ratio was examined next.

The original sucrose gradient that I have used to characterize the reconstituted nAChR samples can identify a fraction of vesicles with high L:P ratio (Figure 4.7), but the separation between the peak of low and high L:P ratio is rather poor. It is important to separate the high from low L:P ratio vesicles so that the high L:P ratio proteoliposomes can be isolated for AFM studies and further characterization purposes. Therefore, the sucrose gradient was optimized to separate the high from low L:P ratio vesicles.

4.4.1. Optimizing the sucrose gradient to separate the high L:P from the low L:P ratio POPC/nAChR

Although a fraction of high L:P ratio vesicles could be obtained with the later reconstitution procedure, the high and low L:P ratio vesicles were not well separated on the original sucrose gradient (0, 5, 10, 20, and 40 % sucrose). In the original sucrose gradient in Figure 4.7, the high and low L:P ratio peaks are strongly overlapped. The original sucrose gradient was modified to optimize the separation between the low and high L:P ratio proteoliposomes. My approach was to modify the original sucrose gradient at the point that separates the high and low L:P ratio proteoliposomes (i.e., between 5 and 10 % sucrose). The nAChR was reconstituted in a POPC bilayer at a targeted L:P ratio of 100:1 (w/w), and the sucrose gradient was optimized to separate the low and high L:P ratio vesicles. Following a few trials, I found that adding a 7.5 % sucrose layer to the original sucrose gradient works well for separating the high L:P ratio proteoliposomes from the undesired lower L:P ratio proteoliposomes (Figure 4.8). The new sucrose gradient is as follows: 0 % (3 ml, containing the sample), 5 % (2.5 ml), 7.5 % (2.5 ml), 10 % (1 ml), 20 % (1 ml) and 40 % (1 ml) sucrose. In this sucrose gradient, the high L:P ratio proteoliposomes tend to settle in between the 5 and 7.5 % sucrose, whereas the lower L:P ratio proteoliposomes settle at 10 % sucrose. It was observed that POPC alone settles just above the high L:P ratio vesicles in Figure 4.8, which indicates that this sucrose gradient may not separate the empty liposomes (settle at 5 % sucrose) from the high L:P ratio proteoliposome satisfactorily. However, I still chose to adopt this sucrose gradient since the densities of the empty liposomes and the high L:P ratio proteoliposomes are very similar, and trying to separate them can be very difficult. Thus, this sucrose gradient was used to characterize subsequent reconstitutions (unless

Figure 4.8. A modification in the sucrose gradient to separate proteoliposomes at high L:P ratio from proteoliposomes at low L:P ratio. The nAChR was reconstituted into POPC at L:P ratio of 100:1 (w/w) with the new reconstitution method and was analyzed on different sucrose gradients. My initial sucrose gradient (0, 5, 10, 20, and 40 %) was not able to separate low from high L:P vesicles (A). However, adding a 7.5 % layer of sucrose allows the separation of vesicles with high L:P ratio from vesicles with low L:P ratio (B). Unfortunately, the high L:P vesicles are not well separated from empty vesicles (C) because these two types of vesicles have very similar density.

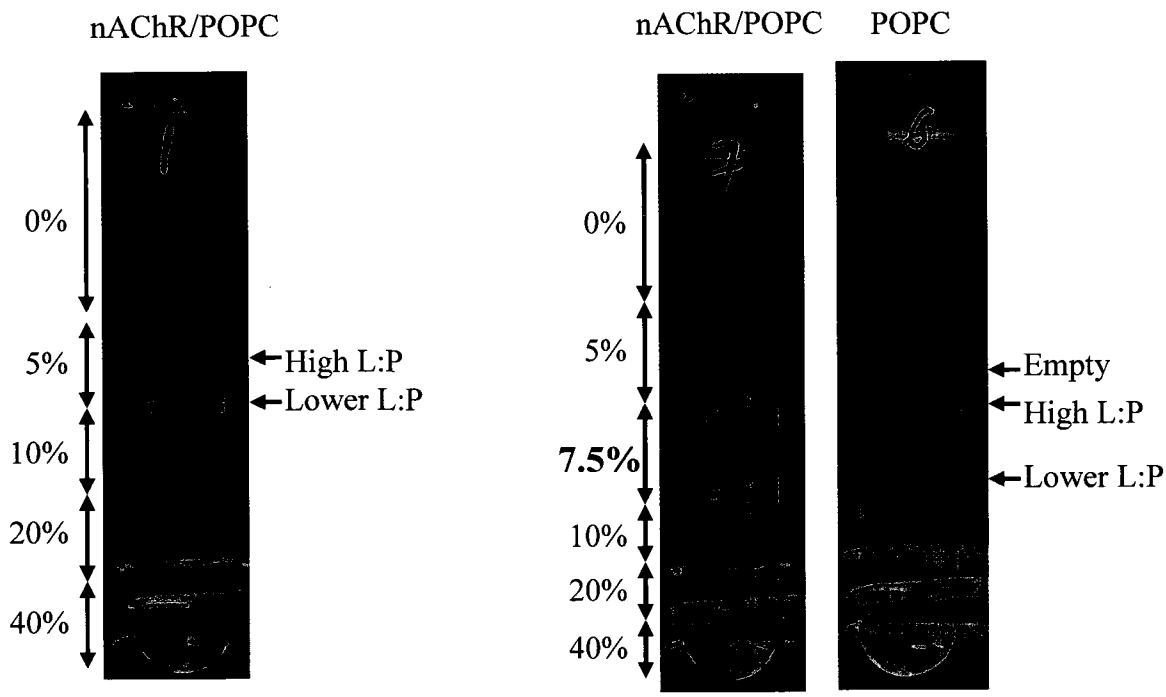
nAChR/POPC
0%
5%
10%
20%
40%
High L:P
Lower L:P
nAChR/POPC
POPC
0%
5%
7.5%
10%
20%
40%
Empty
High L:P
Lower L:P

stated otherwise), and was also used to isolate the high L:P ratio vesicles from subsequent reconstitutions for AFM imaging.

4.4.2 The formation of high L:P ratio vesicles requires a freeze-thaw cycle to the reconstituted POPC/nAChR bilayer specifically after the detergent dialysis step

To understand the mechanism(s) for formation of high L:P ratio vesicles, the earlier and later reconstitution procedures were compared. The reconstitution procedures in the earlier and the later method are identical up to the detergent dialysis point, but the sample treatments are different after the detergent dialysis step (i.e., after a bilayer has formed). In the later method, the sample was simply aliquoted and stored at – 80 °C following dialysis and thawed to room temperature prior to use (i.e., the sample simply underwent a freeze-thaw cycle), and a population of vesicles with high L:P ratio was obtained. In the earlier method, the sample was subjected to ultra-centrifugation and redispersion prior to the freeze-thaw treatment, and vesicles with high L:P ratio were not obtained. The samples were subjected to a freeze-thaw cycle in both methods, but the sample was subjected to ultra-centrifugation and redispersion only in the earlier method. Thus, the ultra-centrifugation and redispersion treatment in the earlier method may affect the formation of high L:P ratio vesicles, or the freeze-thaw cycle immediately after the detergent dialysis step in the later method may promote the formation of vesicles with a high L:P ratio.

In order to determine the mechanism(s) for the formation of vesicles with a high L:P ratio, the nAChR was reconstituted in a POPC bilayer at a targeted L:P ratio of 100:1 (w/w). The sample was divided into four aliquots and these aliquots were subjected to four different treatments after the detergent dialysis step. These are the treatments: 1) Store at 4 °C

(oruntreated), 2) Ultra-centrifuge and redisperse, 3) Freeze-thaw, 4) Freeze-thaw then ultra-centrifuge and redisperse.

By examining the untreated sample I can determine the composition of the sample following the detergent dialysis step. The untreated sample was examined on a sucrose gradient of 0, 5, 7.5, 10, 20 and 40 % sucrose (200 000xg, 4 °C, 20 h) (Figure 4.9A). The analyzed sucrose gradient shows mainly two peaks at 5 and 10 % sucrose. The peak at the higher density sucrose (10 %) corresponds to a population of proteoliposomes with a L:P ratio of about 47:1 (w/w), which is still lower than the desired L:P ratio. The peak in the light density sucrose (5 %) corresponded to the lipid alone liposomes. There was no evidence in the sucrose gradient for the presence of high L:P ratio vesicles (i.e., 100:1 w/w) in this sample. Thus, the reconstituted sample initially consisted of liposomes and proteoliposomes with a L:P ratio of about 47:1 (w/w).

The effect of ultra-centrifugation and redispersion on the sample following the detergent dialysis step was examined next. The sample was subjected to ultra-centrifugation (100 000xg, 4 °C, 2 h) and redispersion (using a homogenizer) after detergent dialysis, and the sample was resuspended back in the same buffer with same (original) volume. The sample was then examined on the same sucrose gradient as above. This sample appears similar to the untreated sample, with a lipid peak at 5 % sucrose, a lipid and protein peak at 10 % sucrose (L:P ratio of 38:1 w/w) (Figure 4.9C) and no detectable proteoliposome with the desired high L:P ratio (i.e., 100:1 w/w). The main difference between this sample and the untreated sample is that both the liposome and proteoliposome peaks were significantly smaller, which indicated that there was a loss of liposomes and proteoliposomes following ultra-centrifugation. Analysis for the total lipid and protein content in this sample showed

Figure 4.9. Characterization of the formation of reconstituted POPC/nAChR vesicles at high L:P ratio. The nAChR was reconstituted in a POPC membrane at a targeted L:P ratio of 100:1 (w/w), then the sample was subjected to a number of treatments after the detergent dialysis step. These are the treatments: A) Keep at 4 °C (or untreated), B) Freeze-thaw, C) Ultra-centrifuge and redisperse, D) Freeze-thaw then ultra-centrifuge and redisperse. For comparison purposes, the same amounts of lipid and protein were used in all of these treatments. The samples were examined on a discontinuous sucrose gradient of 0 % (3 ml, including the sample), 5 % (2.5 ml), 7.5 % (2.5 ml), 10 % (1 ml), 20 % (1 ml) and 40 % sucrose . The samples were subjected to ultracentrifugation at 200 000xg for 20 hours at 4 °C. Following ultra-centrifugation, fractions of 250 µl were drawn from the gradient (starting from the top), and the lipid and protein content of each fraction was analyzed via the Phospholipids C and BCA protein assays. The red arrow points to the high L:P ratio vesicle population that will be used to prepare planar bilayers on mica for AFM and TIRF imaging.

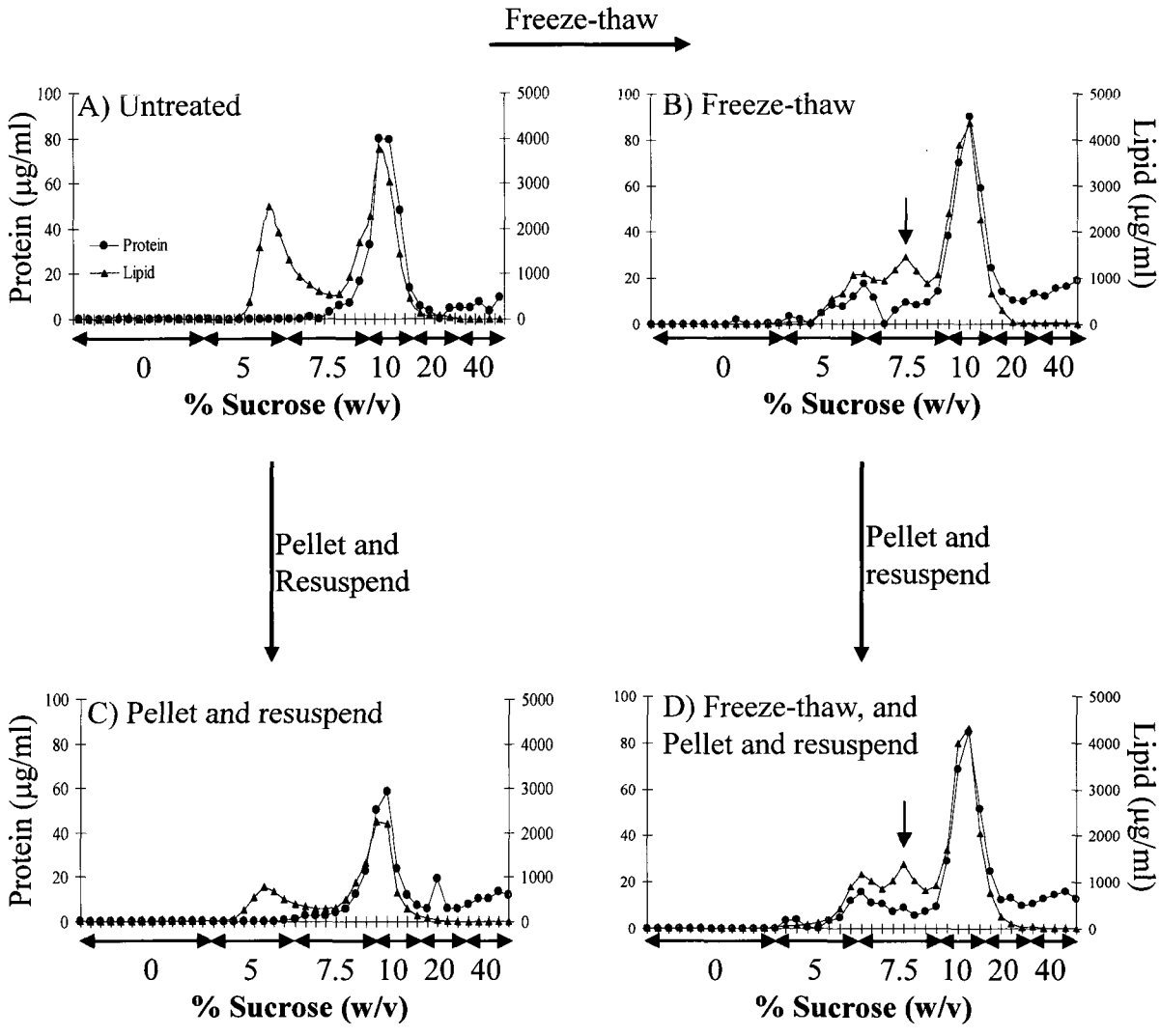
Freeze-thaw
A) Untreated
B) Freeze-thaw
C) Pellet and resuspend
D) Freeze-thaw, and
Pellet and resuspend
Protein
Lipid
Protein (µg/ml)
Lipid (µg/ml)
% Sucrose (w/v)
0 5 7.5 10 20 40
Pellet and
Resuspend
Pellet and
resuspend

that the pellet has lost half the amount of lipid and protein to the supernatant. However, the typical ultra-centrifugation procedure between 0.5 – 2 hour at 100 000 – 160 000 xg has long been used to pellet vesicles that are greater than 30 – 100 nm in diameter (Barenholz et al., 1977; Goll et al., 1982). Thus, my results suggest that the reconstituted sample initially contains a significant amount of small liposomes and proteoliposomes (less than 100 nm in diameter) that are not effectively pelleted by ultra-centrifugation at 100 000 xg for 2 hours at 4 °C. Moreover, the solution containing the reconstituted vesicles following dialysis was quite transparent which suggested that most of the vesicles were fairly small. Unfortunately, the size of the reconstituted liposomes and proteoliposomes by other methods were not analyzed.

The effect of freeze-thaw treatment on the reconstituted sample was then examined. The same reconstituted sample was frozen immediately after the detergent dialysis step at – 80 °C, and then it was thawed to room temperature for analysis by sucrose gradient. The analyzed sucrose gradient for this sample was significantly different from the one for the untreated sample; there were 3 peaks of lipid and protein (overlapped) in the freeze-thaw sample (Figure 4.9B) as compared to only 2 peaks in the untreated one (Figure 4.9A). The 3 peaks of the freeze-thaw sample were found at 5, 7.5 and 10 % sucrose layers. The L:P ratio of the peak at 10 % sucrose was about 50:1 (w/w), the peak at 5 % sucrose had a L:P ratio of about 70:1 (w/w), and the peak at 7.5 % sucrose had a L:P ratio of about 150:1 (w/w). Clearly, a freeze thaw cycle to the reconstituted sample following dialysis assisted the formation of a population of vesicles with high L:P. It has been reported that vesicle fusion can occur upon a freeze-thaw cycle (Anholt et al., 1982; Traikia et al., 2000). Interestingly, it was found that the untreated sample was quite transparent but became turbid after a

freeze-thaw cycle suggesting that there were changes in the vesicle size. Thus, it is likely that the liposomes and proteoliposomes with lower L:P ratio and smaller size in the reconstituted sample may have fused during the freeze-thaw cycle to generate larger proteoliposomes with higher L:P ratio.

Finally, the freeze-thaw sample that was subjected to ultra-centrifugation and redispersion was also analyzed by sucrose gradient. The analyzed sucrose gradient for this sample was identical to the freeze-thaw sample that had not been pelleted (Figure 4.9D). The pattern of lipid and protein peaks was identical, the magnitude of the peaks was very similar, and the L:P ratio for each peak matched extremely well. In addition, the total amount of lipid and protein in this sample was about the same as the freeze-thaw sample that had not been pelleted. This result suggests that the vesicles in the sample that had undergone a freeze-thaw cycle were large, since ultra-centrifugation at 100 000 xg for 2 hours at 4 °C was sufficient to pellet most of them.

4.5 Discussion and Conclusions

The nAChR was normally reconstituted at low L:P ratio (i.e., 1:2 w/w) so that the protein function could be easily examined FTIR *difference* spectroscopy. For AFM imaging, however, it was necessary to reconstitute the nAChR at a high L:P ratio so that the protein could be clearly resolved in the bilayer. In order to increase the L:P ratio of the proteoliposome samples, the reconstitution procedure was slightly altered. However, the alteration(s) may affect the structure and function of the reconstituted nAChR. Thus, the structure and function of the receptor were examined following each alteration.

To increase the L:P ratio of the reconstituted sample, the content of solubilized lipid used in the reconstitution procedure was simply increased (see Materials and Methods). When comparing the functional state of the nAChR reconstituted with a lipid mixture of POPC/POPA/Chol (3:1:1) at the L:P ratio of 1:2 against 10:1 (w/w), the receptor was found to be mainly in a resting state for both L:P ratios. However, the *difference* spectrum was weak and slightly distorted for the sample with the higher L:P ratio (i.e. 10:1), with the signature bands at 1655 and 1547 cm^{-1} barely visible. FTIR *difference* spectra for the nAChR reconstituted at L:P ratios higher than 10:1 (w/w), such as 20:1 or greater, were extremely distorted and the signal was similar to the noise level. Thus, assessing the conformational state of the nAChR reconstituted at high L:P ratio with FTIR *difference* spectroscopy is not possible.

As it seemed the nAChR did not change its structural conformation at a higher L:P ratio, I wanted to reconstitute the nAChR in a simple lipid bilayer such as POPC at a L:P ratio of 100:1 (w/w), which would be used to prepare planar bilayers on mica for AFM imaging. Initially, I assumed that the nAChR could be reconstituted in a POPC bilayer at high L:P ratio if an appropriate amount of detergent solubilized lipid was mixed with a purified protein, and then the detergent was removed by dialysis to form a reconstituted proteoliposome. Unfortunately, the reconstitution procedure did not yield reconstituted POPC/nAChR proteoliposomes at the desired high L:P ratio. Rather, the reconstituted sample typically contained two populations of vesicles, empty vesicles and protein-rich vesicles. In addition, an earlier study that used a similar reconstitution procedure to mine showed that it is very difficult to reconstitute the nAChR into a bilayer at high L:P ratio (Anholt et al., 1981). Initially, I explored an alternative approach to reconstitute the nAChR

at high L:P ratio (i.e., detergent destabilized liposomes reconstitution). However, it was later discovered that the nAChR could be reconstituted at a high L:P ratio with a very similar procedure.

To understand the mechanism(s) for the formation of proteoliposomes with high L:P ratio I compared the conditions used in the earlier and the later reconstitution methods. I found that these two methods differed very slightly in the sample treatment after the receptor has been reconstituted in a bilayer (i.e., after the detergent dialysis step). In the earlier method, the sample was pelleted (which was advantageous to concentrate the sample for FITR study) and was frozen at – 80 °C for storage. In the later method, the sample was simply frozen without pelleting. To identify the mechanism(s) for the formation of high L:P ratio proteoliposomes, the nAChR was reconstituted at a targeted high L:P ratio and the sample was exposed to four different conditions, most of which mimic the conditions in the earlier and the later reconstitution methods. The conditions were: 1) untreated, 2) pelleted, 3) freeze-thaw, and 4) freeze-thaw and pelleted.

When the untreated sample was characterized by sucrose gradient, it was found that the sample contained empty liposomes and proteoliposomes with an average L:P ratio of about 50:1 (w/w), which was much lower than the desired L:P ratio. There were no detectable proteoliposomes at high L:P ratio in the untreated reconstituted sample. Thus, the reconstituted sample initially contains empty liposomes and proteoliposomes with medium L:P ratio.

Examining the pelleted sample by sucrose gradient showed that this sample was not very different from the untreated sample. The main difference between the untreated and pelleted samples was a two-fold reduction in the total amount of liposome and

proteoliposome in the pelleted sample. This result implied that there was a significant loss of vesicles to the supernatant. Moreover, this finding suggested that at least half of the reconstituted proteoliposomes and liposomes were very small in size such that ultra-centrifugation at 100 000 xg for 2 hours at 4 °C was not sufficient to pellet them. This conclusion is based on the observation that similar ultra-centrifugation conditions have been used to separate small vesicles (supernatant) from large vesicles (pellet) (Barenholz et al., 1977; Goll et al., 1982). Moreover, the untreated sample appeared transparent, which provides qualitative support for the hypothesis that most of the reconstituted vesicles were small in size. Therefore, both visual and ultra-centrifugation observations suggested that the reconstituted sample is initially composed of liposomes and proteoliposomes that are small in size.

The freeze-thaw sample, on the other hand, had three population of proteoliposomes with L:P ratio of about 50:1, 70:1 and 150:1 (w/w). The presence of the high L:P ratio proteoliposome at 150:1 (w/w) clearly indicated that a freeze-thaw cycle promoted the formation of vesicles with high L:P ratio. In addition, the sample appeared turbid following freeze-thaw treatment, which suggested that there was an increase in vesicle size after a freeze-thaw cycle. Interestingly, it has been reported that vesicle fusion can be induced through freeze-thaw cycles (Anholt et al., 1982; Traikia et al., 2000). Thus, it is possible that the high L:P ratio proteoliposomes may be formed via fusion between a liposome and proteoliposome with lower L:P ratio.

The sucrose gradient result for the freeze-thaw and pelleted sample appeared identical to the freeze-thaw sample. The total amount of lipid and protein were mostly recovered in the pellet. This result implied that most of the vesicles following a freeze-thaw

cycle were large in size such that ultra-centrifugation at 100 000 xg for 2 hours at 4 °C was sufficient to pellet most of them. Thus, it is safe to conclude that the reconstituted vesicles after a freeze-thaw cycle are large in size.

In summary, the untreated sample showed that the reconstituted sample initially contains empty liposomes and proteoliposomes that have a medium L:P ratio. The result from the pelleted sample suggested that the reconstituted liposomes and proteoliposomes are small in size, because half of the vesicles can not be pelleted via ultra-centrifugation. The result from the freeze-thaw sample showed that a population of proteoliposomes with high L:P ratio (100:1 w/w or more) can be generated from the initial small liposomes and proteoliposomes (medium in L:P ratio). The freeze-thaw and pelleted sample indicated that the initially small vesicles become large after a freeze-thaw cycle, since most of the vesicles can be pelleted after a freeze-thaw cycle. The combined results clearly suggest that the formation of a population of POPC/nAChR vesicles with high L:P ratio occurs via a vesicle fusion mechanism. This is because the reconstitution procedure typically produces small liposomes and proteoliposomes (ranging from low to medium L:P ratio). Small vesicles are known to have high curvature stress and are prone to fusion. When applying a freeze-thaw cycle to the reconstituted sample, the proteoliposomes and liposomes fuse with each other to generate larger vesicles. This hypothesis is based on the fact that vesicle fusion has been observed via freeze-thaw cycles (Anholt et al., 1982; Traikia et al., 2000). If two proteoliposomes with medium L:P ratio fuse together, a larger proteoliposome with the same L:P ratio is formed. However, when a liposome fuses with a proteoliposome, a larger proteoliposome with higher L:P ratio can be generated.

Chapter 5: The preparation of a POPC/nAChR planar bilayer on mica for AFM imaging

5.1 Introduction

The results in the previous chapter showed that the nAChR can be reconstituted in POPC vesicles at a lipid to protein (L:P) ratio of 100:1 (w/w) or more. At such high L:P ratios, the reconstituted proteoliposomes may be used to prepare a planar POPC/nAChR bilayer on mica for AFM imaging. This chapter describes the optimization process which leads to establishment of a procedure to prepare a POPC/nAChR bilayer on mica for AFM and TIRF imaging. Finally, successfully prepared POPC/nAChR planar bilayers on mica were examined thoroughly by both TIRF and AFM.

5.2 Optimizing the preparation of a POPC/nAChR bilayer on mica for AFM and TIRF imaging

5.2.1 Washing the POPC/nAChR planar bilayer with EDTA after sample incubation

The preparation of a POPC/nAChR planar bilayer on mica was first attempted with a reconstituted POPC/nAChR sample at a L:P ratio of 125:1 (w/w). A planar bilayer on mica was prepared by incubating 7 μg of lipid on freshly-cleaved mica in an AFM cell for 1 hour at room temperature in the presence of 10 mM $CaCl_2$. Following incubation, the sample was washed with 100 ml of HEPES buffer, and then imaged by AFM (Figure 5.1A and B). From these images, bilayer patches along with some large particles were observed. However, close examination of these bilayer patches and particles reveals a shadow for every patch and particle observed. The shadows are double tip artifacts that arise from contamination of the AFM tip. The extent of the shadow reflects the size of the contaminant particle stuck to the tip; hence the double tip image may not be apparent in large AFM

Figure 5.1. AFM images of the POPC/nAChR patches. The bilayer patches were prepared with 7 μg of lipid from a sample with a L:P ratio of 125:1 (w/w), and incubated in 10 mM $CaCl_2$ for 1 hour at room temperature. Following incubation, the sample was washed with 100 ml of HEPES buffer (A & B), and then imaged. The same sample was washed with 50 ml of 1 mM EDTA (pH 8.0), followed by 50 ml of HEPES buffer (C & D).

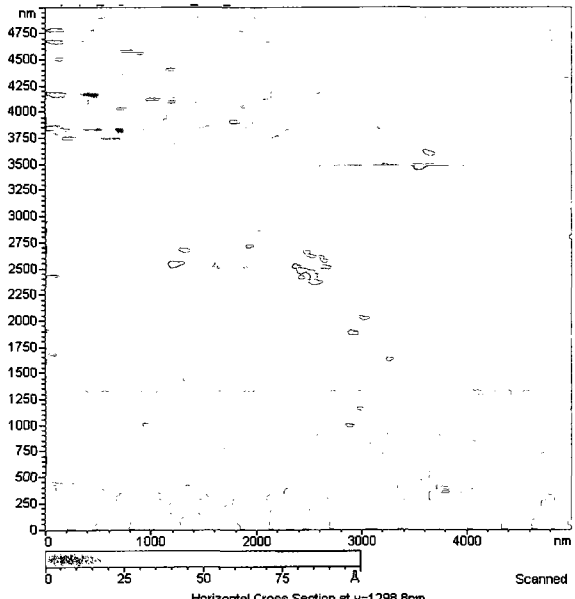
nm
4750
4500
4250
4000
3750
3500
3250
3000
2750
2500
2250
2000
1750
1500
1250
1000
750
500
250
0
0
1000
2000
3000
4000
nm
0
25
50
75
Å
Scanned

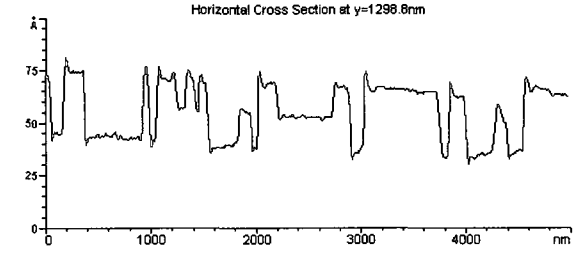
Horizontal Cross Section at y=1296.6nm
Å
75
50
25
0
0
1000
2000
3000
4000
nm

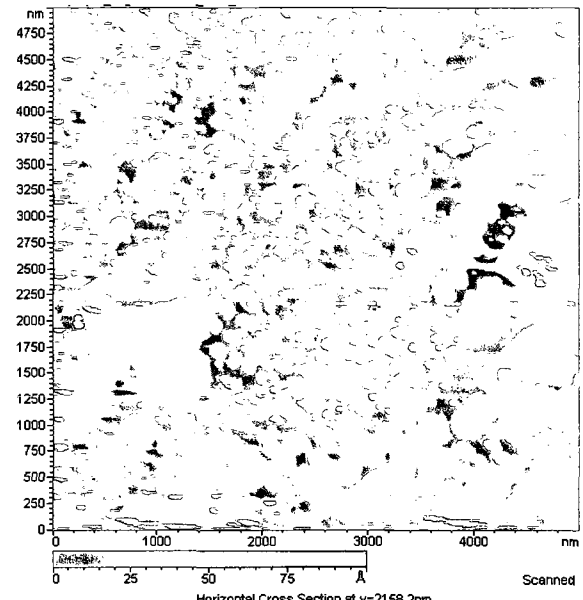
nm
4750
4500
4250
4000
3750
3500
3250
3000
2750
2500
2250
2000
1750
1500
1250
1000
750
500
250
0
0
1000
2000
3000
4000
nm
0
25
50
75
Å
Scanned

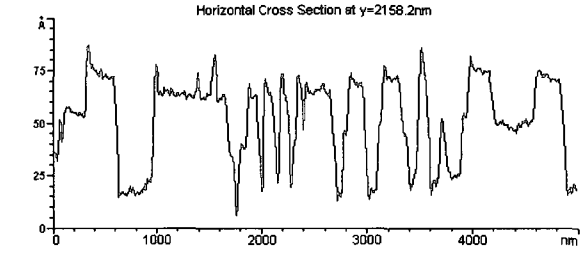
Horizontal Cross Section at y=2158.2nm
Å
75
50
25
0
0
1000
2000
3000
4000
nm

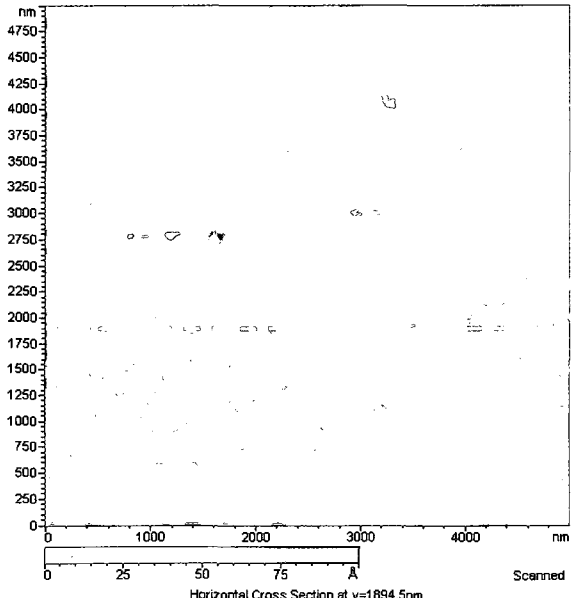
nm
4750
4500
4250
4000
3750
3500
3250
3000
2750
2500
2250
2000
1750
1500
1250
1000
750
500
250
0
0
1000
2000
3000
4000
nm
0
25
50
75
Å
Scanned

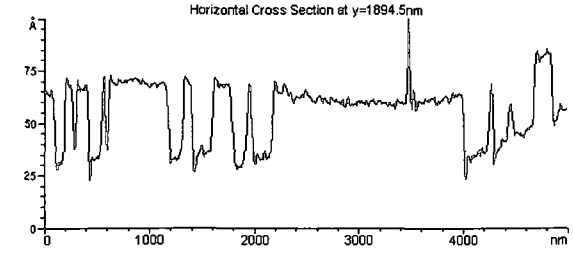
Horizontal Cross Section at y=1894.5nm
Å
75
50
25
0
0
1000
2000
3000
4000
nm

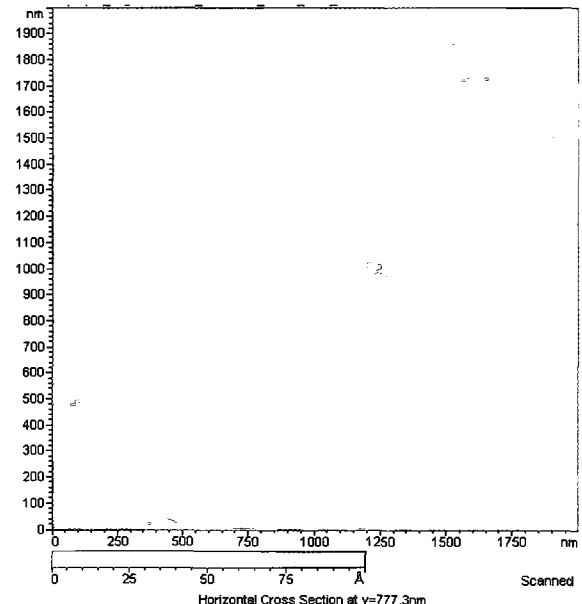
nm
1900
1800
1700
1600
1500
1400
1300
1200
1100
1000
900
800
700
600
500
400
300
200
100
0
0
250
500
750
1000
1250
1500
1750
nm
0
25
50
75
Å
Scanned

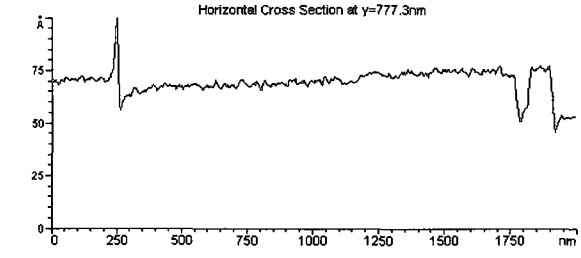
Horizontal Cross Section at y=777.3nm
Å
75
50
25
0
0
250
500
750
1000
1250
1500
1750
nm

images until a smaller image (5 μm or less) was scanned. A particle can be picked up by the AFM tip as the tip scans the sample or the AFM tip could have been initially contaminated. Since the AFM tip was always washed thoroughly (with 75 % ethanol, then water, and then HEPES buffer) prior to imaging, it is unlikely that the tip was contaminated from the beginning. Rather, there must be some loosely bound particles on the bilayer that stick to the AFM tip as it scans across the bilayer. Even when the bilayer was washed extensively with HEPES buffer (200 – 300 ml) and a new tip was used, I could not prevent the tip from picking up these particles on the bilayer.

My approach to eliminate the contaminated tip artifacts was to reduce the source of the loosely bound particles on the mica surface or planar bilayer. Similar problems with particles adhering to the bilayer were not encountered in previous experiments with POPC bilayers. Since the reconstituted protein is the main difference between the POPC and POPC/nAChR samples, it was logically deduced that the nAChR itself was the cause of double tip artifact. The AFM tip could be contaminated by protein present in proteoliposomes, protein aggregates or bilayer fragments that contain the nAChR bound weakly on the planar bilayer or mica surface and that are not washed off with the HEPES buffer. To remove such small weakly bound bilayers or vesicles containing the nAChR, the protein interaction with the bilayer must be weakened. Knowing that the nAChR requires calcium to bridge its interaction with the mica or perhaps with another nAChR in the planar bilayer, I thought that complexing calcium ions in the imaging buffer with a chelating agent such as EDTA might allow these small nAChR fragments to be washed off. To test this theory, the bilayer from Figure 5.1A & B was washed with 50 ml of 1 mM EDTA (pH 8.0), followed by 50 ml of HEPES buffer to displace the EDTA. Figure 5.1C & D show AFM

images of the EDTA washed bilayer. These images are fairly sharp and have no double tip artifacts. This result suggests that the EDTA wash removed most of the small loosely bound particles on the planar bilayer, but did not affect the large bilayer patches on the mica. Note that there were still some particles on the bilayer after the EDTA wash; since they did not cause imaging problems it appears that the EDTA wash also helped to minimize the particles adhering to the AFM tip. Thus, following the incubation step, the planar bilayers formed on mica were routinely washed with 50 ml of 1 mM EDTA (pH8), followed by 50 ml of HEPES buffer. This modification to the washing procedure greatly improved the quality of the AFM images (Figure 5.1C & D).

As the AFM image became sharper and the bilayer patches on mica could be examined closely, it was found that there were only very few bright spots in the bilayer that may correspond to the reconstituted protein (Figure 5.1D). This result suggests that the conditions used to prepare a POPC/nAChR bilayer did not favour the deposition of the protein on mica. Therefore, the incubation conditions were optimized further in order to get an intact planar bilayer on mica with more protein deposited.

Based on the currently available literature, some of the factors that influence the formation of planar bilayers include the incubation temperature, calcium concentration, time and sample loading (Richter et al., 2006; Richter and Brisson, 2005). The latter three variables were examined closely in the following sections. However, the incubation temperature was ignored because the impact of temperature on the formation of a bilayer on mica was reported only for vesicle samples prepared with high Tm lipids (Richter et al., 2006; Richter and Brisson, 2005). Since the Tm of the POPC and POPC/nAChR vesicles are less than 4 °C (daCosta et al., 2002; daCosta et al., 2004) and the samples were prepared

for AFM imaging at room temperature (~20 °C), the incubation temperature should not be a concern. Thus, the effect of incubation time, calcium concentration and sample loading were tested to find an optimum condition to prepare a POPC/nAChR bilayer for AFM imaging.

5.2.2 The effect of calcium on preparation of a POPC/nAChR bilayer at high L:P ratio

As a starting point, the incubation time and quantity of lipid were held constant, while the effect of calcium concentration was assessed. Figure 5.2 shows AFM images of a planar bilayer prepared from reconstituted POPC/nAChR proteoliposomes at the L:P ratio of 160:1 (w/w); the samples were incubated for 1 hour using 6 μg of lipid at various calcium concentrations. At zero calcium concentration, only small bilayer patches ranging from 50 – 300 nm in diameter were observed. These patches are flat and featureless which suggests that they do not have proteins incorporated. As the concentration of calcium increased from 0 up to 10 and 25 mM (Figure 5.2B and C), the bilayer patches grew larger. The observed bilayer patches ranged from 50 – 1,000 nm in diameter when 10 mM calcium was used. At 25 mM, the observed patches ranged from 50 – 2,000 nm. Interestingly, the bilayer patches at either 10 or 25 mM calcium still appeared flat and featureless; there was no evidence for deposited receptor (Figure 5.2A, B and C). The absence of protein spots indicates that the deposited bilayer formed from lipid alone vesicles, which suggests that the POPC/nAChR sample at high L:P ratio (prepared by sucrose gradient) may contain a small population of POPC alone vesicles. Nevertheless, the result here demonstrates that calcium has a positive effect on the deposition of a bilayer on mica such that higher calcium concentration results in more bilayer patches deposited. It can not be concluded at this point what concentration

Figure 5.2. AFM images of planar bilayers prepared with various calcium concentrations. The samples were prepared from reconstituted POPC/nAChR vesicles at a L:P ratio of 160:1 (w/w) and incubated for 1 hour using 7 μg of lipid at various calcium concentrations as indicated.

0 mM $CaCl_2$

10 mM $CaCl_2$

25 mM $CaCl_2$

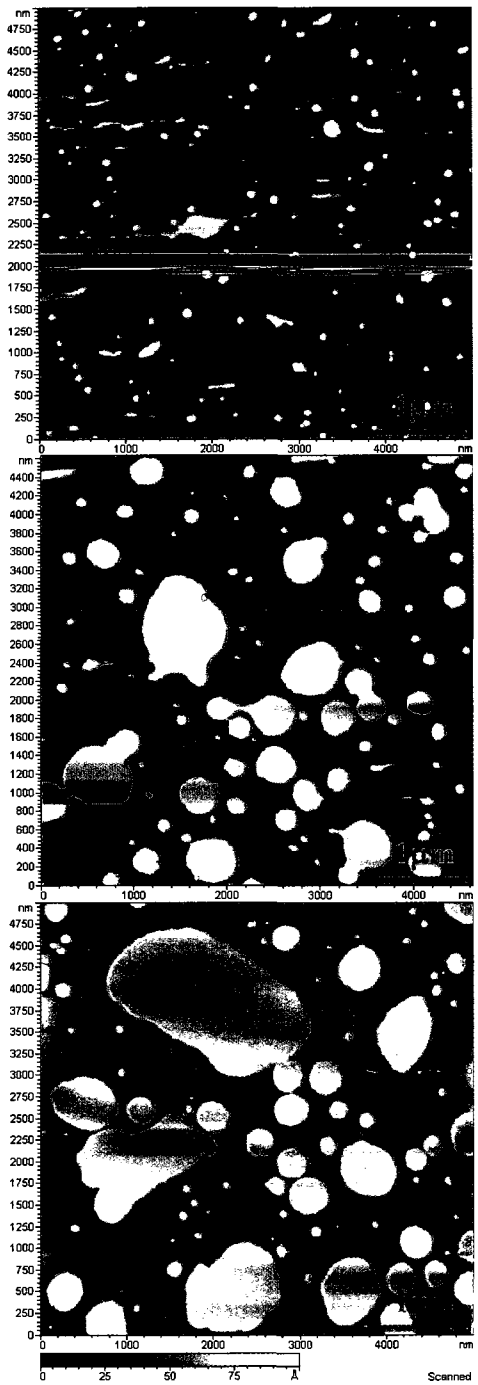

of calcium is best for the preparation of a POPC/nAChR bilayer on mica, but it appears that the incubation time or the amount of sample loaded is not sufficient.

5.2.3 The effect of sample loading

To test the effect of sample loading, the calcium concentration was fixed at 25 mM with an incubation time of 1 h, while the amount of sample loaded was varied. The AFM images in Figure 5.3A & B correspond to a POPC/nAChR bilayer prepared by incubating 10 μg of lipid on mica for 1 hour with 25 mM calcium. These images show an intact planar bilayer on mica. There are small particles in the range of 20 – 50 nm in diameter on the deposited bilayer, and these particles could be the nAChR (possibly as small aggregates) in a POPC bilayer. Unfortunately, these images had artifacts due to tip contamination. In addition, there are a number of large particles about 100 – 250 nm in diameter observed in these images. These large particles can be anything that interacts with the deposited bilayer on mica and can not be removed through washing, even when the bilayer was washed with copious amount of EDTA. These large particles are suspected to be POPC/nAChR vesicles present in excess, which interact with the deposited POPC/nAChR planar bilayer on mica via protein-protein interactions (i.e., protein aggregation). As the AFM tip scans the bilayer, it picks up these proteoliposomes and results in double tip artifacts. Thus, increasing the vesicle loading results in more material adhering to the bilayers, causing increased tip contamination problems.

5.2.4 The effect of time of incubation on the formation of a POPC/nAChR bilayer on mica

My options in preparing and imaging a POPC/nAChR bilayer on mica have now narrowed down to using a minimal sample loading while increasing the incubation time.

Figure 5.3. The effect of sample loading and incubation time on the preparation of a planar bilayer on mica were examined. A & B are AFM images of a bilayer prepared by incubating 10 μg of lipid (using the sample with a L:P ratio of 125:1 w/w) for 1 hour in 25 mM $CaCl_2$. C & D are AFM images of a bilayer prepared with 7 μg of lipid (using the same sample) incubated for 20 hours in 25 mM $CaCl_2$. Both of the samples were prepared in a moist chamber to prevent evaporation of buffer from the AFM cell, especially the 20 hours incubation.

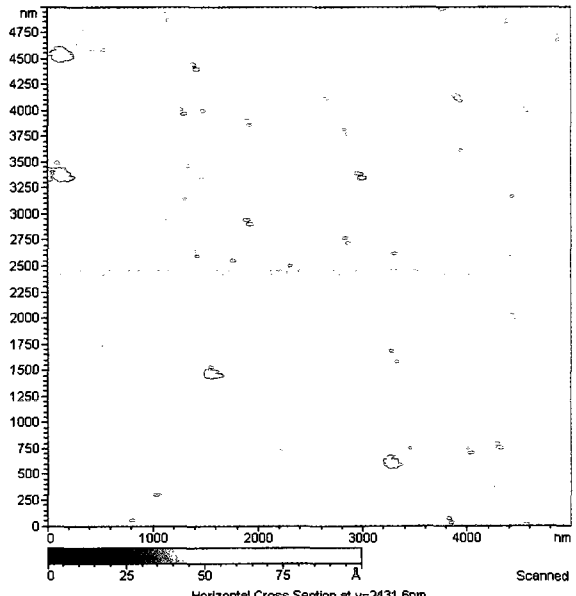
nm
4750
4500
4250
4000
3750
3500
3250
3000
2750
2500
2250
2000
1750
1500
1250
1000
750
500
250
0
0
1000
2000
3000
4000
nm
0
25
50
75
Å
Scanned

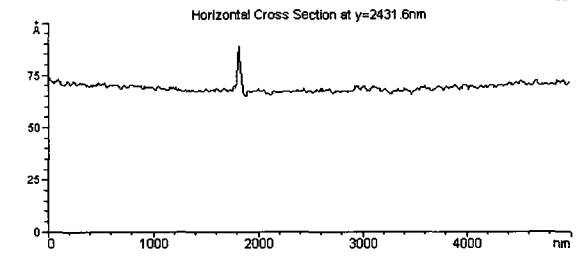
Horizontal Cross Section at y=2431.6nm
Å
75
50
25
0
0
1000
2000
3000
4000
nm

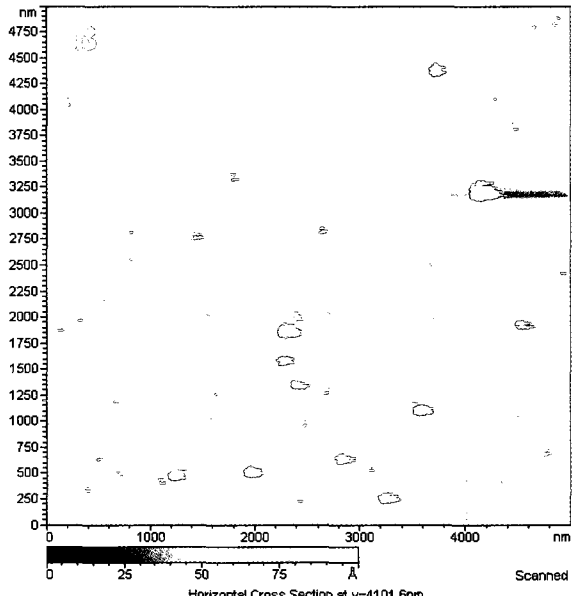
nm
4750
4500
4250
4000
3750
3500
3250
3000
2750
2500
2250
2000
1750
1500
1250
1000
750
500
250
0
0
1000
2000
3000
4000
nm
0
25
50
75
Å
Scanned

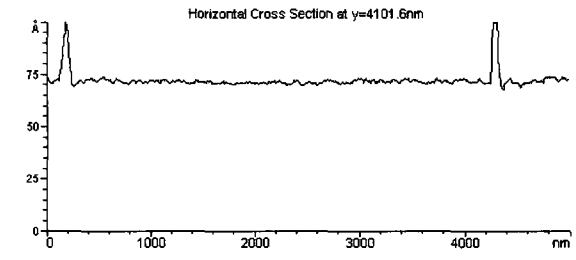
Horizontal Cross Section at y=4101.6nm
Å
75
50
25
0
0
1000
2000
3000
4000
nm

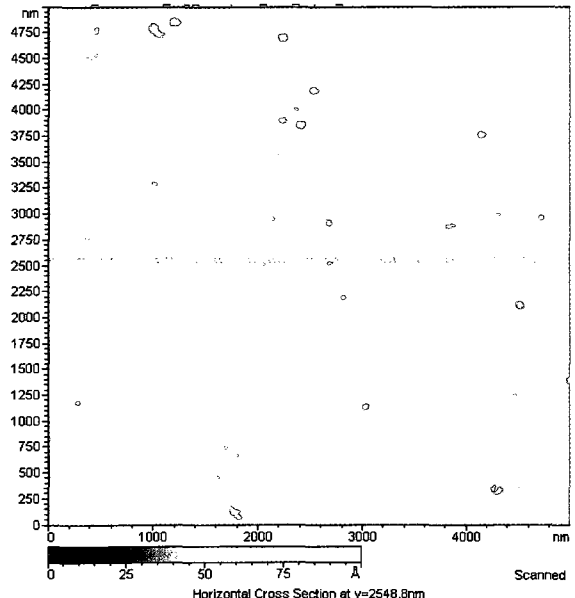
nm
4750
4500
4250
4000
3750
3500
3250
3000
2750
2500
2250
2000
1750
1500
1250
1000
750
500
250
0
0
1000
2000
3000
4000
nm
0
25
50
75
Å
Scanned

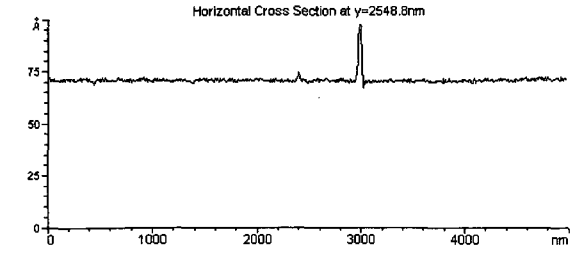
Horizontal Cross Section at y=2548.8nm
Å
75
50
25
0
0
1000
2000
3000
4000
nm

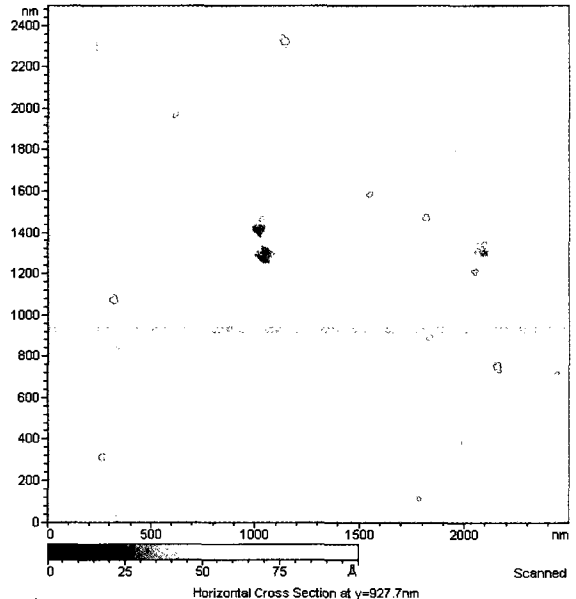
nm
2400
2200
2000
1800
1600
1400
1200
1000
800
600
400
200
0
0
500
1000
1500
2000
nm
0
25
50
75
Å
Scanned

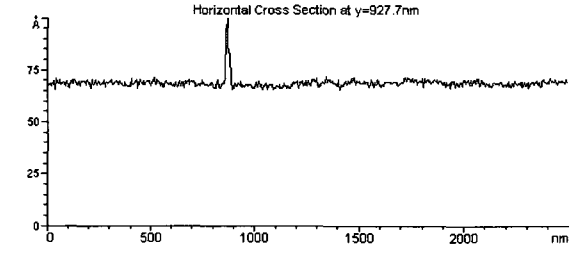
Horizontal Cross Section at y=927.7nm
Å
75
50
25
0
0
500
1000
1500
2000
nm

Thus, a bilayer was prepared on mica by incubating 7 μg of lipid in 25 mM $CaCl_2$ for 20 hours. The AFM images of this bilayer show an intact POPC/nAChR bilayer on mica (Figure 5.3C & D). The bilayer has numerous small particles protruding from a surface that is flat otherwise. These particles have no observable double tip artifacts even in small scale AFM images (for higher resolution) (Figure 5.3D). Such images would allow topographical information regarding the nAChR in a POPC bilayer to be obtained. So far, the best condition to prepare an intact POPC/nAChR bilayer on mica is to use a minimal quantity of reconstituted sample and incubate it for a long period of time (i.e., 20 hours) in the presence of calcium.

To determine the optimal calcium level, a reconstituted POPC bilayer +/- the nAChR was incubated at varying levels of calcium (0, 10 and 25 mM) while holding the incubation time (20 hours) and sample loading (6 μg of lipid) constant. Note that 6 μg of lipid was used to obtain an incomplete bilayer so that the effects of calcium could be better observed; 7 μg of lipid typically results in an intact bilayer. Figure 5.4 A & B correspond to AFM images of the deposited bilayer prepared with POPC vesicles +/- the nAChR in the absence of calcium. In both cases, patches of bilayer were deposited on the mica surface. It is evident that POPC alone vesicles yield larger patches (Figure 5.4B) than do POPC/nAChR vesicles (Figure 5.4A). This result suggests that empty liposomes form a planar bilayer on mica more readily than proteoliposomes in the absence of calcium. When the level of calcium was increased to 10 mM, the amount of bilayer deposited on the mica surface significantly increased for both POPC alone and POPC/nAChR (Figure 5.4 C and D). An intact planar bilayer is formed on mica when POPC vesicles are used, whereas POPC/nAChR vesicles yield a nearly intact bilayer in which some holes can typically be

Figure 5.4. The effect of calcium on the preparation of a bilayer on mica is assessed for POPC +/- the nAChR. The bilayers were prepared by incubating 6 μg of lipid from a reconstituted sample with a L:P ratio of 160:1 (w/w) in 0 (A and B), 10 (C and D) and 25 mM $CaCl_2$ (E and F) for 20 hours. All the samples were prepared in a moist chamber to prevent evaporation of buffer from the AFM cell. Note the artifact at the bottom of images C and E due to the large mica defect.

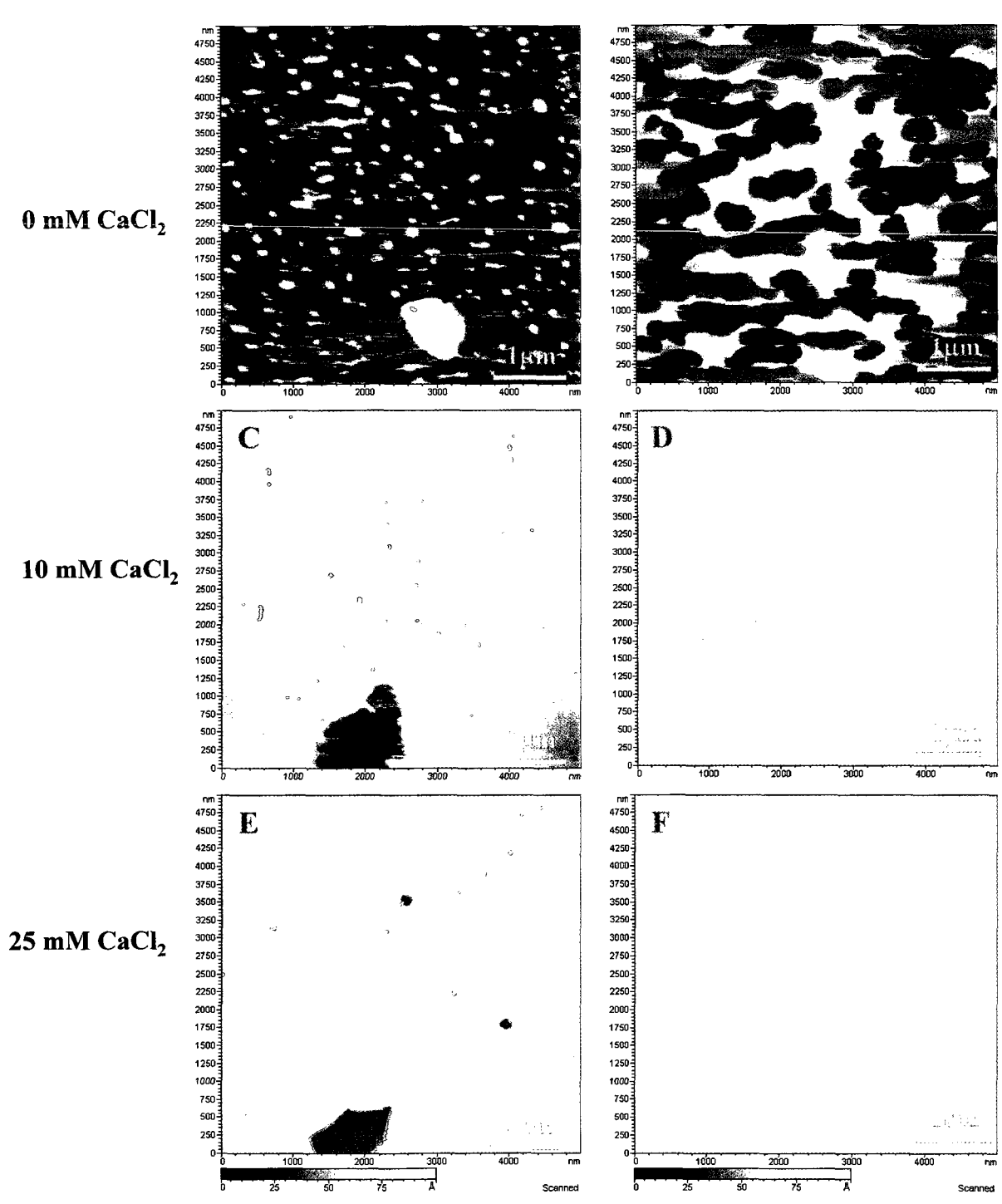
POPC/nAChR
POPC alone
0 mM CaCl2
10 mM CaCl2
25 mM CaCl2
C
D
E
F
1 µm
Scanned

observed. Importantly, the POPC/nAChR vesicles give a bilayer with numerous small spots protruding out of the bilayer (Figure 5.4C). These spots are about 20 nm in diameter and 30 nm in height, but whether such spots correspond to the nAChR in a POPC bilayer would need further examination. As the level of calcium was increased to 25 mM, a very similar result to 10 mM calcium is observed (Figure 5.4 E and F). The results are similar for 10 and 25 mM calcium, suggesting that reconstituted POPC/nAChR vesicles at high L:P ratio (160:1 w/w in this case) only require low calcium concentrations to form a planar bilayer on mica. However, 25 mM calcium was chosen for all subsequent planar bilayer preparations to counteract the variation in L:P ratio in different reconstitutions, just in case slightly lower L:P ratio samples (such as 125:1 used in some experiments) required a slightly higher calcium level.

In summary, the preparation of a POPC/nAChR bilayer on mica for AFM imaging required optimal conditions for the proteoliposomes to deposit on the mica surface and form a planar bilayer without contamination. The key parameters for formation of supported bilayers from reconstituted POPC/nAChR proteoliposomes are the calcium concentration, quantity of sample loaded and length of time. In addition, the deposited bilayer should be washed free of any excess material that may lead to artifacts due to tip contamination. It is established that the conditions to prepare a POPC/nAChR planar bilayer on mica in an AFM cell of approximately 130 mm^2 are to incubate 7 μg of lipid from POPC/nAChR vesicles at high L:P ratio in 25 mM calcium at room temperature for 20 hours. Following the incubation, the excess vesicles are washed off with a solution of EDTA, and then the EDTA solution is replaced with the HEPES imaging buffer prior to imaging. The procedure

described here was used to prepare POPC/nAChR bilayers at high L:P ratio on mica for subsequent experiments.

5.2.5 Imaging the nAChR in a POPC bilayer on mica by TIRF

After the procedure to prepare a POPC/nAChR bilayer on mica was established by AFM, I wanted to confirm that the small particles observed in the AFM images actually corresponded to the nAChR. To serve this purpose, a POPC/nAChR planar bilayer on mica was imaged by TIRF microscopy. In order to view the protein by fluorescence microscopy, the reconstituted POPC vesicles +/- the nAChR were labeled with αBTx-A488 as described in Materials and Methods.

The preparation of a POPC/nAChR planar bilayer on mica for TIRF imaging is slightly different from the procedure for AFM samples due to the larger size of the TIRF cell (see Materials and Methods). A bilayer was prepared by keeping the calcium concentration and incubation time the same as in AFM, but the quantity of sample used was increased to 10 μg of lipid. Furthermore, 1 μg of exogenous POPC vesicles doped with 2 % TR-DHPE (a fluorescent labeled PE) was co-incubated with the sample to allow visualization of the deposited planar bilayer. The TIRF image in Figure 5.5A showed a bilayer prepared from an αBTx-A488 labeled POPC/nAChR bilayer (at L:P ratio of 160:1 w/w); the image shows areas of fluorescence from the αBTx-A488. In contrast, a POPC alone bilayer that was similarly labeled with αBTx-A488 did not show any fluorescence (Figure 5.5B). These results confirm the presence of the nAChR for POPC bilayers on mica prepared with a reconstituted POPC/nAChR sample at high L:P ratio. When a POPC/nAChR bilayer labeled with αBTx-A488 was similarly prepared and imaged by AFM, a number of small particles were observed (Figure 5.5C). On the other hand, the POPC alone bilayer labeled with

Figure 5.5. A comparison of a reconstituted POPC bilayer +/- the nAChR imaged by TIRF and AFM. The bilayers were prepared under similar conditions as in Figure 5.3 C & D, and they were imaged by AFM (A & B) and TIRF (C & D). The negative control was prepared from POPC alone vesicles, where the treatment was identical to the reconstituted nAChR/POPC sample. Both POPC alone and nAChR/POPC vesicles were labeled with aBTx-A488, but the toxin should bind only to the nAChR/POPC sample. For TIRF, a small amount of exogenous POPC vesicles doped with 2 % TR-DHPE (1 μg of lipid in total) were co-incubated with the samples to allow visualization of the bilayer on mica, but only the signal from the nAChR labeled with aBTx-A488 is shown here. The TIRF images were acquired by using a 488 nm laser for excitation and the emission was collected around 543 nm.

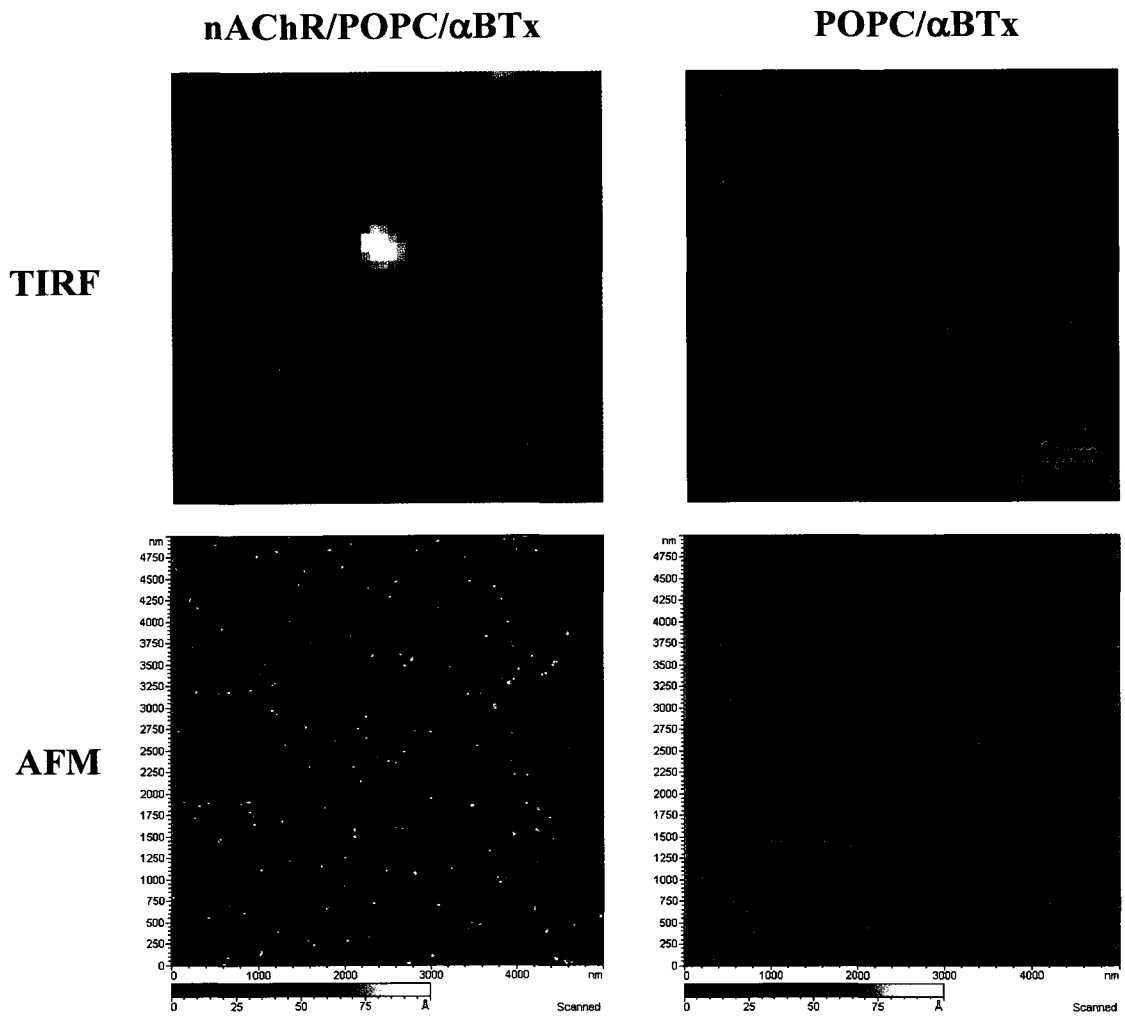
nAChR/POPC/αBTx
POPC/αBTx
TIRF
AFM
nm
4750
4500
4250
4000
3750
3500
3250
3000
2750
2500
2250
2000
1750
1500
1250
1000
750
500
250
0
0
1000
2000
3000
4000
nm
0
25
50
75
Å
Scanned

αBTx-A488 was flat and featureless (Figure 5.5D). Evidently, the fluorescence signal (in TIRF images) or particles (in AFM images) are only observed for POPC bilayers containing the reconstituted nAChR. Thus, the observed fluorescence signal or particles in the TIRF and AFM image, respectively, are likely to correspond to the nAChR. These results encourage further examination and topographical analysis of the raised features observed by AFM.

5.3 Characterizing the nAChR in a POPC bilayer via AFM

As the particles in the AFM images were confirmed to be the nAChR in a POPC bilayer via TIRF microscopy, the next step was to analyze the topographical information on these particles to examine the structure of the nAChR in a POPC bilayer by AFM. Based on AFM images similar to those shown in Figure 5.5C & D, the height distribution for these particles was measured and tabulated in Figure 5.6C. The histogram shows a broad maximum at ~ 3 nm with a small number of features between 5.5 – 9 nm. According to the known cryo-electron microscopy model structure of the nAChR, the nAChR protrudes out of the bilayer by about 3 and 7 nm at the cytoplasmic and extracellular domains, respectively. The major height distribution centered around 3 nm in the histogram coincides closely with the expected height of the cytoplasmic domain of the nAChR. This suggests that the extracellular domain of the receptor is primarily contacting the mica, while the cytoplasmic domain protrudes upward and interacts with the AFM tip during a scan. The features with heights ranging from 5.5 to 9.0 nm could be receptors with the opposite orientation (i.e., with the extracellular domain protruding from the bilayer surface). I have also attempted to image the nAChR at high resolution in the POPC bilayer at high L:P ratio.

Figure 5.6. The height distribution of the observed features protruding from a POPC/nAChR bilayer prepared on mica. The bilayers (A & B) were prepared and imaged under similar condition as in Figure 5.5. The height distribution for the spots observed from at least 3 different reconstitutions were tabulated (C), and at least 2 acquired images per reconstitution were used in this analysis. Based on the height distribution histogram, the nAChR is oriented with the cytoplasmic side protruding from the bilayer surface in most cases. The proposed orientation of the nAChR in the prepared planar bilayer is demonstrated in D.

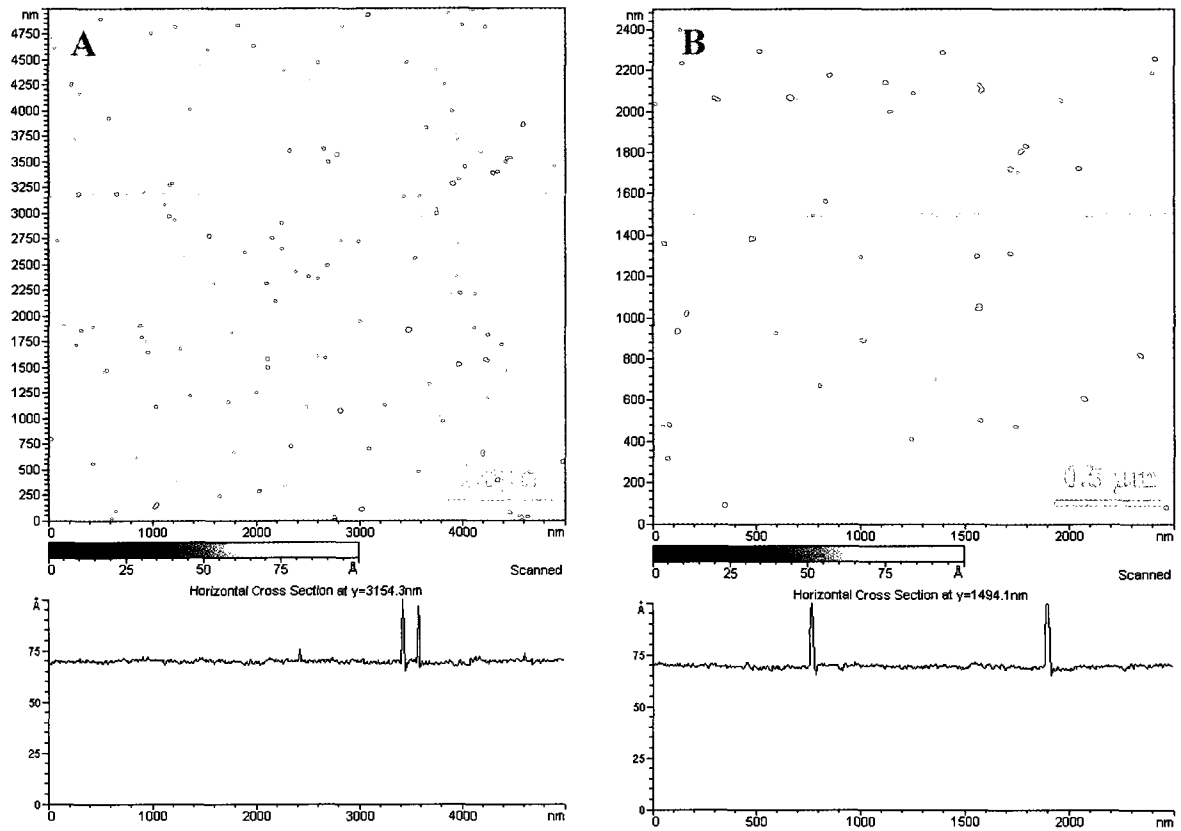
A
B
Scanned
Horizontal Cross Section at y=3154.3nm
Horizontal Cross Section at y=1494.1nm
nm
Å

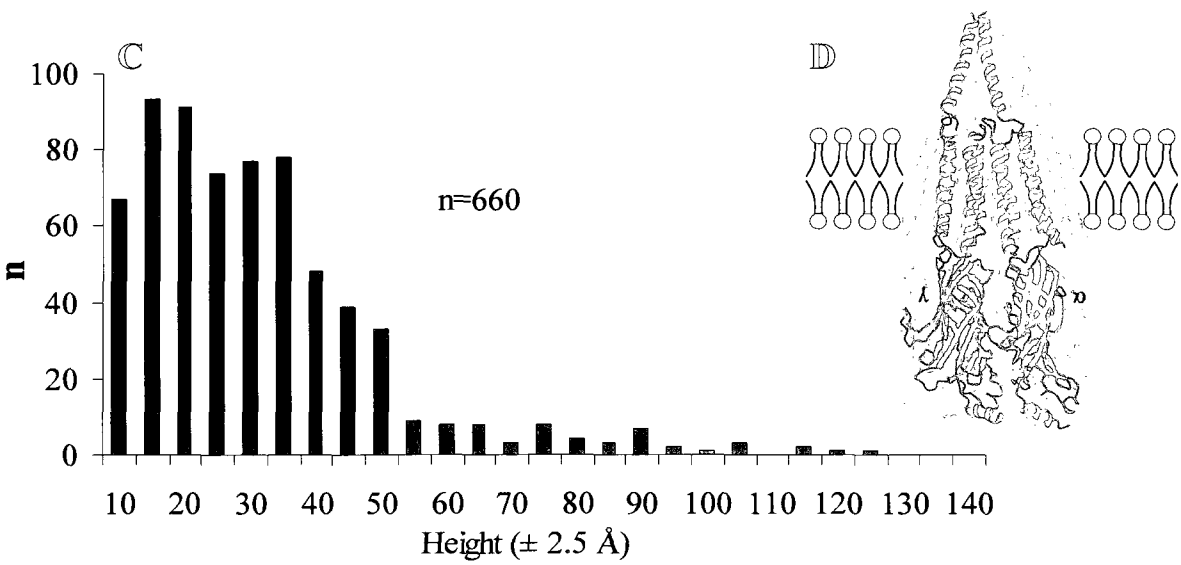
C
D
n=660
n
Height (± 2.5 Å)

To do so, the particles with heights of 3 or 7 nm were zoomed in and scanned at higher resolution (Figure 5.7). Based on these high resolution images, the scanned particles are still not well resolved. It was not possible to acquire an image with adequate resolution to show individual subunits of the nAChR. However, such results were expected since most of the high resolution AFM images of membrane proteins have been acquired from protein rich bilayers that pack in a 2D crystalline manner (Fotiadis et al., 2003; Seelert et al., 2003). For bilayers prepared at high L:P ratio, the individual receptors are well separated in a fluid bilayer, and are not sufficiently rigid to resolve individual subunits by AFM. Nevertheless, the diameter of the particles in the bilayer can be measured from these high resolution AFM images. These particles typically ranged from 14 to 19 nm in diameter (Figure 5.7). It should be noted that the crystal structure of the nAChR by Unwin (2005) did not resolve the cytoplasmic domain of the nAChR well, and the exact diameter of the cytoplasmic domain of the nAChR remains poorly defined. Nevertheless, the diameter of the cytoplasmic domain can not be greater than the extracellular domain based on the amino acid sequence in these domains. Thus, I expect the diameter of the cytoplasmic domains of the nAChR to be smaller than the extracellular domain (~ 9 nm). Yet, the measured diameter for the nAChR ranges from 14 – 19 nm. Clearly these two values do not match. However, this is expected since the measured diameter of the nAChR has not taken the size of the AFM tip into consideration, which tends to over-estimate the lateral measurements.

We need to keep in mind that as the AFM tip scans over an object protruding out of a flat surface, the observed size is a convolution of the sizes of the feature and the AFM tip. The over-estimation in lateral measurements of the insulin receptor by AFM has been well described by Slade (2003) as shown in Figure 5.8; the over-estimation is mathematically

Figure 5.7. Selected small scale AFM images that show high resolution images of the observed features. The observed spots in the bilayers are featureless with a rough diameter of ~150 Å and height of ~35 Å. The reasons that I fail to observe structural features due to individual subunits may include the fact that the POPC membrane is disordered at 20 °C and the protein can be easily moved by the AFM tip. Moreover, the proteins are not densely packed in a 2-D crystalline array; most successful high resolution AFM imaging of membrane proteins has used samples with high protein density.

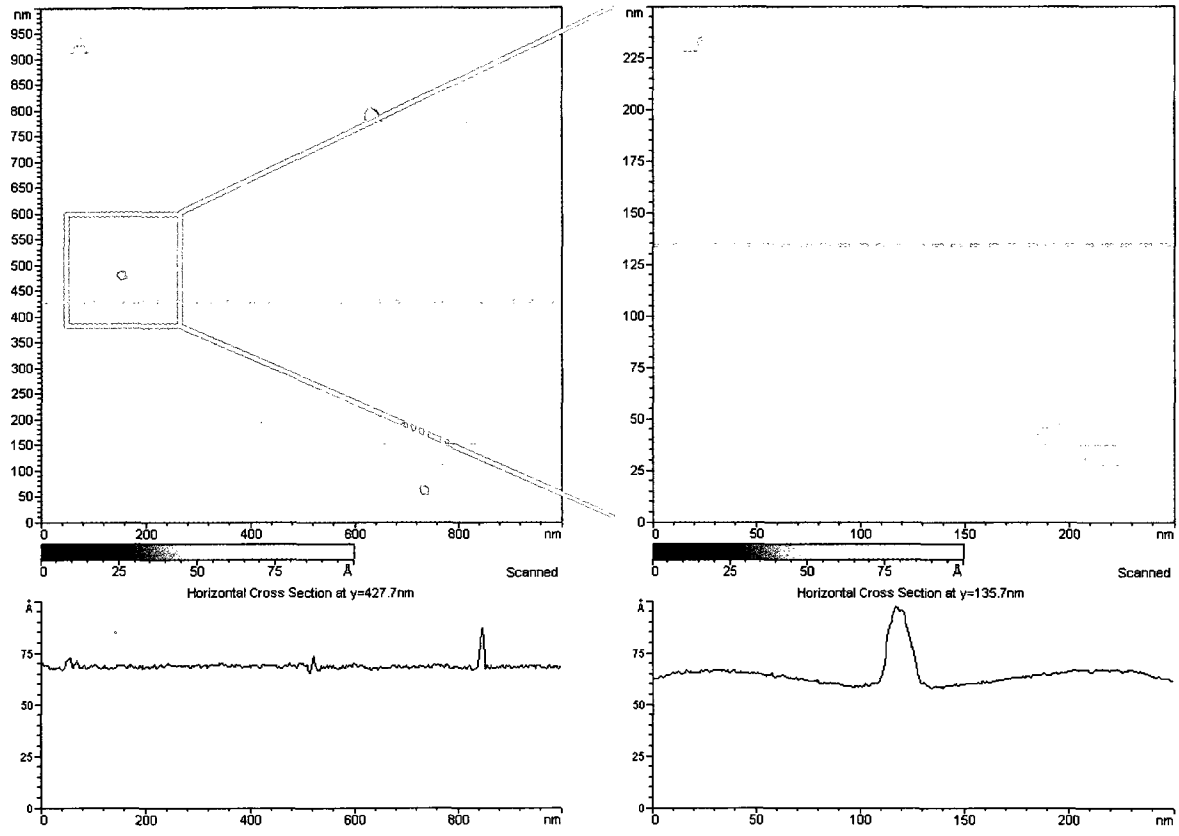
nm
950
900
850
800
750
700
650
600
550
500
450
400
350
300
250
200
150
100
50
0
0
200
400
600
800
nm
0
25
50
75
Å
Scanned
Horizontal Cross Section at y=427.7nm
Å
75
50
25
0
0
200
400
600
800
nm
nm
225
200
175
150
125
100
75
50
25
0
0
50
100
150
200
nm
0
25
50
75
Å
Scanned
Horizontal Cross Section at y=135.7nm
Å
75
50
25
0
0
50
100
150
200
nm

Figure 5.8. A schematic diagram used to calculate the over-estimation in the lateral dimension of an integral membrane protein observed by AFM. The calculation here is based on a model by Slade (2003) used to calculate the overestimation of the insulin receptor reconstituted in a bilayer observed by AFM. In this calculation, r is the half height of the cytoplasmic or extracellular domain of the receptor, R is the radius of the AFM tip apex, and θ is half of the cone angle of the tip.

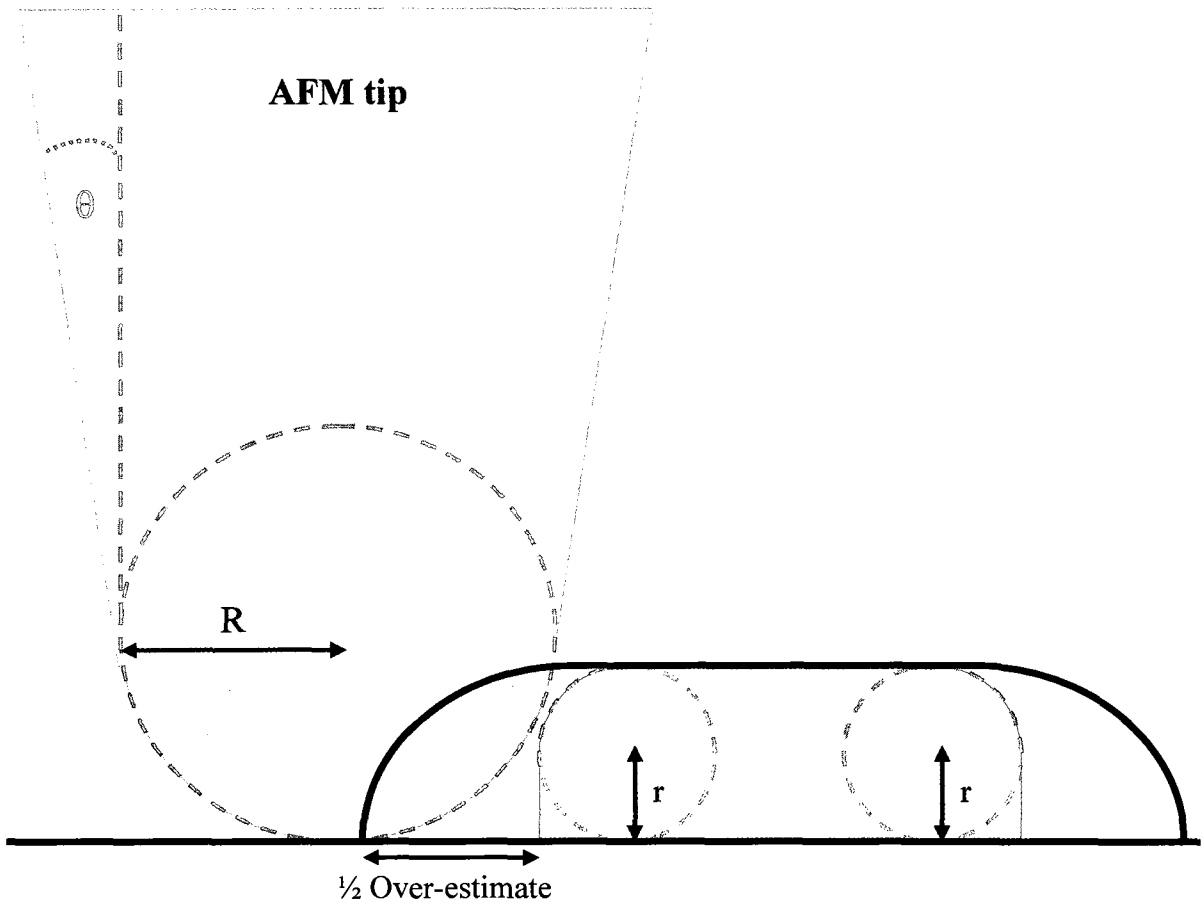

$$(1)\ \text{Over-estimate} = 2\left[\frac{2\,[(r+R)+(r-R)]\,\sin\theta}{2\text{Cos}\theta} - r\right];\ \text{for}\ \sin\theta > (R-r)/(R+r)$$

$$(2)\ \text{Over-estimate} = 2\left[\frac{4\sqrt{R\,r}}{2} - r\right];\ \text{for}\ \sin\theta < (R-r)/(R+r)$$

related to the size of the receptor and the radius and cone angle of the AFM tip. According to the distributor information (*Agilent*), the AFM tip used has a cone angle of 20° at the apex of the tip, and a radius of 7 nm or less. As the size of the nAChR, cone angle and radius of the AFM tip were taken into consideration (Figure 5.9), the over-estimation in the diameter of the nAChR in a bilayer can be calculated with the following equation:

$$\text{Over-estimate} = 2\left[\frac{4\sqrt{R\,r}}{2} - r\right]$$

where r is the half height of the cytoplasmic or extracellular domain of the receptor, R is the radius of the AFM tip apex. Therefore, the over-estimate diameter is about 10 nm if the AFM tip has a radius of 7 nm at the tip apex and the measured height of the receptor is about 3 nm. Subsequently, the actual diameter of the nAChR can be calculated as followed:

Actual diameter = Observed diameter – Over-estimate

Since the observed diameter of the nAChR is found to be about 14 – 19 nm, the actual diameter of the nAChR should be 5 – 10 nm (14 nm – 10 nm = 4 nm, and 19 nm – 10 nm = 9 nm). Thus, the majority of the observed spots have a dimension of about 3 nm in height and 4 – 9 nm in width (lateral diameter). Such dimension is not acceptable for the extracellular domain of the nAChR which is 7 x 9 nm (h x w) (Miyazawa et al., 2003; Unwin, 2005), but the observed dimension would fit the cytoplasmic domain of the nAChR based on the length of the peptide (Unwin, 2005).

Figure 5.9. Schematic diagram to calculate the over-estimation in diameter for the nAChR in a bilayer. The AFM tip used was MAC type II (*Agilent*), which has a cone angle of ~ 20° (i.e., $\theta = 10°$) and tip apex radius (R) of less than 7 nm (I assume that R is between 5 – 7 nm). The extracellular height of the nAChR is about 7 nm (half height, or r = 3.5 nm), and the cytoplasmic height of the nAChR is about 4 nm (half height, or r = 2 nm). If R is 7 nm, then the respective value of (R – r) / (R + r) is 0.333 and 0.555 for the extracellular and cytoplasmic domains. If R is 5 nm, then the respective value of (R – r) / (R + r) is 0.176 and 0.426 for the extracellular and cytoplasmic domain. In all cases, the (R- r) / (R + r) values are greater than Sin(10°) = 0.174. Thus, only equation 2 from Figure 5.8 is applicable when calculating the over-estimate of the diameter of the nAChR.

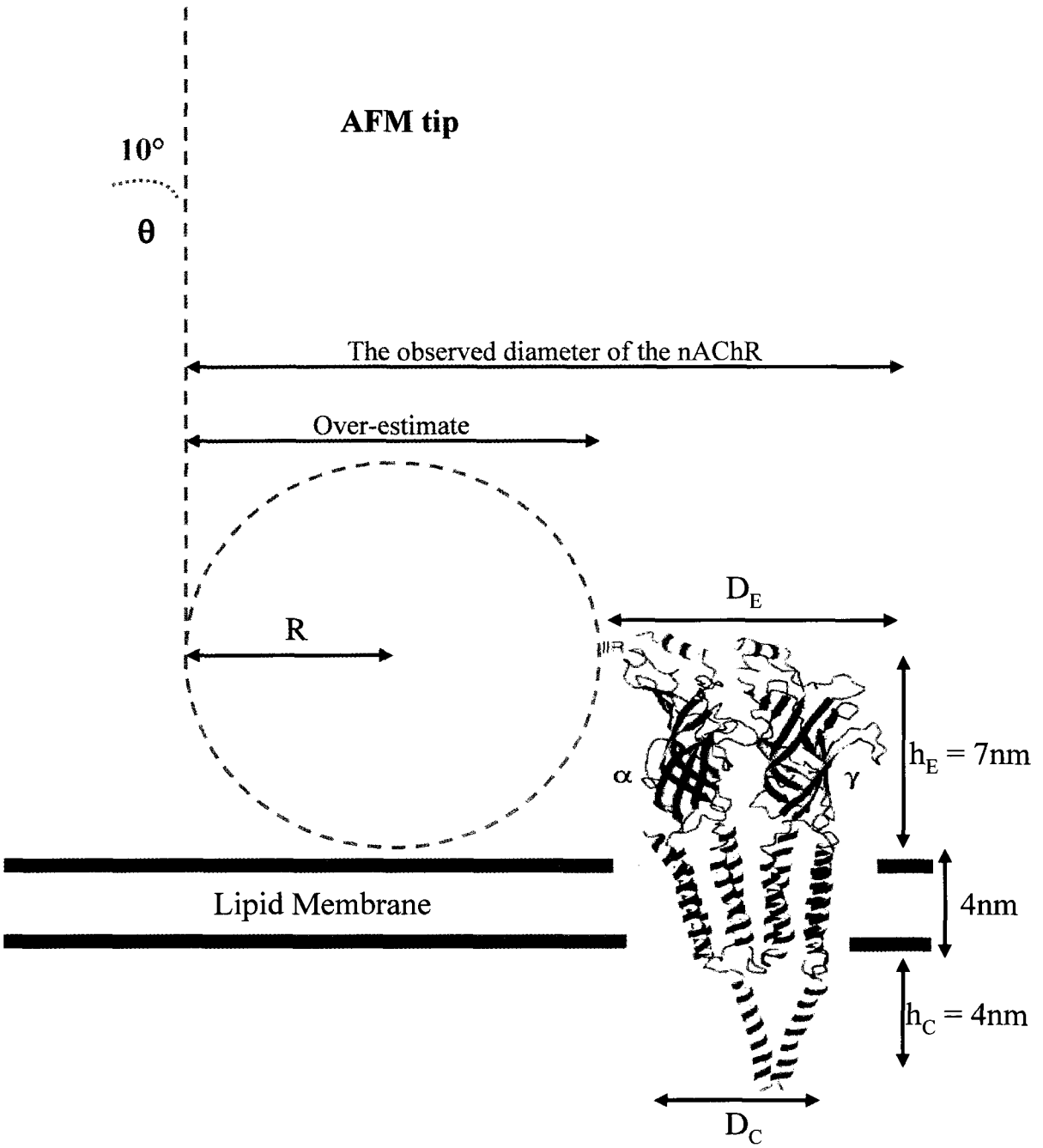

$$(2)\ \text{Over-estimate} = 2\left[\frac{4\sqrt{R\,r}}{2} - r\right];\ \text{for } \sin\theta < (R - r) / (R + r)$$

5.4 Discussion and Conclusions

In order to image a bilayer by AFM, the bilayer has to be a planar bilayer on a solid support (e.g., mica). The process of preparing and imaging a lipid bilayer such as POPC on mica by AFM is not too difficult (see Chapter 3). However, preparing and imaging a POPC bilayer containing the nAChR required extensive optimization.

Firstly, it was found that the presence of calcium is necessary for the formation of a POPC/nAChR bilayer on mica. The TIRF results in Chapter 4 showed that a POPC/nAChR sample at low L:P ratio (i.e., 10:1 w/w) required a high level of calcium (75 mM) for the proteoliposomes to adsorb on the mica surface (Figure 4.8D). The AFM results in this chapter showed that 10 mM calcium is sufficient for a planar bilayer to form on the mica surface with the POPC/nAChR proteoliposomes at high L:P ratio such as 125:1 and 160:1 (w/w) (Figure 5.4C). However, in the absence of calcium only small lipid patches devoid of protein form on the mica surface (Figure 5.4A). The requirement for a divalent cation such as calcium may be due to the fact that the mica (TedPella Inc) and nAChR (Unwin, 2005) surface are both negatively charged, and the presence of calcium most likely bridges the interaction of the two negatively charged surfaces.

Secondly, it is important to use a minimal amount of sample in order to form a POPC/nAChR bilayer that is suitable for AFM imaging. Although excessive sample loading still forms a bilayer on mica, it always leads to double tip artifacts in the AFM image. The artifacts could be due to the surplus POPC/nAChR proteoliposomes adsorbed to the planar bilayer on mica (possibly via protein-protein interaction), and the proteoliposomes can not be removed through washing following the sample deposition stage. As the AFM tip scans the bilayer, it interacts with the adsorbed proteoliposomes leading to tip contamination. It

was found that about 6-7 μg of lipid for a population of POPC/nAChR proteoliposomes at a L:P ratio of 125:1 (w/w) or higher is optimal to form an intact bilayer on a mica surface of about 130 mm^2 (the exposed mica surface in the AFM cell used). Based on my earlier observation, this quantity of proteoliposomes exceeded the absolute amount of lipid required to cover the mica surface, which is about 1 – 2 μg (see chapter 3.2.1). The other 5 – 6 μg of proteoliposome is needed to drive the formation of a planar bilayer on the mica surface (the mechanism is probably equilibration between proteoliposome and planar bilayer on the mica surface), since using less than 7 μg typically led to the formation of a planar bilayer with holes or patches of planar bilayer.

Thirdly, the length of time required to get an intact POPC/nAChR bilayer to form on a mica surface that can be imaged by AFM is also critical. It appears that a long incubation time (i.e., 20 hours) is needed for a minimal loading of POPC/nAChR proteoliposomes to form an intact bilayer on mica (Figure 5.3C&D). When the length of time is insufficient (i.e., 1 hour) the reconstituted nAChR is not deposited on the mica surface and only POPC patches with few or no proteins can be observed (Figure 5.1 and 5.2). The length of incubation time required may not need to be as long as 20 hours, but it was more convenient to incubate overnight and then image the bilayer the following day. The exact minimum incubation time could be much less then 20 hours, but I was not interested in determining the minimum incubation time. Thus, I established that a reconstituted POPC/nAChR sample with a L:P ratio greater than 100:1 w/w can be prepared on mica for AFM imaging by incubating about 7 μg of lipid in 25 mM $CaCl_2$ for 20 hours at room temperature.

Finally, it was found that washing the intact POPC/nAChR planar bilayer on mica with EDTA following the incubation step is useful to reduce the double tip artifacts in the

AFM images (Figure 5.1). Such EDTA washing is believed to remove those excess proteoliposomes bound to the bilayer. The function of EDTA is to competitively complex the calcium ions which allow the intermolecular protein-protein interaction (i.e., bridging the negatively charged surfaces of the nAChR) between the excess proteoliposomes and the planar bilayer.

The TIRF and AFM images shown in Figure 5.5 demonstrate that POPC bilayers with the nAChR reconstituted at high L:P ratio can be prepared and imaged on mica. The observed particles in the AFM images are due to the presence of the nAChR in the POPC bilayer. The height of the particles protruding out of the bilayer has a broad distribution centered around 3 nm, which coincides with the height of the cytoplasmic domain of the nAChR (Figure 5.6). The diameter for the particles measured at high resolution ranged from 14 – 19 nm (Figure 5.7). This observed value clearly does not match the expected diameter of the nAChR. However, when the lateral over-estimation in AFM imaging has been taken into account, the observed diameter can be converted to actual diameter, which gives the cytoplasmic domain of the nAChR a value in the range of 4 – 9 nm. This value fits well with the expected diameter of the cytoplasmic domain of the nAChR (Miyazawa et al., 2003; Unwin, 2005). Therefore, my AFM results suggested that the cytoplasmic domain of the nAChR in a POPC bilayer has a dimension of about 3 nm tall and 4 – 9 nm wide.

Chapter 6: General Discussion and Conclusions

The original goal of this study was to address the controversial question of whether the nAChR can induce segregation of lipids into domains in a reconstituted bilayer. I chose to use AFM to investigate this matter since AFM has been used in recent years to examine several integral membrane proteins in their native membranes at high resolution (Fotiadis et al., 2003; Seelert et al., 2003). However, there is a lack of knowledge in the literature as to how to prepare a reconstituted bilayer containing the nAChR for AFM imaging,,and I had difficulties in imaging a protein reconstituted bilayer in my early experiments. Thus, I decided to devise a method to image the receptor reconstituted in a simple one-component lipid bilayer, before attempting to examine the nAChR reconstituted in more complex bilayers.

The results in this study demonstrated that I was able to devise a method to image the nAChR reconstituted in a simple bilayer (i.e., POPC) by AFM. This method has 2 steps: the first step was to reconstitute the nAChR in POPC vesicles at high L:P ratio (i.e., greater than 100:1 w/w), and the second step was to use the reconstituted sample to prepare a planar bilayer on mica for AFM imaging. Both of these steps were difficult to achieve, and extensive characterization and optimization were needed. However, the characterization and optimization led to the discovery of essential parameters for reconstituting the nAChR in lipid vesicles at high L:P ratio and preparing a planar bilayer containing the reconstituted receptor for AFM imaging. For example, the sample required a freeze-thaw cycle after reconstitution (after dialysis) to reconstitute the nAChR at high L:P ratio (see discussion in section 4.5). The preparation of a POPC/nAChR bilayer on mica for imaging from the high L:P ratio proteoliposomes required optimal conditions and appropriate washing to remove unabsorbed materials to prevent artifact contamination of the AFM tip (see discussion in

section 5.4). Subsequently, it was possible to image the nAChR in a POPC bilayer. The protein protrudes out of the bilayer by about 3 nm and it has a diameter in the range of 4 – 9 nm. These dimensions are consistent with the size of the cytoplasmic side of the nAChR based on electron microscopy data (Miyazawa et al., 2003; Unwin, 1993b; Unwin, 2005). More importantly, I have established a number of key parameters for the reconstitution of the nAChR in a lipid vesicle at high L:P ratio and the preparation of a planar bilayer on mica for microscopic imaging such as TIRF and AFM. Understanding these parameters would undoubtedly be useful in future attempts to reconstitute and image the nAChR in more complex bilayers (e.g., POPC/POPA and POPC/POPA/Chol), and possibly for reconstituting and imaging other integral membrane proteins as well.

For future work, I would reconstitute and image the nAChR either in a POPC/POPA (3:2 mol/mol) or POPC/POPA/Chol (3:1:1 mol/mol) bilayer to address whether the receptor induces segregation of lipids into domains in a reconstituted bilayer. To do so, I would use a similar approach to that used to reconstitute and image the nAChR in a POPC bilayer; the first step is to examine a lipid alone bilayer by TIRF and AFM to assess the morphology of the bilayer. Then I would reconstitute the nAChR in the same bilayer and prepare a planar bilayer for AFM imaging to examine how the presence of the receptor affects the morphology of the bilayer (i.e., whether the receptor induces lipid segregation). As simple as it may sound, I would expect some challenges from preparing and imaging both lipid alone and protein reconstituted bilayer due to the large amount of negatively charged lipid (POPA) present in these bilayers. These challenges could be overcome by optimizing the conditions such as calcium concentration, sample loading, and incubation time and temperature. Perhaps a special washing procedure may also be needed to remove the

unabsorbed materials to prevent contaminated tip artifacts in the AFM images. Hopefully, reconstituting the nAChR in a proteoliposome at high L:P ratio would not lead to significant heterogeneity in the L:P ratio of the proteoliposomes. However, the reconstituted sample would still be carefully characterized by sucrose gradient, and the lipid composition of the proteoliposomes would be examined by TLC.

I wanted to determine whether or not the nAChR can segregate lipids into domains because I wanted to understand how the presence of the receptor in a PC/PA or PC/PA/Chol bilayer increases the Tm of the bilayer. If the nAChR could indeed segregate lipid into domains, it would be a clear indication that this integral membrane protein can somehow interact and control the lipids in its surrounding environment. When this is the case, I would want to look into the mechanism as to how the receptor could do so. If the nAChR does not induce the formation of lipid domains in the bilayer, such result would point out that the presence of this integral membrane protein somehow increases the Tm of the bilayer. In this case, I would still want to investigate how the protein could do so. By examining how a protein influences the property of a lipid bilayer, and vice versa, it would ultimately provide us a better understanding toward the structural and functional role of different lipids and proteins in the cell membrane.

References

Anand R, Conroy WG, Schoepfer R, Whiting P and Lindstrom J (1991) Neuronal nicotinic acetylcholine receptors expressed in Xenopus oocytes have a pentameric quaternary structure. *J Biol Chem* **266**(17):11192-11198.

Anholt R, Fredkin DR, Deerinck T, Ellisman M, Montal M and Lindstrom J (1982) Incorporation of acetylcholine receptors into liposomes. Vesicle structure and acetylcholine receptor function. *J Biol Chem* **257**(12):7122-7134.

Anholt R, Lindstrom J and Montal M (1981) Stabilization of acetylcholine receptor channels by lipids in cholate solution and during reconstitution in vesicles. *J Biol Chem* **256**(9):4377-4387.

Baenziger JE, Miller KW, McCarthy MP and Rothschild KJ (1992a) Probing conformational changes in the nicotinic acetylcholine receptor by Fourier transform infrared difference spectroscopy. *Biophys J* **62**(1):64-66.

Baenziger JE, Miller KW and Rothschild KJ (1992b) Incorporation of the nicotinic acetylcholine receptor into planar multilamellar films: characterization by fluorescence and Fourier transform infrared difference spectroscopy. *Biophys J* **61**(4):983-992.

Baenziger JE, Morris ML, Darsaut TE and Ryan SE (2000) Effect of membrane lipid composition on the conformational equilibria of the nicotinic acetylcholine receptor. *J Biol Chem* **275**(2):777-784.

Barenholz Y, Gibbes D, Litman BJ, Goll J, Thompson TE and Carlson RD (1977) A simple method for the preparation of homogeneous phospholipid vesicles. *Biochemistry* **16**(12):2806-2810.

Baro AM, Miranda R, Alaman J, Garcia N, Binnig G, Rohrer H, Gerber C and Carrascosa JL (1985) Determination of surface topography of biological specimens at high resolution by scanning tunnelling microscopy. *Nature* **315**(6016):253-254.

Barrantes FJ (2002) Lipid matters: nicotinic acetylcholine receptor-lipid interactions (Review). *Mol Membr Biol* **19**(4):277-284.

Benes M, Billy D, Benda A, Speijer H, Hof M and Hermens WT (2004) Surface-dependent transitions during self-assembly of phospholipid membranes on mica, silica, and glass. *Langmuir* **20**(23):10129-10137.

Binnig G, Frank KH, Fuchs H, Garcia N, Reihl B, Rohrer H, Salvan F and Williams AR (1985a) Tunneling spectroscopy and inverse photoemission: Image and field states. *Phys Rev Lett* **55**(9):991-994.

Binnig G, Garcia N and Rohrer H (1985b) Conductivity sensitivity of inelastic scanning tunneling microscopy. *Phys Rev B Condens Matter* **32**(2):1336-1338.

Bligh EG and Dyer WJ (1959) A rapid method of total lipid extraction and purification. *Can J Biochem Physiol* **37**(8):911-917.

Blount P and Merlie JP (1989) Molecular basis of the two nonequivalent ligand binding sites of the muscle nicotinic acetylcholine receptor. *Neuron* **3**(3):349-357.

Boulter J, Connolly J, Deneris E, Goldman D, Heinemann S and Patrick J (1987) Functional expression of two neuronal nicotinic acetylcholine receptors from cDNA clones identifies a gene family. *Proc Natl Acad Sci U S A* **84**(21):7763-7767.

Brejc K, van Dijk WJ, Klaassen RV, Schuurmans M, van Der Oost J, Smit AB and Sixma TK (2001) Crystal structure of an ACh-binding protein reveals the ligand-binding domain of nicotinic receptors. *Nature* **411**(6835):269-276.

Briley MS and Changeux JP (1977) Isolation and purification of the nicotinic acetylcholine receptor and its functional reconstitution into a membrane environment. *Int Rev Neurobiol* **20**:31-63.

Briley MS and Changeux JP (1978) Recovery of some functional properties of the detergent-extracted cholinergic receptor protein from Torpedo marmorata after reintegration into a membrane environment. *Eur J Biochem* **84**(2):429-439.

Brown DA and Rose JK (1992) Sorting of GPI-anchored proteins to glycolipid-enriched membrane subdomains during transport to the apical cell surface. *Cell* **68**(3):533-544.

Bruses JL, Chauvet N and Rutishauser U (2001) Membrane lipid rafts are necessary for the maintenance of the (alpha)7 nicotinic acetylcholine receptor in somatic spines of ciliary neurons. *J Neurosci* **21**(2):504-512.

Campos-Caro A, Sala S, Ballesta JJ, Vicente-Agullo F, Criado M and Sala F (1996) A single residue in the M2-M3 loop is a major determinant of coupling between binding and gating in neuronal nicotinic receptors. *Proc Natl Acad Sci U S A* **93**(12):6118-6123.

Changeux JP (1993) Chemical signaling in the brain. *Sci Am* **269**(5):58-62.

Changeux JP, Devillers-Thiery A and Chemouilli P (1984) Acetylcholine receptor: an allosteric protein. *Science* **225**(4668):1335-1345.

Changeux JP, Kasai M and Lee CY (1970) Use of a snake venom toxin to characterize the cholinergic receptor protein. *Proc Natl Acad Sci U S A* **67**(3):1241-1247.

Choucair A, Chakrapani M, Chakravarthy B, Katsaras J and Johnston LJ (2007) Preferential accumulation of Abeta(1-42) on gel phase domains of lipid bilayers: an AFM and fluorescence study. *Biochim Biophys Acta* **1768**(1):146-154.

Claudio T, Ballivet M, Patrick J and Heinemann S (1983) Nucleotide and deduced amino acid sequences of Torpedo californica acetylcholine receptor gamma subunit. *Proc Natl Acad Sci U S A* **80**(4):1111-1115.

Cooper E, Couturier S and Ballivet M (1991) Pentameric structure and subunit stoichiometry of a neuronal nicotinic acetylcholine receptor. *Nature* **350**(6315):235-238.

Corringer PJ, Le Novere N and Changeux JP (2000) Nicotinic receptors at the amino acid level. *Annu Rev Pharmacol Toxicol* **40**:431-458.

Criado M, Eibl H and Barrantes FJ (1984) Functional properties of the acetylcholine receptor incorporated in model lipid membranes. Differential effects of chain length and head group of phospholipids on receptor affinity states and receptor-mediated ion translocation. *J Biol Chem* **259**(14):9188-9198.

daCosta CJ and Baenziger JE (2009) A lipid-dependent uncoupled conformation of the acetylcholine receptor. *J Biol Chem*.

daCosta CJ, Ogrel AA, McCardy EA, Blanton MP and Baenziger JE (2002) Lipid-protein interactions at the nicotinic acetylcholine receptor. A functional coupling between nicotinic receptors and phosphatidic acid-containing lipid bilayers. *J Biol Chem* **277**(1):201-208.

daCosta CJ, Wagg ID, McKay ME and Baenziger JE (2004) phosphatidic acid and phosphatidylserine have distinct structural and functional interactions with the nicotinic acetylcholine receptor. *J Biol Chem* **279**(15):14967-14974.

Dale HH and Dudley HW (1929) The presence of histamine and acetylcholine in the spleen of the ox and the horse. II. *J Physiol (Lond)* **68**:97-123.

Dalziel AW, Rollins ES and McNamee MG (1980) The effect of cholesterol on agonist-induced flux in reconstituted acetylcholine receptor vesicles. *FEBS Lett* **122**(2):193-196.

Demel R, Schiavo G, de Kruijff B and Montecucco C (1991) Lipid interaction of diphtheria toxin and mutants. A study with phospholipid and protein monolayers. *Eur J Biochem* **197**(2):481-486.

Dennis M, Giraudat J, Kotzyba-Hibert F, Goeldner M, Hirth C, Chang JY, Lazure C, Chretien M and Changeux JP (1988) Amino acids of the Torpedo marmorata acetylcholine receptor alpha subunit labeled by a photoaffinity ligand for the acetylcholine binding site. *Biochemistry* **27**(7):2346-2357.

Elgoyhen AB, Johnson DS, Boulter J, Vetter DE and Heinemann S (1994) Alpha 9: an acetylcholine receptor with novel pharmacological properties expressed in rat cochlear hair cells. *Cell* **79**(4):705-715.

Ellena JF, Blazing MA and McNamee MG (1983) Lipid-protein interactions in reconstituted membranes containing acetylcholine receptor. *Biochemistry* **22**(24):5523-5535.

Epstein M and Racker E (1978) Reconstitution of carbamylcholine-dependent sodium ion flux and desensitization of the acetylcholine receptor from Torpedo californica. *J Biol Chem* **253**(19):6660-6662.

Feller SE, Yin D, Pastor RW and MacKerell AD, Jr. (1997) Molecular dynamics simulation of unsaturated lipid bilayers at low hydration: parameterization and comparison with diffraction studies. *Biophys J* **73**(5):2269-2279.

Filippov A, Oradd G and Lindblom G (2006) Sphingomyelin structure influences the lateral diffusion and raft formation in lipid bilayers. *Biophys J* **90**(6):2086-2092.

Fong TM and McNamee MG (1986) Correlation between acetylcholine receptor function and structural properties of membranes. *Biochemistry* **25**(4):830-840.

Fotiadis D, Liang Y, Filipek S, Saperstein DA, Engel A and Palczewski K (2003) Atomic-force microscopy: Rhodopsin dimers in native disc membranes. *Nature* **421**(6919):127-128.

Fra AM, Williamson E, Simons K and Parton RG (1994) Detergent-insoluble glycolipid microdomains in lymphocytes in the absence of caveolae. *J Biol Chem* **269**(49):30745-30748.

Goll J, Carlson FD, Barenholz Y, Litman BJ and Thompson TE (1982) Photon correlation spectroscopic study of the size distribution of phospholipid vesicles. *Biophys J* **38**(1):7-13.

Gonzalez-Ros JM, Llanillo M, Paraschos A and Martinez-Carrion M (1982) Lipid environment of acetylcholine receptor from Torpedo californica. *Biochemistry* **21**(14):3467-3474.

Gorodinsky A and Harris DA (1995) Glycolipid-anchored proteins in neuroblastoma cells form detergent-resistant complexes without caveolin. *J Cell Biol* **129**(3):619-627.

Goss SL, Lemons KA, Kerstetter JE and Bogner RH (2007) Determination of calcium salt solubility with changes in pH and P(CO(2)), simulating varying gastrointestinal environments. *J Pharm Pharmacol* **59**(11):1485-1492.

Gotti C, Hanke W, Maury K, Moretti M, Ballivet M, Clementi F and Bertrand D (1994) Pharmacology and biophysical properties of alpha 7 and alpha 7-alpha 8 alpha-bungarotoxin receptor subtypes immunopurified from the chick optic lobe. *Eur J Neurosci* **6**(8):1281-1291.

Grosman C, Salamone FN, Sine SM and Auerbach A (2000) The extracellular linker of muscle acetylcholine receptor channels is a gating control element. *J Gen Physiol* **116**(3):327-340.

Hansson GC, Simons K and van Meer G (1986) Two strains of the Madin-Darby canine kidney (MDCK) cell line have distinct glycosphingolipid compositions. *Embo J* **5**(3):483-489.

Hazelbauer GL and Changeux JP (1974) Reconstitution of a chemically excitable membrane. *Proc Natl Acad Sci U S A* **71**(4):1479-1483.

Hodgkin AL and Huxley AF (1952a) The components of membrane conductance in the giant axon of Loligo. *J Physiol* **116**(4):473-496.

Hodgkin AL and Huxley AF (1952b) Currents carried by sodium and potassium ions through the membrane of the giant axon of Loligo. *J Physiol* **116**(4):449-472.

Hodgkin AL and Huxley AF (1952c) The dual effect of membrane potential on sodium conductance in the giant axon of Loligo. *J Physiol* **116**(4):497-506.

Hooper NM and Turner AJ (1988) Ectoenzymes of the kidney microvillar membrane. Differential solubilization by detergents can predict a glycosyl-phosphatidylinositol membrane anchor. *Biochem J* **250**(3):865-869.

Ira and Johnston LJ (2008) Sphingomyelinase generation of ceramide promotes clustering of nanoscale domains in supported bilayer membranes. *Biochim Biophys Acta* **1778**(1):185-197.

Ira and Johnston LJ (2006) Ceramide promotes restructuring of model raft membranes. *Langmuir* **22**(26):11284-11289.

Jorgensen K and Mouritsen OG (1995) Phase separation dynamics and lateral organization of two-component lipid membranes. *Biophys J* **69**(3):942-954.

Karlin A (2002) Emerging structure of the nicotinic acetylcholine receptors. *Nat Rev Neurosci* **3**(2):102-114.

Kusumi A, Nakada C, Ritchie K, Murase K, Suzuki K, Murakoshi H, Kasai RS, Kondo J and Fujiwara T (2005) Paradigm shift of the plasma membrane concept from the two-dimensional continuum fluid to the partitioned fluid: high-speed single-molecule tracking of membrane molecules. *Annu Rev Biophys Biomol Struct* **34**:351-378.

Langenbuch-Cachat J, Bon C, Mulle C, Goeldner M, Hirth C and Changeux JP (1988) Photoaffinity labeling of the acetylcholine binding sites on the nicotinic receptor by an aryldiazonium derivative. *Biochemistry* **27**(7):2337-2345.

Langley JN (1907) On the contraction of muscle chiefly in relation to the presence of receptive substances. Part 1. *J Physiol (Lond)* **36**:347–384

Laude AJ and Prior IA (2004) Plasma membrane microdomains: organization, function and trafficking. *Mol Membr Biol* **21**(3):193-205.

Lee WY and Sine SM (2005) Principal pathway coupling agonist binding to channel gating in nicotinic receptors. *Nature* **438**(7065):243-247.

Leonenko ZV, Carnini A and Cramb DT (2000) Supported planar bilayer formation by vesicle fusion: the interaction of phospholipid vesicles with surfaces and the effect of gramicidin on bilayer properties using atomic force microscopy. *Biochim Biophys Acta* **1509**(1-2):131-147.

Lewis BA and Engelman DM (1983) Lipid bilayer thickness varies linearly with acyl chain length in fluid phosphatidylcholine vesicles. *J Mol Biol* **166**(2):211-217.

Lisanti MP, Sargiacomo M, Graeve L, Saltiel AR and Rodriguez-Boulan E (1988) Polarized apical distribution of glycosyl-phosphatidylinositol-anchored proteins in a renal epithelial cell line. *Proc Natl Acad Sci U S A* **85**(24):9557-9561.

Lushnikov AY, Potaman VN, Oussatcheva EA, Sinden RR and Lyubchenko YL (2006) DNA strand arrangement within the SfiI-DNA complex: atomic force microscopy analysis. *Biochemistry* **45**(1):152-158.

Maehle AH (2004) "Receptive substances": John Newport Langley (1852-1925) and his path to a receptor theory of drug action. *Med Hist* **48**(2):153-174.

Mai A, Weerachatyanukul W, Tomietto M, Wayner DD, Wells G, Balhorn R, Leader A, Cyr JL and Tanphaichitr N (2002) Use of atomic force microscopy for morphological and morphometric analyses of acrosome intact and acrosome-reacted human sperm. *Mol Reprod Dev* **63**(4):471-479.

Marchand S, Devillers-Thiery A, Pons S, Changeux JP and Cartaud J (2002) Rapsyn escorts the nicotinic acetylcholine receptor along the exocytic pathway via association with lipid rafts. *J Neurosci* **22**:8891-8901.

McCarthy MP and Moore MA (1992) Effects of lipids and detergents on the conformation of the nicotinic acetylcholine receptor from Torpedo californica. *J Biol Chem* **267**(11):7655-7663.

Michaelson DM and Raftery MA (1974) Purified acetylcholine receptor: its reconstitution to a chemically excitable membrane. *Proc Natl Acad Sci U S A* **71**(12):4768-4772.

Middleton RE and Cohen JB (1991) Mapping of the acetylcholine binding site of the nicotinic acetylcholine receptor: [3H]nicotine as an agonist photoaffinity label. *Biochemistry* **30**(28):6987-6997.

Miledi R, Molinoff P and Potter LT (1971) Isolation of the cholinergic receptor protein of Torpedo electric tissue. *Nature* **229**(5286):554-557.

Mirre C, Monlauzeur L, Garcia M, Delgrossi MH and Le Bivic A (1996) Detergent-resistant membrane microdomains from Caco-2 cells do not contain caveolin. *Am J Physiol* **271**(3 Pt 1):C887-894.

Miyazawa A, Fujiyoshi Y and Unwin N (2003) Structure and gating mechanism of the acetylcholine receptor pore. *Nature* **424**(6943):949-955.

Monod J, Wyman J and Changeux JP (1965) On the Nature of Allosteric Transitions: a Plausible Model. *J Mol Biol* **12**:88-118.

Montesano R, Roth J, Robert A and Orci L (1982) Non-coated membrane invaginations are involved in binding and internalization of cholera and tetanus toxins. *Nature* **296**(5858):651-653.

Nagle JF, Zhang R, Tristram-Nagle S, Sun W, Petrache HI and Suter RM (1996) X-ray structure determination of fully hydrated L alpha phase dipalmitoylphosphatidylcholine bilayers. *Biophys J* **70**(3):1419-1431.

Nakada C, Ritchie K, Oba Y, Nakamura M, Hotta Y, Iino R, Kasai RS, Yamaguchi K, Fujiwara T and Kusumi A (2003) Accumulation of anchored proteins forms

membrane diffusion barriers during neuronal polarization. *Nat Cell Biol* **5**(7):626-632.

Noda M, Takahashi H, Tanabe T, Toyosato M, Furutani Y, Hirose T, Asai M, Inayama S, Miyata T and Numa S (1982) Primary structure of alpha-subunit precursor of Torpedo californica acetylcholine receptor deduced from cDNA sequence. *Nature* **299**(5886):793-797.

Noda M, Takahashi H, Tanabe T, Toyosato M, Kikyotani S, Furutani Y, Hirose T, Takashima H, Inayama S, Miyata T and Numa S (1983a) Structural homology of Torpedo californica acetylcholine receptor subunits. *Nature* **302**(5908):528-532.

Noda M, Takahashi H, Tanabe T, Toyosato M, Kikyotani S, Hirose T, Asai M, Takashima H, Inayama S, Miyata T and Numa S (1983b) Primary structures of beta- and delta-subunit precursors of Torpedo californica acetylcholine receptor deduced from cDNA sequences. *Nature* **301**(5897):251-255.

Ochoa EL, Dalziel AW and McNamee MG (1983) Reconstitution of acetylcholine receptor function in lipid vesicles of defined composition. *Biochim Biophys Acta* **727**(1):151-162.

Osaka H, Sugiyama N and Taylor P (1998) Distinctions in agonist and antagonist specificity conferred by anionic residues of the nicotinic acetylcholine receptor. *J Biol Chem* **273**(21):12758-12765.

Oshikawa J, Toya Y, Fujita T, Egawa M, Kawabe J, Umemura S and Ishikawa Y (2003) Nicotinic acetylcholine receptor $\alpha 7$ regulates cAMP signal within lipid rafts. *Am J Physiol Cell Physiol* **285**:C567-574.

Oswald RE and Changeux JP (1982) Crosslinking of alpha-bungarotoxin to the acetylcholine receptor from Torpedo marmorata by ultraviolet light irradiation. *FEBS Lett* **139**(2):225-229.

Owicki JC and McConnell HM (1980) Lateral diffusion in inhomogeneous membranes. Model membranes containing cholesterol. *Biophys J* **30**(3):383-397.

Palade GE (1953) An electron microscope study of the mitochondrial structure. *J Histochem Cytochem* **1**(4):188-211.

Parasassi T, De Stasio G, d'Ubaldo A and Gratton E (1990) Phase fluctuation in phospholipid membranes revealed by Laurdan fluorescence. *Biophys J* **57**(6):1179-1186.

Parton RG (1996) Caveolae and caveolins. *Curr Opin Cell Biol* **8**(4):542-548.

Paternostre MT, Roux M and Rigaud JL (1988) Mechanisms of membrane protein insertion into liposomes during reconstitution procedures involving the use of detergents. 1. Solubilization of large unilamellar liposomes (prepared by reverse-phase evaporation) by triton X-100, octyl glucoside, and sodium cholate. *Biochemistry* **27**(8):2668-2677.

Paula S, Volkov AG and Deamer DW (1998) Permeation of halide anions through phospholipid bilayers occurs by the solubility-diffusion mechanism. *Biophys J* **74**(1):319-327.

Paula S, Volkov AG, Van Hoek AN, Haines TH and Deamer DW (1996) Permeation of protons, potassium ions, and small polar molecules through phospholipid bilayers as a function of membrane thickness. *Biophys J* **70**(1):339-348.

Pedersen SE and Cohen JB (1990) d-Tubocurarine binding sites are located at alpha-gamma and alpha-delta subunit interfaces of the nicotinic acetylcholine receptor. *Proc Natl Acad Sci U S A* **87**(7):2785-2789.

Pike LJ (2006) Rafts defined: a report on the Keystone Symposium on Lipid Rafts and Cell Function. *J Lipid Res* **47**(7):1597-1598.

Popot JL, Demel RA, Sobel A, Van Deenen LL and Changeux JP (1978) Interaction of the acetylcholine (nicotinic) receptor protein from Torpedo marmorata electric organ with monolayers of pure lipids. *Eur J Biochem* **85**(1):27-42.

Poveda JA, Encinar JA, Fernandez AM, Mateo CR, Ferragut JA and Gonzalez-Ros JM (2002) Segregation of phosphatidic acid-rich domains in reconstituted acetylcholine receptor membranes. *Biochemistry* **41**(40):12253-12262.

Putman CA, van der Werf KO, de Grooth BG, van Hulst NF and Greve J (1994) Viscoelasticity of living cells allows high resolution imaging by tapping mode atomic force microscopy. *Biophys J* **67**(4):1749-1753.

Raftery MA, Hunkapiller MW, Strader CD and Hood LE (1980) Acetylcholine receptor: complex of homologous subunits. *Science* **208**(4451):1454-1456.

Richter RP, Berat R and Brisson AR (2006) Formation of solid-supported lipid bilayers: an integrated view. *Langmuir* **22**(8):3497-3505.

Richter RP and Brisson AR (2005) Following the formation of supported lipid bilayers on mica: a study combining AFM, QCM-D, and ellipsometry. *Biophys J* **88**(5):3422-3433.

Rigaud JL and Levy D (2003) Reconstitution of membrane proteins into liposomes. *Methods Enzymol* **372**:65-86.

Rigaud JL, Paternostre MT and Bluzat A (1988) Mechanisms of membrane protein insertion into liposomes during reconstitution procedures involving the use of detergents. 2. Incorporation of the light-driven proton pump bacteriorhodopsin. *Biochemistry* **27**(8):2677-2688.

Rigaud JL, Pitard B and Levy D (1995) Reconstitution of membrane proteins into liposomes: application to energy-transducing membrane proteins. *Biochim Biophys Acta* **1231**(3):223-246.

Robinson AL (1986) Electron Microscope Inventors Share Nobel Physics Prize: Ernst Ruska built the first electron microscope in 1931; Gerd Binnig and Heinrich Rohrer developed the scanning tunneling microscope 50 years later. *Science* **234**(4778):821-822.

Rothberg KG, Heuser JE, Donzell WC, Ying YS, Glenney JR and Anderson RG (1992) Caveolin, a protein component of caveolae membrane coats. *Cell* **68**(4):673-682.

Rothberg KG, Ying YS, Kamen BA and Anderson RG (1990) Cholesterol controls the clustering of the glycophospholipid-anchored membrane receptor for 5-methyltetrahydrofolate. *J Cell Biol* **111**(6 Pt 2):2931-2938.

Rovira JC, Ballesta JJ, Vicente-Agullo F, Campos-Caro A, Criado M, Sala F and Sala S (1998) A residue in the middle of the M2-M3 loop of the beta4 subunit specifically affects gating of neuronal nicotinic receptors. *FEBS Lett* **433**(1-2):89-92.

Rovira JC, Vicente-Agullo F, Campos-Caro A, Criado M, Sala F, Sala S and Ballesta JJ (1999) Gating of alpha3beta4 neuronal nicotinic receptor can be controlled by the loop M2-M3 of both alpha3 and beta4 subunits. *Pflugers Arch* **439**(1-2):86-92.

Ryan SE, Demers CN, Chew JP and Baenziger JE (1996) Structural effects of neutral and anionic lipids on the nicotinic acetylcholine receptor. An infrared difference spectroscopy study. *J Biol Chem* **271**(40):24590-24597.

Sako Y and Kusumi A (1995) Barriers for lateral diffusion of transferrin receptor in the plasma membrane as characterized by receptor dragging by laser tweezers: fence versus tether. *J Cell Biol* **129**(6):1559-1574.

Salas PJ, Vega-Salas DE, Hochman J, Rodriguez-Boulan E and Edidin M (1988) Selective anchoring in the specific plasma membrane domain: a role in epithelial cell polarity. *J Cell Biol* **107**(6 Pt 1):2363-2376.

Sargiacomo M, Sudol M, Tang Z and Lisanti MP (1993) Signal transducing molecules and glycosyl-phosphatidylinositol-linked proteins form a caveolin-rich insoluble complex in MDCK cells. *J Cell Biol* **122**(4):789-807.

Schiebler W and Hucho F (1978) Membranes rich in acetylcholine receptor: characterization and reconstitution to excitable membranes from exogenous lipids. *Eur J Biochem* **85**(1):55-63.

Seelert H, Dencher NA and Muller DJ (2003) Fourteen protomers compose the oligomer III of the proton-rotor in spinach chloroplast ATP synthase. *J Mol Biol* **333**(2):337-344.

Shlyakhtenko LS, Gall AA, Filonov A, Cerovac Z, Lushnikov A and Lyubchenko YL (2003) Silatrane-based surface chemistry for immobilization of DNA, protein-DNA complexes and other biological materials. *Ultramicroscopy* **97**(1-4):279-287.

Simons K and Ikonen E (1997) Functional rafts in cell membranes. *Nature* **387**(6633):569-572.

Simons K and Ikonen E (2000) How cells handle cholesterol. *Science* **290**(5497):1721-1726.

Singer SJ and Nicolson GL (1972) The fluid mosaic model of the structure of cell membranes. *Science* **175**(23):720-731.

Smart EJ, Ying Y, Donzell WC and Anderson RG (1996) A role for caveolin in transport of cholesterol from endoplasmic reticulum to plasma membrane. *J Biol Chem* **271**(46):29427-29435.

Sunshine C and McNamee MG (1992) Lipid modulation of nicotinic acetylcholine receptor function: the role of neutral and negatively charged lipids. *Biochim Biophys Acta* **1108**(2):240-246.

Tahara Y and Fujiyoshi Y (1994) A new method to measure bilayer thickness: cryo-electron microscopy of frozen hydrated liposomes and image simulation. *Micron* **25**(2):141-149.

Traikia M, Warschawski DE, Recouvreur M, Cartaud J and Devaux PF (2000) Formation of unilamellar vesicles by repetitive freeze-thaw cycles: characterization by electron microscopy and 31P-nuclear magnetic resonance. *Eur Biophys J* **29**(3):184-195.

Tristram-Nagle S, Petrache HI and Nagle JF (1998) Structure and interactions of fully hydrated dioleoylphosphatidylcholine bilayers. *Biophys J* **75**(2):917-925.

Unwin N (1993a) Neurotransmitter action: opening of ligand-gated ion channels. *Cell* **72 Suppl**:31-41.

Unwin N (1993b) Nicotinic acetylcholine receptor at 9 A resolution. *J Mol Biol* **229**(4):1101-1124.

Unwin N (2003) Structure and action of the nicotinic acetylcholine receptor explored by electron microscopy. *FEBS Lett* **555**(1):91-95.

Unwin N (2005) Refined structure of the nicotinic acetylcholine receptor at 4A resolution. *J Mol Biol* **346**(4):967-989.

Unwin N, Toyoshima C and Kubalek E (1988) Arrangement of the acetylcholine receptor subunits in the resting and desensitized states, determined by cryoelectron microscopy of crystallized Torpedo postsynaptic membranes. *J Cell Biol* **107**(3):1123-1138.

van Meer G and Simons K (1986) The function of tight junctions in maintaining differences in lipid composition between the apical and the basolateral cell surface domains of MDCK cells. *Embo J* **5**(7):1455-1464.

van Meer G, Stelzer EH, Wijnaendts-van-Resandt RW and Simons K (1987) Sorting of sphingolipids in epithelial (Madin-Darby canine kidney) cells. *J Cell Biol* **105**(4):1623-1635.

Veatch SL and Keller SL (2003) Separation of liquid phases in giant vesicles of ternary mixtures of phospholipids and cholesterol. *Biophys J* **85**(5):3074-3083.

Vega-Salas DE, Salas PJ and Rodriguez-Boulan E (1988) Exocytosis of vacuolar apical compartment (VAC): a cell-cell contact controlled mechanism for the establishment of the apical plasma membrane domain in epithelial cells. *J Cell Biol* **107**(5):1717-1728.

Vereb G, Szollosi J, Matko J, Nagy P, Farkas T, Vigh L, Matyus L, Waldmann TA and Damjanovich S (2003) Dynamic, yet structured: The cell membrane three decades after the Singer-Nicolson model. *Proc Natl Acad Sci U S A* **100**(14):8053-8058.

Voet D, Voet JG and Pratt CW (1999) *Fundamentals of Biochemistry*. John Wiley & Sons, Inc., New York.

Wallin E and von Heijne G (1998) Genome-wide analysis of integral membrane proteins from eubacterial, archaean, and eukaryotic organisms. *Protein Sci* **7**(4):1029-1038.

Weerachatyanukul W, Probodh I, Kongmanas K, Tanphaichitr N and Johnston LJ (2007) Visualizing the localization of sulfoglycolipids in lipid raft domains in model membranes and sperm membrane extracts. *Biochim Biophys Acta* **1768**(2):299-310.

Weill CL, McNamee MG and Karlin A (1974) Affinity-labeling of purified acetylcholine receptor from Torpedo californica. *Biochem Biophys Res Commun* **61**(3):997-1003.

Wenz JJ and Barrantes FJ (2005) Nicotinic acetylcholine receptor induces lateral segregation of phosphatidic acid and phosphatidylcholine in reconstituted membranes. *Biochemistry* **44**(1):398-410.

Xiang TX and Anderson BD (1998) Phase structures of binary lipid bilayers as revealed by permeability of small molecules. *Biochim Biophys Acta* **1370**(1):64-76.

Yamada E (1955a) The fine structure of the gall bladder epithelium of the mouse. *J Biophys Biochem Cytol* **1**(5):445-458.

Yamada E (1955b) The fine structure of the renal glomerulus of the mouse. *J Biophys Biochem Cytol* **1**(6):551-566.

Yamada E (1955c) The fine structure of the renal glomerulus of the mouse. *J Histochem Cytochem* **3**(4):309.

Yang J, Tamm LK, Tillack TW and Shao Z (1993) New approach for atomic force microscopy of membrane proteins. The imaging of cholera toxin. *J Mol Biol* **229**(2):286-290.

Yellin N and Levin IW (1977) Hydrocarbon trans-gauche isomerization in phospholipid bilayer gel assemblies. *Biochemistry* **16**(4):642-647.

Zeyda M and Stulnig TM (2006) Lipid Rafts & Co.: an integrated model of membrane organization in T cell activation. *Prog Lipid Res* **45**(3):187-202.

NOTES

Curriculum Vitae

Ngoc Vuong
97 Glamorgan Drive, Ottawa ON K2L1R5, CANADA
Email: ngocvuong@yahoo.com
Phone: 613-863-8664

SUMMARY OF QUALIFICATIONS

-B.Sc. and M.Sc. in Biochemistry, and 7+ years of research experience.
-Three years of supervising and managing university science students.
-More than 5 years of experience in UV/Vis, FTIR and fluorescence spectroscopy.
-Experience with electron, fluorescence (TIRF and Confocal) and atomic force microscopy.
-Column chromatography: affinity, ion exchange, silica, HPLC.
-SDS-PAGE, immunoblot, TLC, 2-D gel and enzymatic assays for proteins and lipids.
-Handling animals (surgical and experimental), and cells/tissues culturing.
-Knowledgeable in molecular biology such as RT-PCR
-Excellent in data organization, statistic, oral (verbal) communication and presentation.
-Computer skills: Microsoft Excel (level 3 training), Word, and PowerPoint.
-Work well independently, as well as team work (strong interpersonal skill).

WORK EXPERIENCE

Biologist 2008 – present
Health Canada, Ottawa, Ontario Canada
-Investigate the toxicological effect of air pollutions on the cardiovasicular system via *in vivo* and *in vitro* studies with cutting edge technologies.

Technical Officer 2007 – 2008
National Research Council of Canada, Ottawa, Ontario, Canada
-Coordinate microscopic training and scheduling for researchers/collaborators in the institute.
-Provide care and trouble shoot microscopic instruments, and ordering chemical reagents.
-Purify and reconstitute membrane proteins to examine the protein's structure and function.

Teaching Assistant 2005 – 2007
University of Ottawa, Ottawa, Ontario, Canada
Introduction to Organic Chemistry Laboratory
-Supervise and instruct a large group of students to perform and interpret simple experiments such as recrystallization, distillation, extraction, as well as Grignard, E1, S_N1 and S_N2 reactions.
-Teach the students to write report in a concise manner, and assess their comprehension.

Introduction to Biochemistry Laboratory
-Demonstrate to second year students basic biochemistry experiments such as ion exchange chromatography, amino acid titration and SDS-PAGE in a precise and time efficient manner.
-Constructively criticize lab reports to encourage students to develop critical thinking.
Protein Structure and Function
-Assist third year students to grasp the principles behind modern physics methods use to study protein structures and function, protein folding and engineering, mechanisms of enzyme action, enzyme kinetics, and regulation of enzyme activity.
-Teach the students to view and generate protein structure model from Protein Data Bank.

Technical Officer 2003 – 2004
National Research Council of Canada, Ottawa, Ontario, Canada
-Develop a protocol for the preparation of a solid support bilayer and monolayer.
-Use atomic force microscopy (AFM) to examine whether the reconstituted rhodopsin has preferential interaction with liquid disordered phase in a domain forming membrane.
-Assist in the photochemistry study of psoralen and coumarin in HSA complexes and DMPC vesicle by UV/Vis and fluorescence spectroscopy.

Research Assistant 2002 – 2003
Ottawa Health Reseach Institute (OHRI), Ottawa, Ontario, Canada
-Coordinate and conduct a collaborative project between the OHRI and Health Canada.
-Investigate the toxicological effect on rat sperm upon exposing the animal to air particles such as ozone and suspended particulates around the Environmental Health Canada building in the Ottawa region.
-Organize and document data, identify problems in the project, and provide solutions to the problems.

EDUCATION

M.Sc. in Biochemistry 2010
University of Ottawa, Ottawa, Ontario, Canada
Thesis: Imaging the nicotinic acetylcholine receptor reconstituted in a POPC membrane.

B.Sc. in Biochemistry 2002
University of Ottawa, Ottawa, Ontario, Canada
Thesis: Elucidation of the lipid composition of rafts isolated from non-capacitated and capacitated pig sperm.

AWARDS

University of Ottawa Biochemistry, Microbiology & Immunology graduate student poster presentations. 2007. 1st Place Winner.

PUBLICATIONS

1. **Vuong N**, Baenziger JE and Johnston JL. Preparation of reconstituted acetylcholine receptor membranes suitable for AFM imaging of lipid-protein interactions. Chemistry and Physics of Lipids. 2010 Feb; 163 (2): 117-126.

2. Baenziger JE, Ryan SE, Goodreid MM, **Vuong NQ**, Sturgeon RM, and daCosta CJ. Lipid composition alters drug action at the nicotinic acetylcholine receptor. Molecular Pharmacology. 2008 Mar; 73(3):880-90.

3. Bou Khalil M, Chakrabhandu K, Xu H, Weerachatyanukul W, Buhr M, Berger T, Carmona E, **Vuong N**, Kumarathasan P, Wong TTP, Carrier D, and Tanphaichitr N. Sperm Capacitation Induces an Increase in Lipid Rafts Having Zona Pellucida Binding Ability and Containing Sulfogalactosylglycerolipid. Developmental Biology. 2006 Feb; 290(1):220-35.

4. Chen L, Rinco O, Popov J, **Vuong N** and Johnston JL. Psoralen and Coumarin Photochemistry in HSA Complexes and DMPC Vesicle. Photochemistry and Photobiology. 2006 Jan-Feb; 82(1):31-7.

5. Furimsky A, **Vuong N**, Xu H, Kumarathasan P, Xu M, Weerachatyanukul W, Bou Khalil M, Kates M, Tanphaichitr N. Percoll gradient-centrifuged capacitated mouse sperm have increased fertilizing ability and higher contents of sulfogalactosylglycerolipid and docosahexaenoic acid-containing phosphatidylcholine compared to washed capacitated mouse sperm. Biology of Reproduction. 2005 Mar; 72(3):574-83.

CONFERENCES

1. **Vuong N**, Baenziger J and Johnston L. (2007) Imaging the nicotinic acetylcholine receptor in a POPC membrane. University of Ottawa Biochemistry, Microbiology & Immunology graduate student poster presentations.

2. **Vuong N**, Baenziger J and Johnston L. (2007) Imaging the nicotinic acetylcholine receptor in a POPC membrane. Chemical Biophysics Symposium, Toronto, Canada. Poster presentation.

3. **Vuong N**, Johnston L and Baenziger J. (2005) Localization of the nicotinic acetylcholine receptor in the membrane. First Annual McGill Biophysical Chemistry Symposium. Montreal, QC, Canada. Poster presentation.

4. **Vuong N**, Loewen M, Ianoul A and Johnston L. (2004) Rhodopsin preferentially localized in the fluid phase of the membrane. Genomic and Health Initiative Conference. Montreal, QC, Canada. Poster presentation.